HELSINGIN YLIOPISTO

Proton-Transfer-Reaction Mass Spectrometry in Atmospheric Analysis

Master’s Program in Chemistry and Molecular Sciences
Master's thesis

Author:
Anna Murdoch

Supervisors:
Professor Mikael Ehn
Professor Susanne Wiedmer
Post-doctoral Researcher Jian Zhao

17.3.2025
Helsinki

Faculty: Faculty of Science

Degree program: Master's Program in Chemistry and Molecular Sciences

Study track: Analytical Chemistry

Author: Anna Murdoch

Title: Proton-Transfer-Reaction Mass Spectrometry in Atmospheric Analysis

Level: MSc

Month and year: March 2025

Number of pages: 57

Keywords: environmental analysis, proton-transfer—reaction mass spectrometry, vaporization inlet for aerosols, volatile organic compound, atmospheric science

Supervisor or supervisors: Professor Mikael Ehn; Professor Susanne Wiedmer; Post-doctoral Researcher Jian Zhao

Where deposited: University of Helsinki digital archive

Additional information:

Abstract:

Proton-transfer-reaction mass spectrometry (PTR-MS) is an analytical technique developed for the detection of volatile organic compounds (VOCs). In the field of atmospheric science, its uses are numerous. VOC emissions may be monitored for long-term data, atmospheric concentrations can be traced back to emission sources, and emission phenomena can be captured due to the high time-resolution of the technique. In addition, atmospheric VOC oxidation reactions leading to ozone and secondary organic aerosol (SOA) formation are studied. The technique has also been applied in the study of particles, namely as an assisting method in SOA studies and as a detection method for environmental micro and nano plastics (MNPs).

The applicability of PTR-MS ranges from the investigation of complex gas mixtures to the most detailed study targets, from laboratory chamber studies to field campaigns. The merits of this relatively novel form of mass spectrometry include its sensitivity to atmospheric trace compounds and its ever-growing mass resolution. Moreover, mass spectra of analyte mixtures consist mainly of protonated molecular ions, MH^+, since fragmentation of molecular ions is quite minimal in this form of chemical ionization MS.

The experimental project of this thesis featured the investigation of evaporation products from SOA produced in the ozonolysis of α- and β-pinene in an atmospheric chamber. The analysis was performed by coupling a recently developed vaporization inlet for aerosols (VIA) to a Vocus PTR time-of-flight (ToF) mass spectrometer. The operation of the VIA consisted of a VOC-stripping charcoal gas denuder and a flight-tube surrounded by a heating wire to enable a temperature-ramping program in the tube. The flow of particles through the VIA and into the Vocus was held constant, thus producing temperature-specific data on particle evaporation. As this was the first time the VIA was used with a PTR-MS, the primary goal was to test the applicability of the inlet to the Vocus.

Data analysis of mass spectra and plotted thermograms from several set-ups showed much potential for the use of VIA-Vocus in particle-phase studies, but that the method still requires optimization. Preliminary results indicated the presence of several oxygenated species, as expected. However, many peaks not fitting our expectations were detected in particle phase spectra. This was most probably due to VOC leaching through the gas-phase denuder and contamination of the VIA tube's inner walls. In future measurements, the conditioning of the gas denuders and the sufficient recording of blank measurements is most significant to ensure the improved quality of data.

Table of contents

Abbreviations

BTEX	Benzene, toluene, ethylbenzene and xylenes
BVOC	Biogenic volatile organic compound
CHARON	Chemical analysis of aerosols on-line
CIMS	Chemical ionization mass spectrometry
CPF	Conditional probability function
CPS	Counts per second
DF	Dilution factor
EF	Emission factor
EI	Electron impact ionization/
EESI	Extractive electrospray ionization
ESI	Electrospray ionization
FIGAERO	Filter inlet for gases and aerosols
FIMR	Focusing ion molecule reactor
GC-FID	Gas chromatography flame ionization detector
GC-MS	Gas chromatography mass spectrometry
HEPA	High efficiency particulate air
HOM	Highly oxygenated organic molecule
HYSPLIT	Hybrid single-particle lagrangian integrated trajectory model
MIR	Maximum incremental reactivity
MNP	Micro and nano plastic
NNMF	Non-negative matrix factorization
NPF	New particle formation
OFP	Ozone formation potential
OGD	Oil and gas development
OVOC	Oxygenated volatile organic compound
PAH	Polyaromatic hydrocarbon
PMF	Positive matrix factorization
PSCF	Potential source contribution function
PTFE	Polytetrafluoroethylene
PTR-MS	Proton-transfer-reaction mass spectrometry
SIFT-MS	Selective ion flow tube mass spectrometry
SOA	Secondary organic aerosol
SOAP	SOA formation potential
SP-AMS	Soot particle aerosol mass spectrometer
SRI	Selective reagent ionization
SVOC	Semi-volatile organic compounds
TD	Thermal desorption
TIC	Total ion concentration
TOF	Time-of-flight
VCP	Volatile chemical product
VIA	Vaporization inlet for aerosols
VOC	Volatile organic compound

1 Introduction

Proton-transfer-reaction mass spectrometry (PTR-MS), an analytical technique developed by Hansel *et al.* in 1995, is most suitable for the detection of volatile organic compounds (VOCs).[1] Due to the fundamental nature of VOCs to volatilize in ambient conditions, the technique of PTR-MS is relevant in atmospheric analytical chemistry and reactivity studies.

PTR-MS represents a form of chemical ionization mass spectrometry (CIMS), differing from other chemical ionization techniques by its unique applicability and fine sensitivity.[1–3] PTR doesn't require vacuum conditions, which opens possibilities for hyphenation with other analytical techniques. Instrument-wise, a variety of alternatives exists regarding price, sensitivity, mass resolution, and instrument size. Sampling, while typically conducted continuously in gas-phase, can also be conducted quite liberally using connective inlets. Thanks to the merits of excellent time-resolution and sensitivity, PTR-MS has taken a steady place among analytical techniques, producing on-line data otherwise left uncaptured. Its rivalling techniques should better be called complementary, since they offer just that, while lacking in ways that PTR-MS does not.

Applications discussed in this thesis have been limited to those relevant to atmospheric sciences. VOC pollution in terms of source attribution, point source analysis or the impact of a specific anthropogenic activity are heavily researched topics and thus handled extensively. VOC reactivities, specifically the formation of oxygenated VOCs (OVOCs), ozone and secondary organic aerosol, are an important factor in climate chemistry. These types of studies feature both field measurements and chamber studies in laboratories. Aerosol research focuses typically either on anthropogenic or biogenic sources. More recently, PTR-MS of micro- and nano plastics has emerged as a valid technique. Since particles by their significant mass are beyond the detection range of PTR-MS, aerosol research is typically studied together with other particle detection techniques.

As the topic of the experimental part of the work, a novel vaporization inlet for aerosols (VIA) was combined with high resolution PTR-ToF-MS to characterize any VOC presence in sampled air consisting of volatilized secondary organic aerosol (SOA), born from the reactions between selected VOCs and controlled amounts of ozone. Secondary organic aerosol was produced in an atmospheric chamber and measurements of the

chamber's gas and particle content were conducted alternately. As the use of the VIA inlet has only been published on a few occasions[4,5], the primary goal of the experiment was using PTR in testing a method, which was thus far optimized for NO3-ToF-CIMS measurements.

2 Literature review

2.1 Instrument and set-ups

2.1.1 Chemical ionization and sensitivity

A highly essential part in PTR-MS is its characteristic ionization method by proton transfer. Chemical ionization techniques appearing in the scope of this thesis are featured in Figure 1.

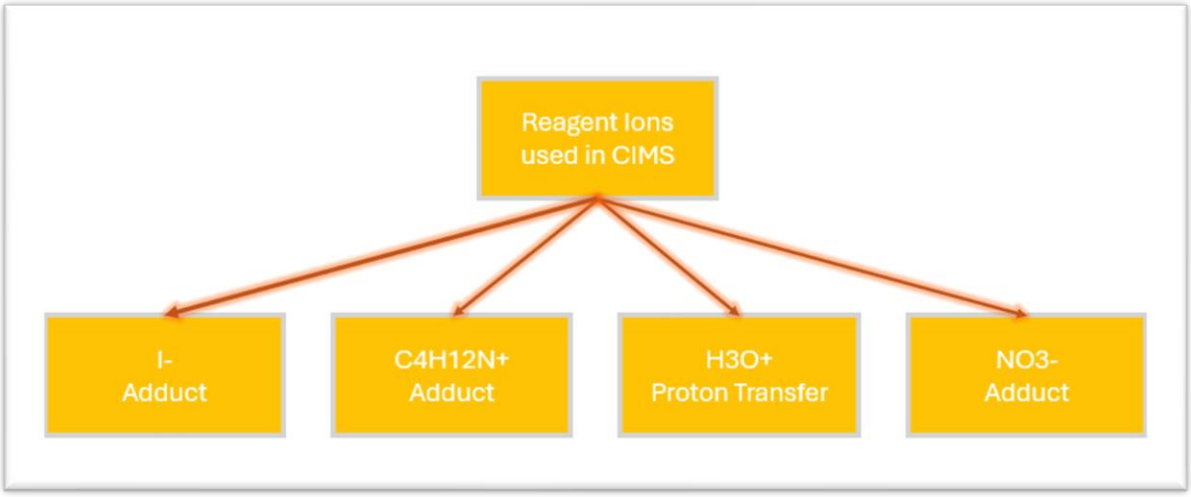

Figure 1. Chemical ionization techniques used in atmospheric mass spectrometry. CIMS= Chemical ionization mass spectrometry.

The proton affinity of analytes establishes the basis for analysis by PTR-MS. Whether an analyte gets ionized by PTR depends on its proton affinity compared to that of water, $PA_{H_2O} = 697 \frac{kJ}{mol}$[6]. Protonation of sample analytes is achieved through collision induced proton transfer reactions with the reagent ion H_3O^+, as expressed by Hansel *et al.*[1] (see reaction equation (1), where M represents a combination of atoms present in the organic analyte, typically C, N *and* S.). The reagent ions are produced by directing

a hollow cathode sourced high voltage through ultrapure water vapor, which then flows into an ion-molecule reactor.[1,7]

$$H_3O^+ + M_iH_j \rightarrow H_2O + M_iH_{j+1}^+ \quad (1)$$

Compounds with a lower proton affinity than that of water will not be protonated during chemical ionization and remain thus entirely undetected. This is a fact to remain mindful of when conducting untargeted analysis by PTR-MS. Inorganic gases such as $CO_2, N_2O,$ and CO fall on this list of undetectable compounds, but also atmospherically significant volatile organic compounds such as methane and glyoxal[8] exhibit a proton affinity too low for PTR.[1]

Proton-transfer-reaction as an ionization mode is relatively gentle, so less fragmentation occurs in the ionization process than in electron impact (EI) ionization. As a result, molecular ion peaks can be identified with high likelihood, and analysis of sample mixtures is possible. It is however worth noting, that evidence of occasional PTR-induced fragmentation does exist, namely in the case of peroxidated[9] monoterpenes. Coggon *et al.*[10] studied fragmentation disturbances in atmospheric measurement data and developed corrective measures for key ions affected by fragmentation.

The conditions within the inlet and drift tube are optimized so that proton transfer via collisions between reagent ions and analytes can occur maximally without product ion wall losses. In practice, the pressure is held near-vacuum at a single mbar level and the temperature elevated above ambient. A longitudinal electric field in the drift tube enables a quick analyte exit into the ion transfer unit before further reactions can occur.[3] The reduced electric field (E/N), where E depends on the length of the drift tube and the voltage applied $[\frac{V}{cm}]$, and N represents the number density of molecules $[cm^{-3}]$,[2] is a highly essential parameter to optimize. The number density of molecules can be derived from the ideal gas law (eq. 1) Boltzmann constant). This in turn explains the importance of pressure and temperature within the drift tube.

$$\frac{N}{V} = \frac{p}{kT} \quad \text{(eq. 1)}$$

Peng *et al.*[11] discuss the effects of the reduced electric field as balancing between water clustering in the lower E/N range and product ion fragmentation in the higher E/N range. Due to the effect of water clustering, some VOCs (benzene & toluene) exhibit

humidity-dependent reduction in sensitivity.[3] The afore discussed parameters are usually disclosed in PTR-MS publications, as the set drift tube conditions affect the MS results. Table 1 includes a list of drift tube parameters used in PTR-MS studies.

Table 1. Drift tube operating parameters in proton-transfer-reaction mass spectrometry. The highlighted rows represent the maximum and minimum reduced electric field encountered.

Pressure	Drift Tube Temperature	Voltage	*Reduced Electric field*	*Reference*
2.2 mbar	60 C	600 V	*130 Td*	[12]
3.0 mbar	120 C	603 V	*120 Td*	[13]
2.3 mbar	60 C	600 V	*135 Td*	[14]
4.0 mbar	80 C	1000 V	*132 Td*	[15]
4.0 mbar	80 C	1000 V	*132 Td*	[16]
2.0 mbar	60 C	600 V	*145 Td*	[17]
2.5 mbar	110 C	650 V	*140 Td*	[10]
2.1 mbar	120 C	550 V	*120 Td*	[10]
2.0 mbar	60 C	590 V	*130 Td*	[10]
2.2 mbar	100 C	600 V	*125 Td*	[10]
2.3 mbar	60 C	600 V	*130 Td*	[10]
2.5 mbar	110 C	650 V	*140 Td*	[10]
3.8 mbar	60 C	900 V	*120 Td*	[18]
3.3 mbar	80 C	850 V	*135 Td*	[19]
3.0 mbar	60 C	815 V	*135 Td*	[20]
2.8 mbar	80 C	460 V	*90 Td*	[21]
3.2 mbar	80 C	710 V	*120 Td*	[22]
2.9 mbar	120 C	500 V	*100 Td*	[11]
2.2 mbar	45 C	570 V	*122 Td*	[23]
3.8 mbar	120 C	760 V	*120 Td*	[24]

The set E/N is on average 120 to 130 Td, with the voltage ranging from below 500 V to 1000V. The drift tube pressure is typically in the order of 2 to 4 mbar and the temperature ranging from 60 to 120 °C with the exception of one study where 45 °C was used. Instrumentation has been developed so that sensitivity has been improved by a factor of 10^3 from single ppb level[1] to single ppt level[7] over the course of two decades. Riva *et al.*[17] estimate a successful mass spectrometric analysis to depend on two major factors: how well the analyte is ionized and how well the ionized analyte is detected by the mass analyser. The ionization efficiency has been improved by developing new ion-molecule reactors. The most recent developments involve ion-focusing systems in which radiofrequency fields are applied inside the drift tube.[3,7] A more detailed description of such a novel reactor is provided in the experimental section of this thesis. Some set-ups involve ion funnels formed out of ring electrodes,[3,25]

originally introduced to PTR-MS instruments by Barber *et al.* in 2012.[26] This increases the number of charged analytes exiting the ion-molecule reactor through a charge-based focusing effect on the travelling ions. Also quadrupole[9–11,22,27] and hexapole[3,25,28] ion guides are commonly used between the ion-molecule reactor and the mass analyser. Some evidence has however been reported on analyte fragmentation with the use of ion guides.[10]

Estimations of analyte concentrations can be obtained by the use of corresponding proton-transfer-reaction rate constants[13,29,30], readily available VOC calibration mixtures[10,17,18,20], or gravimetrically prepared standards[10,27]. Normalization to reagent ion signal is commonly implemented,[11,17,31,32] due to the fact that the primary reagent ion signal may not stay constant throughout the measurement period.[33] An example of an experimentally derived transmission formula with a reported accuracy of ~30 % is presented below in (eq. 2).[34] Here, $[VOCH^+]$ and $[H_3O^+]_0$ are the transmission corrected concentrations of the protonated analyte and the primary ion respectively, $[VOC]$ the VOC mixing ratio, k the corresponding proton-transfer-reaction rate constant and t the ion residence time in the drift tube.

$$[VOCH^+] = [H_3O^+]_0[VOC]kt \qquad \text{(eq. 2)}$$

When applied beyond available calibrants, a quantitative approach by PTR-MS gives mainly direction of what the actual mixing ratios may be. Even within analysis of target VOCs with existing calibrants, long-term quantitative measurements are challenged by drifting transmission.[25] Calibrations are conventionally performed at the beginning and the end of a measurement period, and when conducting long-running experiments, the drift may become problematic. Notø and Holzinger[25] propose the use of atmospherically relevant halogenated compounds to derive real-time transmission data, which in turn can enhance measurement accuracy.[25] Trichlorofluromethane and carbon tetrachloride are persistent, continuously monitored compounds with negligible emissions, which makes them ideal internal calibrants in all ambient measurements.[25]

More recent developments describe PTR-instruments with fast-switching multiple reagent ion capabilities (NH_4^+, NO^+, and O_2^+),[3] which means that the same sample can be ionized with various reagent ions in a quick-alternating pace, broadening the range of detection beyond that of PTR-MS. The use of O_2^+ for instance is more tuned for

chlorinated compounds,[35] and as such useful in pollutant analysis. A schematic of one such instrument is depicted in Figure 2.

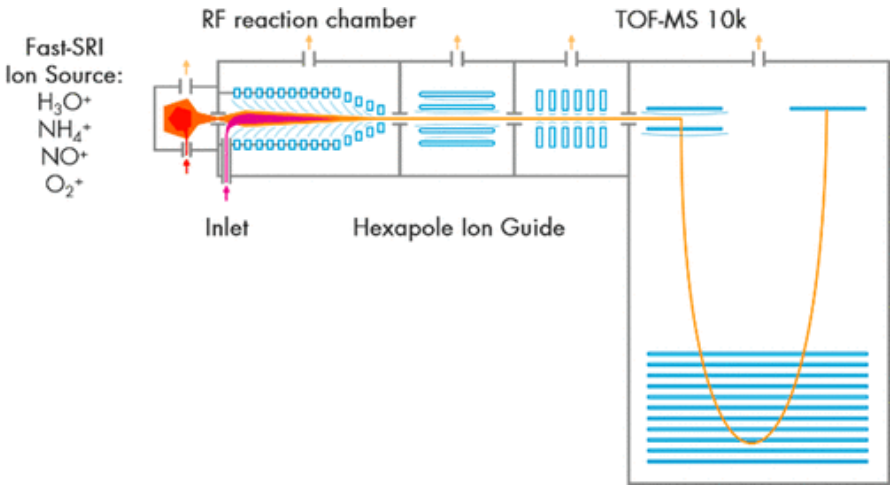

Figure 2. A schematic of a novel multiple reagent ion proton-transfer-reaction mass spectrometer. SRI= selective reagent ionization Reprinted with permission from American Chemical Society (open access).[3]

2.1.2 Mass analysis and resolution

As the method of ionization lies at the heart of PTR-MS, less attention is directed at mass analysis. Selection of mass analyser seems to depend on the required mass resolution and budget available. Two types of mass analysers are favoured in PTR-MS instruments: quadrupole[14,23,31,36–42], and time-of-flight[2,8,10–13,15,17–22,24,25,27,28,30,33,39,43–63]. In terms of mass resolution, R, quadrupole instruments can be considered at the lower end. PTR-ToF instruments on the other hand may range from low (1200)[28] to high ($10000 - 15000$)[3,17,56] resolution depending on their inner components and the length of the flight tube.

In context of atmospheric research and the fact that pre-separation of sample analytes is extremely rare, demands on the mass analysis and mass resolution are high. At the same time, units fit for field use must be easily transportable, often eliminating the most high-resolution options. This contradiction has resulted in a wide range in instrumentation.

The original PTR-MS publication by Hansel *et al.*[1] focused entirely on the novel ionization method, referring to the mass analyser merely as a detection system. In 2010, a high-resolution instrument was introduced by Graus *et al.*[2], featuring a time-of-flight tube including a resolution-enhancing reflectron. Reflectrons, also known as

ion mirrors, curve the path of the analytes according to their existing kinetic energies in such a way that the angular distance within any travelling pack of ions decreases,[6] effectively narrowing the peak width on the resulting mass spectrum. In addition, mass resolution has been increased through the development of longer flight tubes.[7] These high-resolution mass analysers enable the separation of isobaric compounds. In data analysis, this development can be observed in the number of partially overlapping peaks identified. Krechmer *et al.* exemplify this by running data deconvolution on a cluster of peaks with various resolving powers (see Figure 3Table 1).

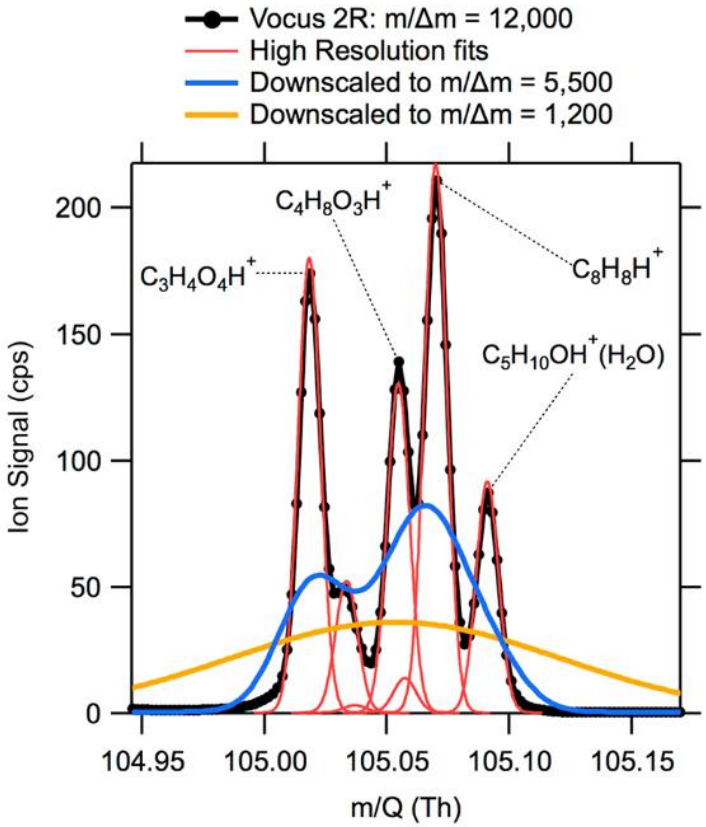

Figure 3. A mass spectrum of ambient air from one 2-Hz saved spectrum (24 September 2017, 18:48:34 UTC) at m/Q = 105 Th. With a mass resolving power m/Δm = 12 000, five peaks were resolved in the deconvolution. The same mass spectrum was then down-sampled to lower resolving powers of 5500 and 1200. Reprinted (adapted) with permission from Krechmer et al.[7] Copyright 2018 American Chemical Society.

2.1.3 Sampling

Sampling in PTR-MS can be divided into continuous direct sampling into instrument and the collection of grab samples into vessels[38,51] or filters[13,43,48,57,64]. In both cases, the general challenges of VOC sampling exist. Often being in the level of trace analysis, any sample losses during the sampling process can cause significant bias to the results.

Unfortunately, sample loss may be tedious to combat since the chemical nature of VOCs is to interact with surfaces and get lost on the way to the detector. For this reason, care must be taken when choosing sampling equipment. Both surface materials and tubing dimensions matter.

The majority of VOC analyses by PTR-MS occur as on-line measurements[2,8,10–12,14,17–21,23,24,27,28,30,31,33,36,37,39–42,44,45,49,52,54,56,59–63,65], as originally intended by Hansel et al[1]. This usually means fast continuous measurements and minimal sample corruption. On the other hand, quantitative studies will require frequent instrumental calibration, because transmission tends to change over time as circumstances change[25]. In laboratory studies sampling lines may be optimized to minimize the risk of sample losses, but the reality of conducting field measurements is often different. A typical field set-up consists of instrumentation inside a field station[10,12,18,21,24,40,54,63] or a mobile laboratory[10,14,19,28,44,45,56] with the sampling line reaching lengths of several meters and the sample flow split into various inlets. Some field studies do exist where outdoor measurements with a minimal length inlet have been conducted[31,41,60–62].

The sample line often features an inner polymer surface such as polytetrafluoroethylene (PTFE)[8,10,18,19,40,45,54,62,63], polyether ether ketone [10,14,19–21,28,40], perfluoroalkoxy [11,12,20,23,24,28,31,36,41,44,56,59–61,66] or fluorinated ethylene propylene[53]. These are known to be highly inert materials and are therefore favoured in trace analysis, with the exception of nano plastic analysis[48], in which plastic tubing is sometimes avoided to minimize sample contamination. However, more often this issue in micro and nano plastic (MNP) sampling is addressed by a copious number of blank measurements and respective background subtraction.[13,57,64,67]

Particle filters[37,54,60,61] may be added to the sampling system to avoid contamination, or to trap analytes[43,49] for subsequent analysis. Also filters to eliminate gases have been used in particle analysis.[30] Sample air is occasionally dried[36,66], but caution should be exercised when considering the use of cold traps for instance. Jobson *et al.*[66] observed enhanced sensitivity and reduced water clustering in the measurement of formaldehyde and several other volatile species, when sample air was dried in a cold trap. Losses were however observed for some aromatic species, especially at trace level analysis.[66] The effect of humidity has also been tackled post-measurement during data-analysis.[9] With the recent development of the Focusing Ion-molecule reactor (FIMR) for the ToFwerk Mass spectrometer Vocus, no link between sensitivity and sample humidity was observed.[7]

The use of heated inlets[10,20,21,28,40,45] is relatively common to prevent condensation on the walls of the sampling line, the temperature ranging typically between 60 and 80 °C. Sample inlet flow varies from as low as 10^{-3} L/min level[23] to several liters per minute[10,27] depending on the sample and target analytes. As demonstrated above, consideration for detail is called for when building set-ups for on-line measurements. It is therefore unfortunate that the details of the sampling set-up are not always described explicitly and reproducibly in publications. From an analytical perspective, the omitting of details of the sampling protocol is dubious, especially in the context of trace VOC analysis. As a curiosity among on-line analysis exists a tracer flux ratio study[56], which used an unmanned aerial vehicle to sample air on a vertical axis of 25 m while connected to a mobile laboratory via a perfluoroalkoxy line.

Offline measurements are also performed[13,25,43,48,51,57,64], albeit rarely. This usually means the collection of a field sample and its subsequent transportation, storage and laboratory analysis. The most common case of offline PTR-MS is the capture of analytes onto filters and instrumental coupling to a thermal desorption (TD) unit.[13,43,48,57,64]

Occasionally, gaseous samples are collected for offline analysis. Wang *et al.*[38] performed headspace sampling into Tedlar® bags .Yang *et al.*[51] developed a method with a drone carrying an aircore sampler equipped with a coiled stainless steel sampling tube for gases. Analysis was performed by connecting the Aircore sampler into a PTR-MS instrument via PTFE tubing. Method development[25,51] in general often requires an offline approach, since the use of calibrants is involved. Notø *et al.*[25] injected controlled amounts of atmospherically relevant calibrants into a PTR-MS inlet in the development of an on-line method which measures atmospheric constituents quantitatively in long-running measurements.

In addition to strictly on-line/offline measurements, cases in-between exist, where field samples are employed in an experimental set-up, but the instrumental analysis itself is conducted on-line-style.[15,38,46,47,53] This typically involves the collection of an aqueous or solid field sample and the consecutive measurement of any volatile emissions. Matrices such as soil[38], manure[46], sewage sludge[15,47] and plant litter[53] have been targeted in an atmospheric context so far. Here, sample headspace is sampled from an atmosphere mimicking chamber either by syringe[15,46,47,53] or pumped straight into an instrument via sample line. In the case of offline and the above-mentioned experimental measurements, sample preparation is often conducted in the form of

sample drying[38,43,48] or dilution, washing[38], filtering[13,38,43,64], or homogenization[38,53]. Sample transfers in such cases are thus unavoidable.

2.1.4 Special inlets

The existence of various inlets to PTR-MS instrumentation extends its analytical possibilities beyond the analysis of gas phase VOCs. The function of available inlets varies from evaporation of solid phase samples to on-line collection and subsequent evaporation of particulate samples. It is worth noting that the entire composition of sampled particles may not be decipherable by PTR-MS, but that the research focus here lies mostly on the semi-volatile sample components[11].

One method features the analysis of filter-collected NPs by TD-PTR-MS[13,43,48,57,64]. Here, the aim was to gather MS spectra characteristic to different plastic types and compose a library for prospective NP identification. Thermal desorption involves applying a temperature ramp on a sample holder such as a quartz[48,57] or PTFE[64] filter containing trapped analytes, in this case NPs. Applying hot temperatures to particulate samples causes the evaporation of volatile and semi-volatile compounds, which are then led into the PTR-MS inlet for subsequent ionization and mass analysis. Materić *et al.*[13] succeeded in analyzing complex environmental samples for a variety of NPs without sample pretreatment such as digestion of organic matter or density-based NP separation. The identification of NPs from a sample mixture was based on the idea of plastic and temperature specific characteristic ions.[13] In addition to particle analysis, TD inlets may be used when VOCs have been trapped onto adsorbents in a form of sample enrichment[8] or for the sake of offline analysis[46].

Inlets developed for the study of aerosol include the chemical analysis of aerosols, on-line (CHARON)[11,30],and the vaporization inlet for aerosols (VIA)[4,68], both of which operate by separating particles from gas phase molecules and thermal desorption of the isolated particles. The basic structure in these two inlets is quite similar, comprising a gas denuder and a TD unit. The CHARON in addition includes a particle collimating aerodynamic lens between the two components. The CHARON operates at a low pressure and a constant temperature <10 mbar,[11] whereas the VIA functions on a temperature gradient in atmospheric pressure[68]. Residence time of analytes in the VIA is characterized as remarkably short, which leaves particles less time to evaporate but also enables the rapid detection of species prone to degradation during the TD process.[68] While the VIA operates by an on-line-principle, the CHARON inlet provides

a somewhat longer residence time and concentrates particles by a factor of 15.[11] More information on the VIA is included in the experimental section (see 3.1.2.)

A somewhat more complex particle sampling system is the filter inlet for gases and aerosols (FIGAERO)[49], which differs from the inlets mentioned above in its manifold structure. The separate collection points of particles and gases enable simultaneous sampling of the two phases and minimize the risk of cross-contamination. In addition, the FIGAERO features a built-in mechanism for measuring particle-phase blanks. Similarly to the VIA[4], the FIGAERO's particle evaporation is based on a temperature gradient.[49,50] However, while the VIA operates on an on-line principle, particle analysis by the FIGAERO is performed by collecting particles onto a PTFE filter over a distinct period, followed by an evaporation period and MS analysis.[50]

2.2 Comparison to other set-ups and hyphenation

2.2.1 Proton-transfer-reaction as an ionization method

PTR ionization falls in the group of CIMS, as illustrated in Figure 1, and as such is much softer than electron impact ionization (EI). Conventionally, PTR-MS has been used to identify molecular ions from mass spectra, whereas identification by EI-MS is performed by spectral comparison with existing databases. However, it must be noted, that even PTR-MS is nowadays used in so-called fingerprinting methods based on matching mass spectra.[13,48,57]

When compared to other CIMS methods, PTR stands out by producing mass spectra relatively simple to interpret. Majority of peaks may be identified by the subtraction of one hydrogen from the m/z value, i.e. complex clusters or adducts are rarely formed and the possibility of multiple charges can be neglected. Electrospray on the other hand is known for the production of multiply charged ions, whereas ionization techniques such as NO_3^- and $C_4H_{12}N^+$ are known for the formation of clusters and adducts, sometimes following fragmentation[17]. Extractive electrospray (EESI) produces such a mixture of chemical reactions, that dopants such as NaI are used for the formation of Na^+ adducts to curb a wide range of other bond formations.[50]

A key difference between PTR and other CIMS methods is its selectivity to VOCs. While ESI typically targets macromolecules such as peptides,[6] adduct forming CIMS methods tend to detect molecules in the range of intermediate and low volatility. Figure 4 illustrates the detection range of these methods when applied to the study of SOA

formation and the unique mass range possessed by PTR-MS. Note that the x-axes depict the number of oxygen atoms in specific organic molecules and not the m/z of a mass spectrum.

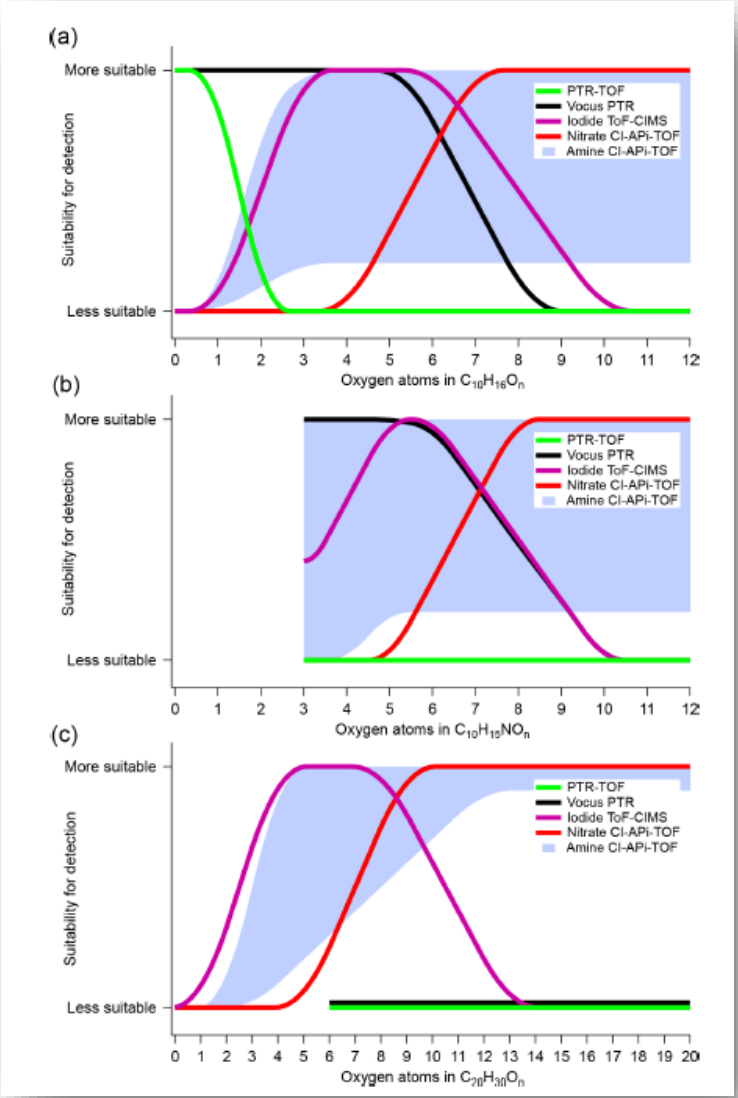

Figure 4. Selectivity of various chemical ionization techniques in a secondary organic aerosol study. (a) features α-Pinene oxidation products, (b) the organonitrate form of oxygenated α-pinene, and (c) the respective dimers of (a). Reprinted with permission from EGU publications (open access).[17]

As PTR was initially developed for the measurement of VOCs,[1] the structure of the instrumentation is prone to losing heavier molecules as wall losses[17]. It is thus plausible, that through further instrumental development the mass detection range could be extended. Until now however, the developmental focus has been on increasing sensitivity to the point of ultra-high[3].

2.2.2 Proton-transfer-reaction mass spectrometry - stand-alone or a complementing technique

As with all direct MS methods, the amount of information produced by PTR-MS is limited to masses detected, often in a semi-quantitative manner. This means that at most, the molecular formula of an analyte with several possible structures may be deduced. It is thus in a sense of validation that supporting techniques are selected to complement a PTR-MS analysis. Instrumental techniques can be combined in various ways: 1. Parallel measurements with instruments of similar selectivity to improve the overall accuracy of work; 2. Parallel measurements with instruments with different selectivity to increase the amount of information gained. The latter is seen especially in climate and aerosol research.[17,20,60,61]

It is typically gas chromatography mass spectrometry (GC-MS) and PTR-MS that go together for their complementing aspects in respect to each other.[10,27,42] Also GC-flame ionization detection (FID) has been used analogously.[52] While the often field-deployable PTR-MS produces vast amounts of high-sensitivity data via continuous sampling, identification of analytes may be challenging depending on the sampled air and the mass resolution of the instrument. GC-MS on the other hand is a laboratory-bound slow technique, used due to its high accuracy.[42] It enables the analysis of highly complex mixtures due to the pre-separation of analytes and the fact that retention indices can be used to verify identifications. Furthermore, the possible elucidation of structural isomers adds valuable information to atmospheric chemistry studies.[8,27] Sampling in GC-MS is somewhat more involved than in PTR-MS, often limited to trapping of sampled air into canisters[42] or onto solid phase adsorbents[8,52] before separation and mass analysis. Reasons for this include the need for sample transportation[42] or enrichment of analytes[8,52]. In the case of adsorbents, a further step of TD is added to the process.[8,52] It should be noted that in comparison to continuous on-line sampling, much information may be lost in the process of grab sampling followed by potential sample preprocessing. In addition, sample contamination is always an existing risk in manual sampling.

A curiosity in the field of PTR-MS is its hyphenation with GC. Coggon *et al.*[10,27] conducted several field studies where GC-PTR-TOF-MS was applied as a complementing technique to direct PTR-MS to aid in the analysis of structural isomers.

The use of GC also served in the study of unwanted collision induced fragmentation in PTR-MS and the caused bias to common MS peaks in atmospheric analysis.[10]

Some comparative studies between PTR-MS and other techniques have been conducted in the field of atmospheric analysis. As illustrated in the previous section, GC-MS as highly different but equally VOC-selective seems to be the most popular technique used to compare measurement results. Riva *et al.*[17] compared a variety of CIMS techniques from the perspective of highly oxygenated organic molecule (HOM) detection techniques with the result that while PTR-MS in general is limited to the detection of VOCs, the detection range of the Vocus extends to oxygenated volatile organic compounds (OVOCs). In terms of particle analysis, CHARON-PTR-MS has been compared to EESI-MS in aircraft sampling conditions.[50]

A similar VOC-selective form of direct MS, selective ion flow tube MS (SIFT-MS) provides a less costly method for the analysis of complex gas mixtures [69] While its detection limits have been observed considerably higher than those of PTR-MS, it is still considered a fitting trace gas analytical tool.[69,70] In fact, in cases of structural isomers the availability of several reagent ions (NO^+, O_2^+, H_3O^+) may produce more information on analyte composition.[69] Pagonis *et al.* composed a spectral library to aid in the interpretation of spectra obtained by PTR-MS and SIFT-MS and highlight the role of fragmentation patterns in the structural identification of product ions.[70]

While some alternative techniques exist, it is the view of the undersigned that PTR-MS has truly earned its place among the established analytical techniques in atmospheric trace gas analysis. Extending beyond VOC analysis through its capacity to be coupled with inlets, and methods reaching ever superior sensitivities, PTR-MS provides a worthy alternative to rivalling techniques. Due to the ionization in non-vacuum conditions, sampling options via various inlets are flexible and hyphenation with other techniques entirely possible.

2.3 Applications in environmental research

PTR-MS, while not available as a miniaturized field unit yet, is used widely in environmental research. Studies are conducted both in the field and in laboratories with experimental set-ups. Field measurements are typically conducted from measurement stations and mobile laboratories. Occasionally field samples are transported into laboratories, where after potential pretreatment, sample emissions or composition may be studied in controlled, climate-like conditions.

Information can be gained from not only atmospheric volatile organic compounds, but also from the interactions between atmospheric gases and particles, or between different environmental compartments. Even some particles themselves allow analysis by PTR-MS. Environmental research by PTR-MS is driven by goals to improve climate modelling, gaining emission data for better regulation, and to create more accurate policies to protect the environment.

2.3.1 Research on atmospheric volatile organic compounds

There are numerous approaches in the study of atmospheric VOCs. One heavily practiced type of approach is VOC source apportionment[36] i.e. the study atmospheric VOC levels following the categorization of emission sources and the individual impact of each source. Source apportionment is conducted in various ways, and little unison exists in this area of atmospheric research. Perhaps the most abundant type of VOC source apportionment is entirely untargeted, and classification follows generally that of biogenic/anthropogenic/primary/secondary VOCs.

An alternative way to categorize emissions is narrowing down the topic of interest. These types of studies often feature a background category, and classification of emissions outside that of the target class is superfluous. Coggon *et al.*[27] studied the impact of cooking emissions in a restaurant heavy tourist destination while conducting comparative measurements in a residential neighbourhood. Pan *et al.*[23] focused on oil and gas development and its connection to high ozone levels. An anthropogenic impact study was conducted by Li *et al.*[24] in the midst of a crowded tourist area. Mass spectra attributed to various dominant sources are depicted in Figure 5. Even more targeted studies have been performed by way of narrowing down the group of targeted VOCs.[14,36,52,65] Targeted groups of VOCs feature such as ozone precursors[36], haze[14] and oxygenated VOCs[65]. Volatile chemical products (VCPs) rise on several source apportionment papers, such as Li *et al.*'s, as a topic of interest.[24,62]

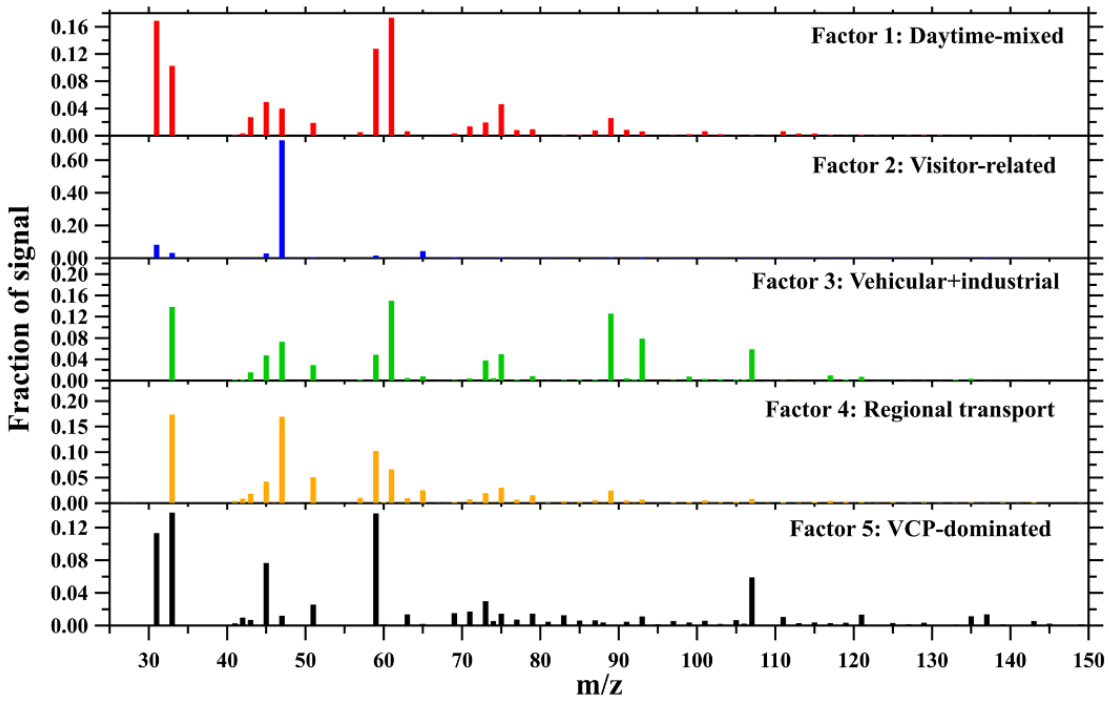

Figure 5. Urban mass spectra attributed to five sources of volatile organic compounds by positive matrix factorization. Image modified and reprinted with permission from EGU publications (open access).[24]

The number of classes ranges from 2[14] to 8[62] and is typically determined by statistical correlation analysis, positive matrix factorization (PMF) being the most common one. The frequently applied PMF is a mathematical method which can be applied in source apportionment to derive common emission source categories among groups of analytes.[21,39,40,52,59] Equation (eq. 3) describes the basic PMF principle. Here, x_{ij} is species j in sample i, g_{ik} the concentration contribution of factor k in sample i, f_{kj} the percentage of species j in factor k, e_{ij}=residue factor for species j in sample i, and p the number of assumed emission sources.

$$x_{ij} = \sum_{k=1}^{p} g_{ik} f_{kj} + e_{ij} \qquad \text{(eq. 3)}$$

A highly relevant part of PMF in source apportionment is determining the number of categories (described as p in equation (eq. 3)). Typically, the factorization is performed on several values of k and the results compared to select the most appropriate value.[18,21,36,51,52,59] At times, other data is included in this decision process.[39] Here, a certain level of subjectiveness exists, starting from the choice which values of k are

chosen into the preliminary analyses. As a deeper investigation of mathematical and statistical methods is beyond the scope of this review, more information and supporting formulae are accessible in the original article by Paatero and Tapper[71].

An alternative statistical approach to source apportionment is non-negative matrix factorization (NNMF)[62]. NNMF, unlike PMF, requires no assumption of source categories and iterates the factorization with different number of categories until arrival at ideal solution ((eq. 4), where $\underset{F}{\leftrightarrow}$ is the measured intensity matrix, $\underset{W}{\leftrightarrow}$ the species fingerprint, $\underset{H}{\leftrightarrow}$ the species temporal patterns, and $\underset{r}{\leftrightarrow}$ =the residual matrix, which should have a minimal value at the end).[62]

$$\underset{F}{\leftrightarrow} = \underset{W}{\leftrightarrow} \times \underset{H}{\leftrightarrow} + \underset{r}{\leftrightarrow} \qquad \text{(eq. 4)}$$

Due to the complexity of the atmospheric processes and chemistry, other analytical tools are often required in data analysis and interpretation. To gain understanding on the impact of travelling airmasses, backward trajectories of air are modelled in various ways[14,21,23,36,59], the hybrid single-particle lagrangian integrated trajectory model (HYSPLIT) [23,40,42] being perhaps the most well-known. A modelling tool combining air backward trajectory analysis with measured pollutant data is the potential source contribution function (PSCF).[21,40] In addition, the photochemical age of identified compounds is often of interest and thus calculated to aid source apportionment.[23,54,62,65] Borbon *et al.* describe the premise of the photochemical age parameterization method as four key assumptions: 1. all measured OVOCs are proportional in measured intensity to an inert tracer gas; 2. The main reactant in the removal of atmospheric OVOCs is the hydroxyl radical 3. If the ratio of two OVOCs, whose reaction rates with hydroxyl radicals vary, is known, then the photochemical age of these gases may be calculated; 4. OVOCs of biogenic origin are proportional to isoprene emissions.[65]

Pan *et al.* used the concentrations of selected alkanes and their nitrated analogues to determine the aging of analysed air via photochemical clocks.[23] Other, often relevant calculations feature OH reactivity[18,21] and ozone formation potential[18,21]. The source apportionment studies featuring classification and various analytical approaches encountered in this work are compiled in Table 2.

Table 2. Source apportionment of atmospheric compounds – a compilation of published results.

Setting	Selectivity	Source Apportionment	Further analysis	Emission Sources	Ref.
Urban Texas	15 VOCs related to ozone formation	PMF; Cluster analysis of backward trajectories	Temporal trends, diurnal variations; high ozone events	1. biogenic (19 %); 2. aged urban mixed sources (anthropogenic and combustion VOCs) (37 %); 3. acetone factor (44 %)	[36]
Nine cities in northwest China	18 VOCs related to haze formation	Various trajectory statistical models	Diurnal variations	1. anthropogenic pollution (40 %); 2. dust pollution (50 %)	[14]
Urban-industrial France	44 VOCs	PMF	Terpenoid industrial emission analysis	1. Background and industrial (18 %); 2. traffic and fuel storage (9 %); 3. petrochemical, metallurgy, and coal-fired industry (8 %); 4. C8–C9 aromatics from traffic and industrial-residential solvents (8 %); 5. metallurgical processes and diesel-LPG industry (11 %); 6. industrial chemical storage and food cooking processes (27.7 %); 7. Toluene solvent use (5 %) 8. natural gas use and gasoline evaporation and (potentially offshore oil and gas production from long distance) (13 %)	[52]
Urban Beirut	OVOCs	Photochemical age calculation, linear regression analysis	Seasonal and diurnal variations	1. anthropogenic; 2. background; 3. biogenic; 4. secondary; 5. Biomass burning	[65]
Las Vegas, Los Angeles, and Boulder	Cooking emissions	PMF	Diurnal variations	1. mobile source (30-40%); 5. local solvent source; 2. VCP-dominated factor (40-80 %); 3. cooking-dominated factor (10-30 %); 4. regional background + secondary oxidation processes	[27]
South-East China mountain site		PMF	Impact of weather	1. Biogenic primary (18 %); 5. aromatic -related (21 %); 2. isoprene oxidation (21 %); 6. regional industry (4 %); 3. monoterpene oxidation (15 %); 4. sesquiterpene oxidation (21 %)	[12]
Regional background site in Hong Kong		PMF, backward trajectory analysis		1. vehicles and industry (20.8 %); 5. secondary OVOCs 2 (6.7 %); 2. solvent usage (10.5 %); 6. biogenic (4.3 %); 3. primary OVOCs (13.1 %); 7. background + biomass burning (10.9 %); 4. secondary OVOCs 1 (33.6 %);	[18]
Barcelona urban background & Montseny rural background	11 VOCs quantified	PMF	Ozone formation potential, SOA formation potential	1. Anthropogenic I: traffic & industry; 2. Anthropogenic II: traffic & biomass burning; 3. Isoprene oxidation; 4. Monoterpenes; 5. Long-lifetime VOCs	[39]
Urban and rural China	Atmospheric formaldehyde	Photochemical age-based parameterization method	Tempo-spatial variation, ozone formation potential	1. Primary anthropogenic; 2. Secondary anthropogenic; 3. biogenic; 4. Biomass burning; 5. Background	[54]
Hong Kong		PMF, Backward trajectory clustering, potential source contribution function (PSCF)	Diurnal variations, OH reactivity and O3 formation potential	1. Biogenic; 2. Vehicle; 3. Solid fuel combustion; 4. secondary formation 5. mixed regional	[21]

Table 2 continues

Setting	Selectivity	Source Apportionment	Further analysis	Emission Sources	Ref.
Coastal industrial China		Conditional probability function analysis, PSCF, HYSPLIT, PMF	Seasonal variations	1. Secondary formation; 2. unknown acetonitrile source; 3. Biomass burning; 4. Biogenic; 5. paint solvent; 6. electronics industry	[40]
Urban Beijing		PMF; HYSPLIT	VOC connection to SOA formation	1. Vehicle (gasoline); 2. Vehicle (diesel); 3. Biogenic; 4. Solid fuel combustion; 5. OVOC 1; 6. OVOC 2	[59]
New Mexico National Park	O&G pollution	PMF; HYSPLIT	OH reactivity	1. longer-lived O&G.; 2. shorter-lived O&G; 3. process-specific O&G; 4. Longer-lived secondary; 5. shorter-lived secondary; 6. alkenes; 7. Background	[23]
Urban Georgia (US)		non-negative matrix factorization (NNMF); MEGAN	Seasonal variations	1. Biogenic isoprene; 2. Biogenic other terpenes; 3. Traffic fresh; 4. Traffic aged; 5. Cooking/ burning 6. VCPs dominated 7. Acetone-dominated; 8. Secondary	[62]
Crowded urban China		PMF	Diurnal variations	1. daytime mixed (biogenic and secondary) (21 %); 2. visitor-related (30 %); 3. vehicular-industrial (28 %); 4. regional transport (10 %); 5. VCPs (11 %)	[24]

[1] VCP= Volatile Chemical Produts
[2]O&G= Oil and Gas Development
[3]HYSPLIT= Hybrid single-particle lagrangian integrated trajectory model
[4]MEGAN= The Model of Emissions of Gases and Aerosols from Nature

Due to the various approaches within source apportionment regarding measurement location (urban/rural/industrial), selectivity, campaign length (short-term/long-term) and overall resulting categories, comparisons between studies are difficult to draw and reducing emissions by category to single average percentages is often not possible. All published average emission values are included in parentheses in Table 2.

A more targeted approach in atmospheric analysis is studying the impact of point sources, where only target analytes are considered. This approach revolves heavily around anthropogenic emissions ranging from routinely conducted human operations to accident scenarios. The scope of the study target varies from detailed phenomena to areal studies affected by pollution. Common point sources investigated by PTR-MS include oil and gas development (OGD)[44,56], industrial emissions[42,58], and waste management[31,32,15,52]. As traffic is infamously known for its emissions, including those of VOCs, studies targeted even further such as to the effect of vehicle cold start emissions[37] exist.

The effect of anthropogenic activities on air quality and human health directs research to areas with high concern of elevated pollution[35,42,44,56,58], often combined with a source apportionment approach.[40,52,59] These measurements are typically performed

from mobile laboratories[19,27,35,45,56,58], i.e. instruments housed in vans or larger vehicles. Oil and gas development sites have been studied for VOC pollution by methods such as tracer flux ratio methodology[56].West Virginia based tracer flux ratio measurements were conducted in a downwind location from the point of interest and included the controlled release of tracer gases such as N_2O and acetylene. Controlled methane emissions to augment any existing methane pollution were also used to improve the accuracy of the emission estimations. Estimation of the measured VOC emission rates was based on comparison of the deliberately released methane and tracer gas levels. Industrial point source analyses have been conducted in France (targeting industrial terpenes)[52], China[40,58], and Taiwan[42]. Wang *et al.*[58] developed a supplementary assessment system for the globally applied air quality index[72], which thus far has not included VOC pollution as a factor. Measurements by Wang *et al.* revealed extremely high periodic concentrations of VOCs assumed as industrial monomers, with atmospheric concentrations ranging from below 100 to over 3000 $\frac{\mu g}{m^3}$.[58]

Fractions of waste management have been investigated for climate effects through measurements of flue gas emitted via waste incineration[60,61] and VOC emissions from sewage sludge[15,61]. In addition, aerosol formation following the agricultural repurposing of sewage sludge has been studied by R. Ciuraru *et al.*[47]. An even more narrow focus was adopted by Wang *et al.*[38], who studied the volatility of biodegrable plastic degradation products in soil. Escape of volatiles through the incineration of garbage and sewage sludge in Japan has been studied by Fujitani *et al.*[60] through flue gas measurements under various dilution factors (DF). The corresponding emission factors, while lower than those sourced from traffic, can still be seen as significant due to the high annual combustion of waste.[60] The calculation of emission factors (EF), a most relevant concept in point source analysis as it describes the ratio of emission source and the actual pollution, is performed differently depending on measurement circumstances. Equation (eq. 5), where c_i is the concentration of target analyte, Q_{dry} the dry flow rate of flue gas and M_{MSW} the waste burning rate, describes emission factors defined with the help of flue gas dilution factors and the rate of waste combustion.[60]

$$EF_i = \frac{c_i \times DF \times Q_{dry}}{M_{MSW}} \qquad \text{(eq. 5)}$$

Post-incineration emissions of sewage sludge have been studied similarly on-site by the dilution approach[61]. Another approach to the study of point sources has been taken in analysing manure, soil, and sewage sludge emissions in controlled laboratory conditions[15,38,46,47]: these studies have been conducted by collecting field samples and placing them in environmental chambers which mimic atmospheric conditions. This simplified approach reduces the number of changing parameters and so base comprehension on the studied atmospheric impact in standard conditions can be gained.

Dominutti *et al.*[41] studied the effects of various anthropogenic sources on a long-term campaign: waste burning, road transportation and charcoal burning in two highly populated Vietnamese cities were monitored by PTR-MS. Perhaps unsurprisingly, traffic emissions were deemed to have the highest impact of the studied sources, corresponding to the research of Fujitani et al[60]. Here too, data was interpreted via *EF*s, while somewhat differently defined. Equation (eq. 6), derived by Keita *et al.*[73], describes the calculation of emission factors based on a carbon balancing method. Here, fc is the carbon mass fraction of the corresponding fuel. ΔVOC, ΔCO, and ΔCO_2 are the background subtracted mixing ratios of said analytes, and M_{VOC} the molar mass of the VOC in question.

$$EF_{VOC} = \frac{\frac{\Delta VOC}{\Delta CO + \Delta CO_2} \times M_{VOC}}{12} \times fc \times 10^3 \qquad \text{(eq. 6)}$$

Source apportionment and targeted point source analysis are tools to gain understanding over consistent VOC emissions and their atmospheric impact. PTR-MS can however be a useful technique in recording VOC emitting events such as accidents or wildfire scenarios. The importance of obtaining VOC data from these uncontrolled events lies in 1. the ability to perform accurate hazard assessment in field conditions[19] and 2. the detection of potential atmospheric phenomena such as ozone or aerosol formation. Vitucci *et al.*[19] investigated post-fire emissions from a plastic recycling plant and successfully generated a hazard assessment through non-targeted analysis by PTR-MS (see corresponding hazard assessment in Figure 6). Vitucci *et al.* quote the number of annual recycling plant fires being in the hundreds in United States alone, and with an increasing trend. Hence, such development of rapid analytical techniques in environmental risk assessment can be seen as highly relevant.

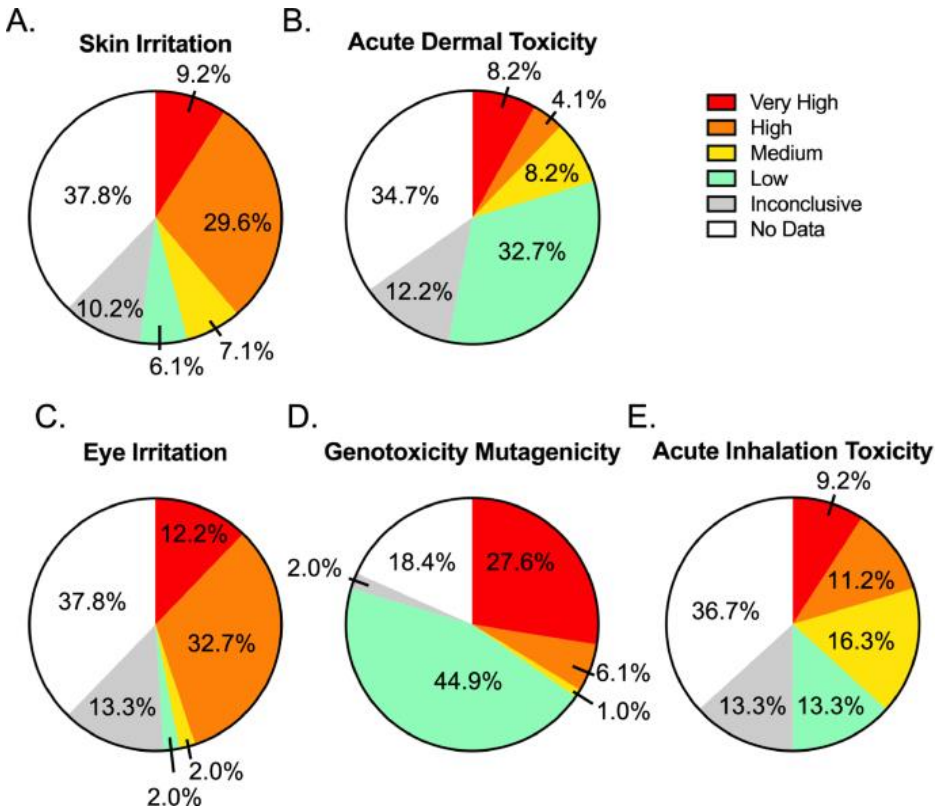

Figure 6. Section from a hazard assessment following a recycling plant fire. Data obtained by proton-transfer-reaction mass spectrometry. Image reprinted with the permission of Springer Nature (open access).[19]

Dead vegetation emissions during wildfire scenarios[53] have been studied in atmospheric chambers by temperature ramping. More generally, wildfire effect on VOC emissions has been recorded during the massive Australian wildfires of 2019-2020[63]. Smoke plumes containing long-lived VOCs, having survived a distance of several hundred kilometers, were measured in a field station. Despite the distance to the fire area, a total of 150 VOCs were identified and confirmed by investigation of correlation with known smoke tracers.[63]

2.3.2 Reactivity of atmospheric volatile organic compounds

In addition to the colourful research related directly to VOC concentrations, PTR-MS is also applied in the study of atmospheric chemistry. For instance, specific reactivities or VOC lifetimes can be studied to gain comprehension on the production of ozone and secondary pollutants. Certain VOCs known as ozone precursors are targeted for their ozone formation potential (OFP). While serving an important protective function in the stratosphere, tropospheric production of ozone is a known driver of aerosol

formation. The production of ozone and the subsequent climate events are in fact the underlying motivation for many atmospheric PTR-MS studies.[15,21,27,36,39,40,47]

Shrestra *et al.*[36] studied events of high ozone concentration: In addition to the travelling of airmasses and the presence of elevated background levels of O_3, elevated levels of so-called ozone precursors were observed prior to high ozone days. Zhou *et al.*[14] report acetaldehyde, trimethylbenzenes, propene, isoprene, and methanol, in decreasing order, totalling to 88 % of OFP_{VOCs}, as the most significant ozone precursors in North-West urban China. Other studies have identified formaldehyde[20], alkenes[20] and OVOCs[20,21] as most significant ozone precursors.

Carter *et al.*[74] summarize the relevant chemistry behind OFP to the following three reactions:

$$VOC + \cdot OH \rightarrow RO_2 + products \quad (2)$$

$$RO_2 + NO \rightarrow \rightarrow NO_2 + radicals \quad (3)$$

$$radicals \rightarrow \rightarrow \cdot OH + products \quad (4)$$

The significance of VOCs in the ozone formation process lies in the production of peroxy radicals (RO_2, reaction equation (2)), which in turn produce NO_2, the key species responsible for ozone formation (reaction equation (3)). Further radical reactions return hydroxyl radicals into the atmosphere (reaction equation (4)), promoting in turn additional peroxy radical formation.

OFP has been observed to vary seasonally. Figure 7 summarizes the results of a comparative study gathering seasonal measurement data from a rural and an urban site.[39] In 't Veld *et al.*[39] calculated the seasonal ozone formation potential and secondary organic aerosol potential (SOAP) for both sites. As can be seen from the sector diagrams, a distinct difference between the OFP and the respective SOAP is that certain compounds tend to dominate in SOAP, mainly toluene and C_8 aromatics in the city and rural winter. Rural summertime SOAP on the other hand is driven by monoterpene emissions,[39] which is rational since monoterpenes are known to be emitted from vegetation[12]. Moreover, weather has been observed to affect VOC emissions similarly, cloudy weather indicating dominating anthropogenic emissions and sunny weather indicating biogenic emissions.[12]

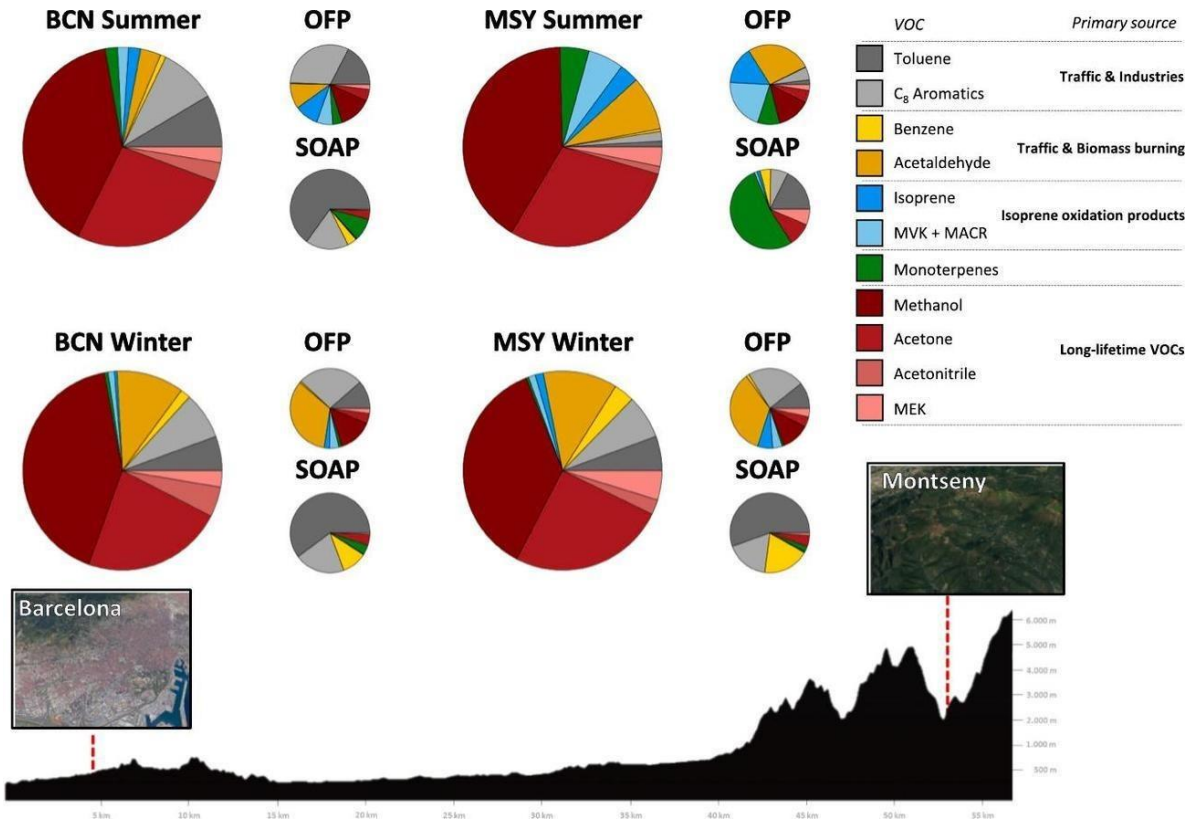

Figure 7. Tempo-spatial comparison of volatile organic compound concentrations and linked ozone formation potential (OFP) and secondary organic aerosol formation potential (SOAP); BCN= Barcelona urban area; MACR= methacrolein; MSY= Montseny rural area MVK= methyl vinyl ketone with Reprinted permission from Elsevier Ltd. (open access).[39]

Various approaches exist to obtaining VOC related OFPs. One such approach features the MIR method (see equation (eq. 7)),[39,54] in which MIR_i is the maximum incremental reactivity of species i obtained from literature[74].

$$OFP = [VOC]_i \times MIR_i \qquad \text{(eq. 7)}$$

SOAP [14,39] has been calculated based on experimental data alone. Zhou *et al.* reference (eq. 8) which considers the yield of SOA corresponding to each VOC in question (SOA_{yield/VOC_i}).

$$SOAP_i = [VOC]_i \times SOA_{yield/VOC_i} \qquad \text{(eq. 8)}$$

An alternative method for calculating OFP, independent of MIR values, is via the calculated hydroxyl reactivity R_{OH}. with (eq. 9), where n is the molar number of

conversions of NO to NO_2 in the VOC oxidation process and $[\cdot OH]$ the hydroxyl concentration[14].

$$OFP_{OH} = R_{OH} \times [\cdot OH] \times n \quad \text{(eq. 9)}$$

The relevant hydroxyl ($\cdot OH$) reactivity[14,21,23] noted as R_{OH} can be calculated as the sum of reactivities between hydroxyl radical and each detected VOC (eq. 10). Here, k_{VOC_i+OH} is the first order rate coefficient for the reaction between VOC_i and OH.

$$R_{OH} = \sum k_{VOC_i+OH} \times [VOC_i] \quad \text{(eq. 10)}$$

2.3.3 Aerosol research

Aerosol research is typically conducted with techniques with a detection range suited for particles or at least highly oxygenated compounds. PTR-MS can however be a useful approach, especially when considering the atmospheric chemistry proceeding aerosol formation. VOCs are related to SOA through oxidation reactions in which the former produces the latter. The motivation in this line of research lies in the climate and health effects of atmospheric particles. The potential climate effects of the studied particles are two-fold. Firstly, particles affect the course of solar radiation through light scattering and absorption effects. Secondly, SOA are known to contribute to cloud formation. Increasing comprehension on our climate system plays a crucial role in the efforts to combat global warming. Aerosol particles, whether organic or anthropogenic, are known to possess adverse health effects in all shapes and sizes.

So far, biogenic particle analysis has been conducted with other techniques aimed at detecting HOMs or particles themselves. One heavily used instrument is the Aerodyne aerosol mass spectrometer, which uses electron impact as ionization mode. Other common methods feature the FIGAERO[49] inlet, typically coupled with I^--CIMS, and extractive electrospray (EESI) ToF-MS[50]. NO_3^--CIMS[4,68] as an ionization mode has gained relevance more recently through the development of the VIA. One disadvantage of this approach however is its limited mass range. As a result, any potential HOM fragmentation products, and the smallest mass HOMs may remain undetected. Introducing PTR-MS into the study of SOA increases the amount of information gained on SOA composition, since the detection range covers lower mass compounds beyond

the scope of NO_3^--CIMS. The role of PTR-MS is therefore to act as a complementing analytical technique in the study of particle composition.

The complexity of the chemistry occurring in atmospheric conditions can perhaps be summarized to: 1. the multitude of organic/inorganic compounds, ions, and radicals; 2. The presence of several phases; 3. The everchanging meteorological conditions. Therefore, it is logical that aerosol precursors and their chemistry are studied via model compounds in stripped down chamber conditions. The oxidation chemistry and climate impact of one such model compound, 2,4-hexadienedial, is depicted in a simplified manner in Figure 8. This study conducted by N. Brun *et al.*[33] included numerous reactions in both aqueous (cloud-like) and gas-phase conditions leading from its ring-opening formation to its final products still detectable by PTR-MS. The authors discovered photolysis and hydroxyl radicals as the major 2,4-hexadienedial sinks in wet daytime conditions.[33] The relevance of such compound specific research was emphasised by the discovery that the reactivity of the model compound varied from another bifunctional model compound (2-butenedial) used in previous studies[75].[33] Another compound specific example is the oxidation of skatole (C_9H_9N) in a chamber environment.[47] Skatole, used as a proxy to recycled organic waste, was found to boost new particle formation (NPF) when in the presence of SO_2.

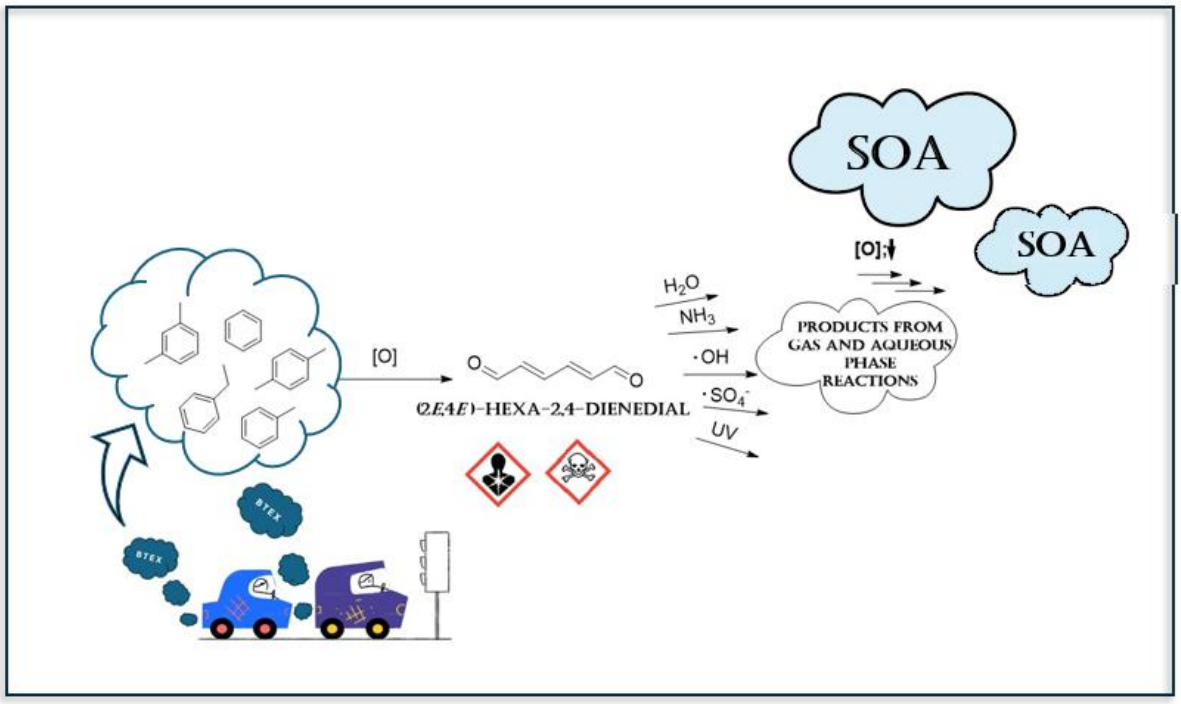

Figure 8. Illustration of the role of aromatic oxidation products such as 2,4-hexadienedial in atmospheric chemistry. BTEX refers to the group of benzene, toluene, ethylbenzene, and xylenes.

The atmospheric impact of a single VOC such as benzene may be obscure without consideration of the chain of potential processes involving said compound. The formation of a toxic intermediate, aerial transportation, further oxidation or the formation of hydrates for instance, and finally, the condensation into aerosol form are illustrated above (Figure 8).

Anthropogenic factors behind NPF have been identified via targeted studies. The incineration of sewage and garbage have been studied comprehensively: Fujitani *et al.*[60,61] studied gas-particle partitioning by analysing gas-phase organics with various dilution factors. The results were compared with soot particle aerosol mass spectrometer (SP-AMS) particle data to obtain volatility distributions. Peng *et al.*[11] on the other hand studied gas-particle phase partitioning of urban aerosol semi-volatile organic compounds (SVOCs) by PTR-TOF-MS with the aid of the CHARON inlet (see section2.1.4).

Chamber studies have also been conducted on the basis of an aerosol precursor emitting sample matrix such as manure[46] or sewage sludge[15], both of which have been observed to emit an extensive VOC/OVOC profile. Even the atmospheric effect of forest litter exposed to high temperatures (wildfire conditions) has been addressed via an experimental chamber study.[53] In the case of studying the emissions of an environmental sample, the emitting matrix is typically spread evenly along the bottom of the chamber and the chamber air continuously sampled in tightly controlled conditions.[15,46] Parameters to control and monitor include air flow rate[9,15,17,46,49,53], temperature[8,17,38,46,49,53], relative humidity[9,17,38,46,49,53], concentration/flow rate of reactive gases[8,9,17,49] such as O_3, NO_x, H_2O_2, and irradiation parameters[8,49]. Hydrocarbon traps are used to ensure that measured background stays minimal.[47,53] An important matter to consider despite the inert chamber materials is the occurrence of wall losses. These are typically estimated during calibration.[8,17,47]

Zhou *et al.*[14] conducted an extensive field study on the relationship between VOCs and particulate matter. SOA formation was observed to be driven in part by the oxidation of VOCs such as Benzene, C_{10} aromatics, and xylene in North-West cities of China. As a noteworthy observation of the study, the contribution of VOCs to particle composition was found to correlate inversely with particle size.[14] It should be noted that aerosol study campaigns such as this harness a larger set of instrumentation and that the role of PTR-MS among techniques remains in VOC detection. Zhao *et al.*[5,76]

have studied SOA composition in chamber conditions by other mass spectrometric means, and as a recent addition, PTR-TOF-MS measurements were conducted to increase understanding on the composition of SOA born from monoterpene oxidation.

2.3.4 Environmental micro and nano plastics

The research applications of PTR-MS also extend to the global challenge of MNP pollution. PTR-MS measurements have been performed both on MNPs and their degradation products. Materić *et al.*[13] developed a semi-quantitative fingerprinting methodology to analyse NPs from environmental samples by coupling a thermal desorption unit (TD) to a PTR-MS instrument. They have thus far sampled plastics from areas such as Siberian lakes[64], the Dutch Wadden sea[77], polar ice[67] and Alpine snow[13,43]. This approach broadens the application range of PTR-MS from gaseous VOCs to the analysis of particle matter collected from any environmental compartment. The estimation of NP concentrations is based on the known kinetics of proton-transfer-reactions and the ion count ratio between the reagent ion and the analyte, as presented in (eq. 11), where k is the analyte specific PTR rate coefficient, t the primary ion residence time in the drift tube, $[MH^+]$ the ion count of the protonated analyte, and $[H_3O^+]$ the reagent ion count. $\frac{m}{z}$.is the analyte mass-to-charge ratio. Despite the reoccurrence of this method[43,48,57,64,67,77], the use of PTR-MS in MNP research remains a curiosity among other detection methods.

$$[c] = \frac{1}{kt}\frac{[MH^+]}{[H_3O^+]} \times \frac{\sqrt{\left(\frac{m}{z}\right)_{H_3O^+}}}{\sqrt{\left(\frac{m}{z}\right)_{MH^+}}} \qquad \text{(eq. 11)}$$

By combining TD-PTR-MS with backward trajectory analysis, information on the aerial transportation of NPs have been gained and the ubiquitousness of MNP pollution established.[43,48,64] Urban measurements of MNPs have been conducted in Austria with a further analytical target of polyaromatic hydrocarbons (PAHs).[57] Kirchsteiger *et al.*[57] observed correlations between polypropylene and polyethylene and certain PAH concentrations, indicating that MNPs may act as vectors for these pollutants (see Figure 9).

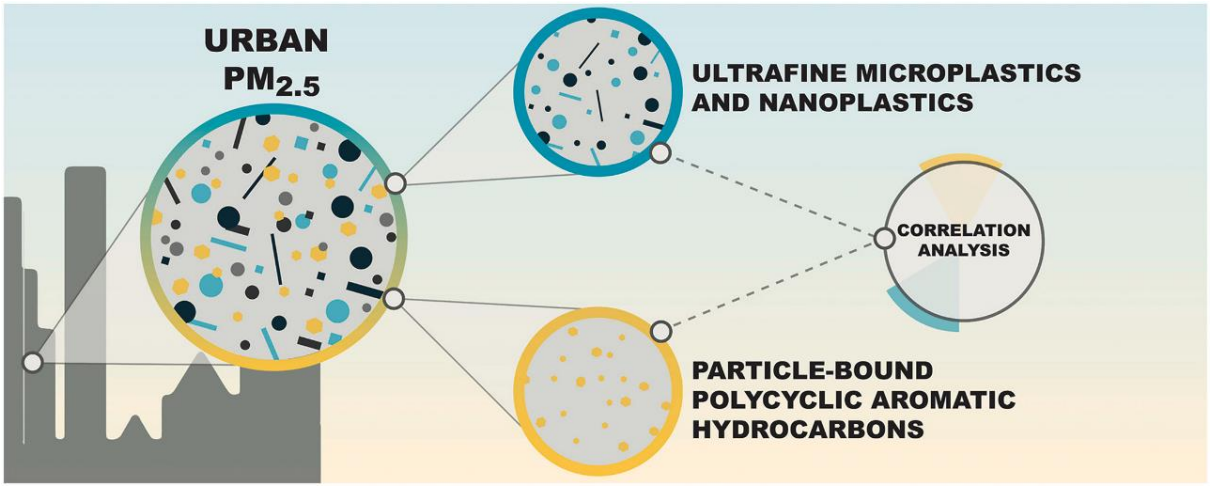

Figure 9. Connection between atmospheric nanoplastics and polycyclic aromatic hydrocarbons. Reprinted with permission from Elsevier Ltd. (open access).[57]

In addition to MNP analysis and the study of interactions with other pollutants, also the degradation products of MPs have been analysed by PTR-MS. Wang *et al.*[38] studied VOC emissions from soil-mixed biodegradable MPs in a chamber study. Each studied polymer type was observed to trigger a characteristic change in the soil CH_4 and CO_2 emissions as well as a VOC profile.[38]

2.4 Atmospheric reactions producing secondary organic aerosol

In the interest of explaining the significance of the research related to the experimental part of the work, an overview of atmospheric SOA formation is presented. Biogenic volatile organic compounds (BVOCs) are molecules emitted by living organisms. In the context of atmospheric aerosol formation, monoterpenes emitted by plant life comprise a significant group of compounds, although their share of BVOCs is only approx. 15 %[78]. A VOC heavily present in the boreal region is α-pinene, a commonly used model compound for studying aerosol formation from BVOCs. In the presence of atmospheric oxidants, VOCs can undergo oxidation reactions leading to the formation of HOMs[79], significantly lower in volatility than VOCs.[80] This decrease in volatility in turn leads to condensation and the formation of SOA, the composition of which is the target of this study. The percentage of HOMs in SOA particles has been estimated as 10 – 20 % based on previous chamber studies[4].

Majority of the HOMs that contribute to NPF are born through oxidation by atmospheric ozone (O_3) or hydroxyl radicals (OH).[81] HOMs, recently newly defined by Bianchi *et al.*[79], include three key features to narrow down this class of compounds:

1. HOMs are products of one or several autoxidation reactions with peroxyradicals.
2. Formation occurs in gas-phase and atmospheric conditions.
3. Minimum number of oxygen atoms per molecule is 6.

HOMs are detected both as monomers and dimers by NO_3-CIMS.[80] As the oxygen count is remarkably high in these molecules, their formation requires multiple successive reactions. One reaction sequence postulated by Ehn *et al.*[80] involves VOC ozonolysis followed by multiple H-shift reactions and the addition of O_2 (see Figure 10).. This means that oxidation of a volatile organic compound can advance as long as its structure allows, resulting in highly oxygenated organic molecules which then condense into particle from.

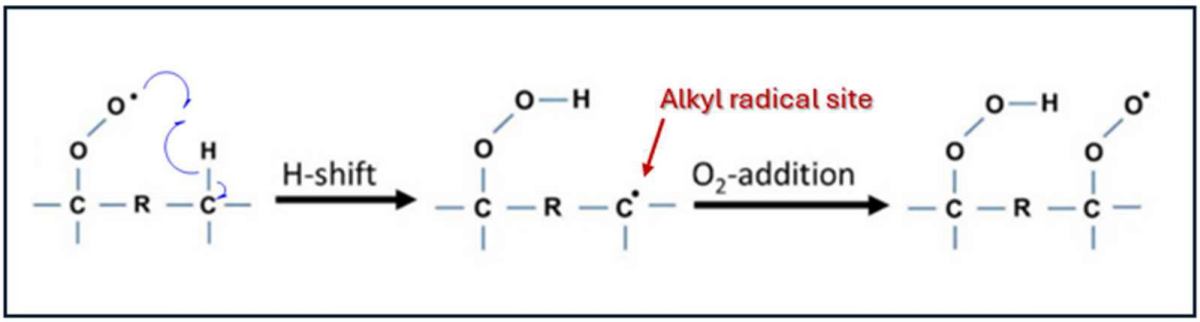

Figure 10. Illustration of an oxidation sequence via alkyl radicals formed by hydrogen shift reactions. Figure adapted and reproduced with permission from Springer Nature.[80]

Analysis by direct mass spectrometry can only go so far as identification of molecular formulas. As a result, there remains a gap in the understanding of specific reaction mechanisms in HOM formation.[79] The complexity of the chemistry behind SOA formation must be stressed, as the study of even one VOC oxidation process produces hundreds of gas phase compounds, some of which less volatile and easily condensed. Another knowledge gap remains through the selectivity of the detection methods. By coupling both a HOM-selective CIMS and a VOC-selective PTR-MS instrument parallel to the sample line, a more comprehensive picture may be gained on the structure of secondary organic aerosols.

3 Experimental

The topic of the experimental project was to test the applicability of the recently developed VIA inlet to SOA measurements by Vocus, a high-resolution PTR-TOF-MS. This inlet had been used in previous experiments measuring particle-phase composition by other CIMS instrumentation.[4,68] While the compounds expected to be found in the particles produced by monoterpene ozonolysis were mainly beyond the detection range of the Vocus, the scientific aim was to detect fragments of compounds once condensed into particle form.

3.1 Instrumentation

Instrumentation and equipment relevant in this experimental report feature the atmospheric conditions modelling COALA-Chamber, vaporization inlet for aerosols and the Vocus Mass Spectrometer. A schematic of the used instrumental set-up is presented in Figure 11. In the following sections, the basic operating principles of the Vocus and VIA will be described.

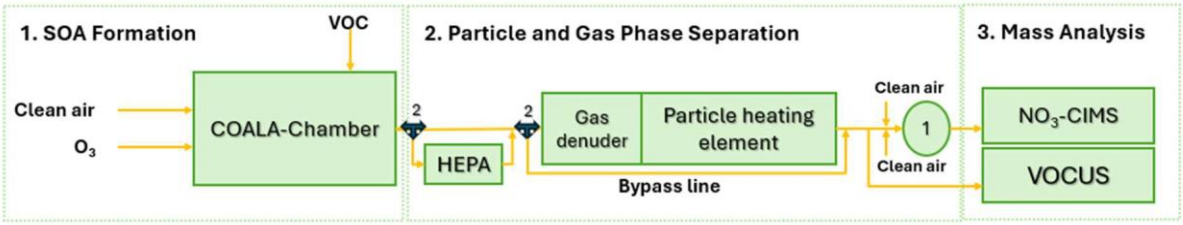

Figure 11. Illustration of the instrumental set-up used in the measurements. [1]Sheath flow unit ensures a laminar flow into the NO3-CIMS.[2]Valves for the use of various sampling lines enable chamber and VIA measurements and their respective background measurements.

3.1.1 Vocus

Proton-transfer-reaction time-of-flight mass spectrometry (PTR-TOF-MS) is an instrumental approach in which a wide range of detection and high-resolution meet. The instrument used in the experimental section of this work is a Vocus 2R by TOFWERK, originally evaluated and published by Krechmer *et al.*[7] in 2018. Proton-transfer-reaction as ionization mode is relatively gentle, so less fragmentation occurs in the ionization process than in electron impact ionization. As a result, molecular ion peaks can be identified with high likelihood, and analysis of sample mixtures is

possible. It is however worth noting, that evidence of occasional PTR-induced fragmentation does exist, namely in the case peroxidated[9] monoterpenes.

Vocus 2R features a focusing ion-molecule reactor (FIMR), in which ionization occurs. First, water vapor is ionized through an electric discharge of approximately 450 V. The reagent ions enter the FIMR angled such that collision with sample species is inevitable. The trajectory of the reagent ions and analytes is illustrated in Figure 12. Due to a quadrupole installed around the glass tube in which the analytes travel, the ions are further focused into a narrow beam before exiting through the sampling orifice. This results in ions entering the mass analyzer to a higher extent, thus improving sensitivity in detection. Ions arriving from the FIMR fly through a quadrupole serving as an ion guide and continue to a long v-TOF chamber for mass analysis. The resolution achieved by our instrument in the course of the experiment was approximately 9000.

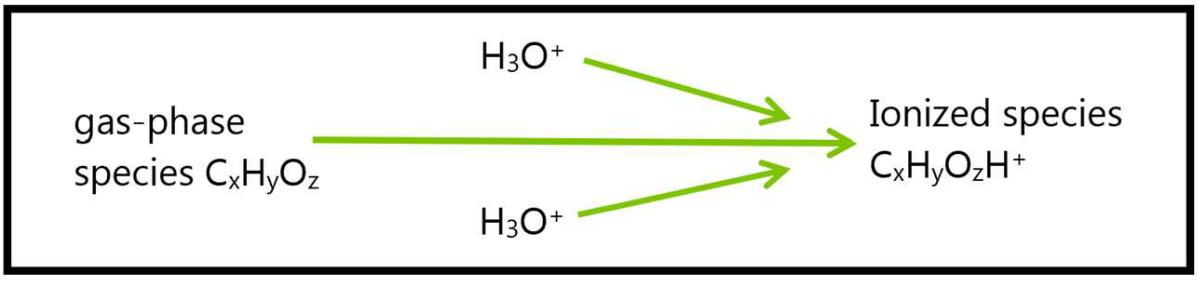

Figure 12. Ionization process in the focusing ion-molecule reactor.

The relevance of PTR-MS as detection mode in the study of SOA composition lies in its selectivity range. An extensive comparative study was performed with several CIMS techniques by Riva *et al.*[17] concerning the ozonolysis of α-pinene. NO3--CIMS and iodide-CIMS were found to be suitable mainly for the detection of HOMs, I—CIMS being able to detect only the less oxygenated, semi-volatile HOMs. In addition to SVOCs, even some volatile species such as acetic acid and formic acid can be detected due to clustering with the heavy reagent ion[82]. With PTR-MS on the other hand, nearly the entire class of volatile and semi-volatile of compounds can be detected, the Vocus having more detection overlap with I–CIMS than a conventional PTR-TOF.[17] As the detection of volatile species is a piece of a puzzle missing in the determination of SOA particle composition, the development of a method to detect these elusive species may help in completing the picture.

3.1.2 Vaporization inlet for aerosols

The basic operating principle of the VIA is to separate the formed particles from reactor gases and induce particle evaporation by applying heat to the sample flow. The VIA is composed of a gas denuder and a heated vaporization tube. The honeycomb structure activated carbon gas denuder filters out organic gases while particles are transmitted through to the vaporization tube. The tube itself is 40 cm in length and composed of Sulfinert® coated stainless steel,[76] rendering the inner surface highly inert. The vaporization tube is enwrapped by a coiled heating wire and glass wool insulation.
The applied heat induces particle evaporation in the flowing sample. These evaporated compounds and fragments can then be detected by mass spectrometry. Since all VOCs have their own characteristic temperature of evaporation, a unique mass spectrum should ideally be produced at any given time point of the temperature ramp. Figure 13 is a free illustration of the data acquired during a VIA-Vocus measurement.

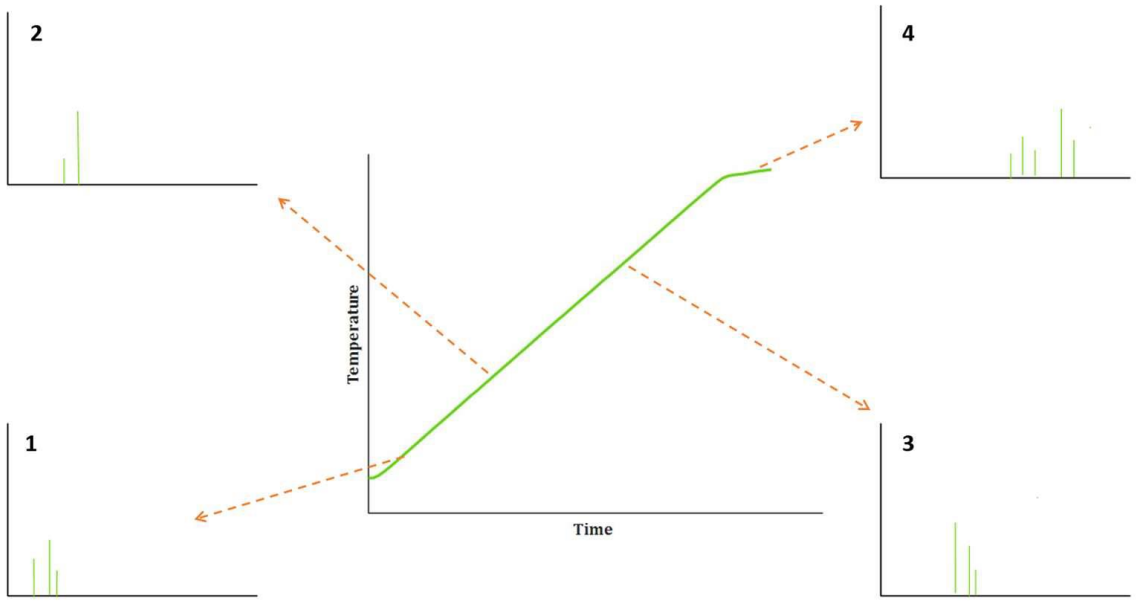

Figure 13. Visualization of the complexity of the VIA-Vocus measurement. Graphs 1 to 4 refer to mass spectra produced at different time points of an experiment. A unique spectrum should form at any given point during the measurement. Whether lighter species remain detectable in higher temperatures is debatable.

The gas removal efficiency and particle transmission of the VIA were evaluated in a recent paper by Zhao *et al.*[68] The gas removal efficiency was determined by measuring a certified VOC mixture by PTR-TOF, with and without the denuder, at various temperatures (25, 100, 200, and 300 °C). Out of the studied VOCs, 97.2-99.9% were successfully removed depending on the compound. In addition, the removal

efficiencies of the reagent gases (relevant also in the current study) were determined at approximately 80 % for 500-800 ppb α-pinene and above 95 % for 4 ppm O3. It should be noted that extremely high concentrations, non-comparable to atmospheric conditions, were used in these tests.

The particle transmission was studied by measuring atomizer generated ammonium sulfate particle counts by condensation particle counter (CPC). Determined transmission level for particles above 50 nm in size was >95 %.[68] Challenges affiliated with VOC and particle measurements include analyte losses in the measurement process. Despite the VIA being designed to minimize surface adsorption (silica modified inner surface layer), the risk for particle loss via surface collisions is to be considered. Sample loss via incomplete evaporation or collision into tube walls can be minimized by optimizing the sample flow and applied temperature. In addition, a risk of thermal decomposition exists if compounds are exposed to high temperatures for a prolonged period. Zhao *et al.*[83] observed distinct differences in particle phase HOM measurements by different methods (AMS vs VIA-NO3-CIMS). However, it is unclear whether these differences stem from VIA or instrumental differences.

3.2 Chemicals and gases

Two monoterpenes were used as starter VOCs in the SOA production, namely α-pinene (7785-26-4, >98 %, 136.24 g/mol, 858 g/l, Sigma-Aldrich Germany) and β-pinene (18172-67-3, >99 %, 136.24 g/mol, 872 g/l, Sigma-Aldrich Germany).

Gases used in the chamber experiment featured ultrapure air and ozone. Ozone was produced by an ozone generator from Dasibi Environmental Corp with built-in changes made in-house. Ozone level in the chamber was approximately 60 ppb. Nitrogen was used as a carrier gas in the VOC injection. VOCs measured during the experiment were detected by a ToFwerk Vocus PTR-TOF-MS on loan to the University of Helsinki by the courtesy of University of Eastern Finland.

3.3 Methods

The mixing ratios (see Table 3) of the injected VOCs were calculated from calibration equation (eq. 12). in which ρ_{VOC} is VOC density, $c_{injection}$ the concentration of injected VOC, M_{VOC} the molar mass, and v_V the total volumetric flow rate. This equation was

determined by calibrating the syringe pump and the respective syringe system. An example calculation is presented for the lowest α-pinene mixing ratio:

$$X = \frac{815.0578 \times \rho_{VOC} \times c_{injection}}{M_{VOC} \times v_V} \quad \text{(eq. 12)}$$

$$X_{apinene} = \frac{815.0578 \times 858 \frac{\text{g}}{\text{l}} \times 0.01062 \frac{\mu\text{l}}{\text{h}}}{136.24 \frac{\text{g}}{\text{mol}} \times 40 \text{ l/min}}$$

$$= 59.96 \ldots \text{ ppb} \approx 60 \text{ ppb}$$

Table 3.The calculation of mixing ratios for α-pinene and β-pinene.

α-pinene Injection Rate [µL/h]	Total Chamber Flow [L/min]	Mixing Ratio [ppb]
0.01062	35+5	60[1]
0.62	35+5	80
0.0158	35+5	90[1]
0.02124	35+5	120[1]
β-pienene Injection Rate [µL/h]	Total Chamber flow [L/min]	Mixing Ratio [ppm]
0.0105	35+5	60[1]
0.01755	35+5	100[1]
0.02633	35+5	150[1]
0.02633	35+5	200[1]

[1] *After the Vocus-only measurement, a different syringe was installed, and since then, a factor of 44 was applied in all respective calculations.*

3.3.1 Instrumental set-ups

Gas-phase measurements were conducted by analyzing chamber air led through a bypass line. A particle absorbing high efficiency particulate air (HEPA) filter between the atmospheric chamber and the MS inlet ensured a gas-only sample flow. Particle-phase measurements were conducted by letting chamber air flow through the honeycomb activated carbon gas denuder, which led to the trapping of gas phase organics. The particles flowed through the VIA tube and depending on the current temperature in the tube, compounds or their fragments evaporated and flowed into the Vocus inlet. The temperature ramping program was set to heat the tube in a controlled manner up to approximately 338 °C and then allowed for the tube to cool down in an unregulated manner. Majority of the measurements were conducted simultaneously

with the NO_3^-CIMS and the Vocus i.e. by the combination set-up. One particle phase measurement was conducted with a Vocus-only set-up.

The objective in setting up the sample flow was achieving a stable flow rate of approximately 3 LPM. Flow rates significantly higher than this were not considered a feasible option due to the possibility of increased leaching through the gas denuder. Flow rates considerably smaller on the other hand would have decreased the quality of the simultaneous NO_3^-CIMS measurements. The obtained flows through the VIA and the Vocus inlet are tabled below (Table 4). Complete repeatability in sample flow could not be attained due to uncertainties related to the complex set-up.

Table 4.Recorded flow rates in the sample line and the Vocus inlet during measurements.

Measurement	Total sample flow rate [L/min]	Vocus Inlet flow given as a percentage of total flow [%]	Vocus Inlet flow [L/min]
Chamber measurement	3.4	15	0.51
Combination Set-up	3.2	10	0.32
Vocus-only Set-up	2.95	37	1.09

3.4 Data processing

3.4.1 ToFware analysis

The raw MS data was processed by ToFware v3.3.0, a graphical user interface built on Igor Pro. ToFware is specifically designed for processing data produced by ToFwerk instruments such as the Vocus. The workflow is depicted below in Figure 14. Analysis was begun by mass calibration. Initial calibration ions were chosen based on the injected VOC and ions commonly present in PTR-MS measurements. After an initial attempt at mass calibration, peaks identified in the process were added as calibrants to improve accuracy. The accuracy of the calibration ion m/Q was assessed with the help of plots drawn by ToFware during mass calibration, see Figure 15a.

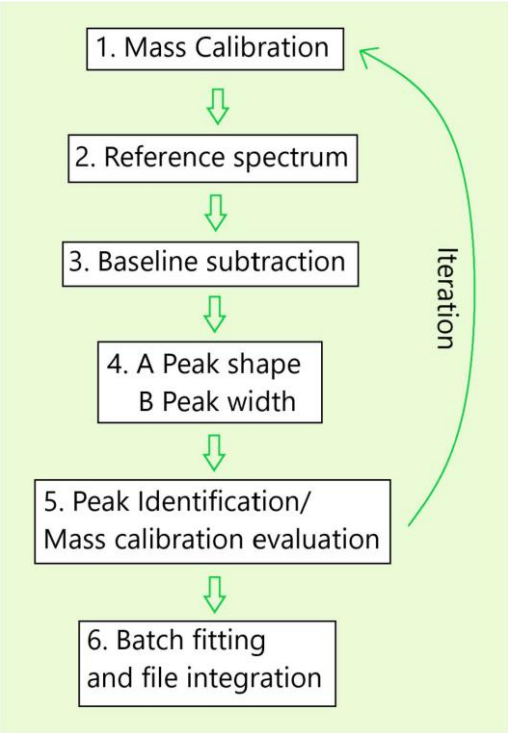

Figure 14. Workflow for processing of the raw mass spectrometry data on ToFware.

The reference spectrum was determined by choosing an interval from the measured timeseries where the offset in the fitted m/Q position was relatively stable and minimal (see Figure 15b). An average MS was then produced from the chosen datapoints. The baseline was then subtracted from the reference spectrum by adjusting experimental parameters where necessary. Baseline subtraction was saved to processed files.

Peak shape was adjusted with an interactive tool, with which unsuitable peaks were removed from a selection of overlayed peaks. The goal was to obtain a gaussian shape with minimal shouldering. The workings of the peak shape tool are illustrated in Figure 15c. The peak width was then refined by adjusting experimental parameters and removing outlier ions from a plot that depicts the full width of a peak at 50 % of maximum intensity, see Figure 15d.

These basic steps were followed by the examination of the now-processed reference spectrum and the first attempt at assigning peaks. This process was repeated until a satisfactory mass calibration was achieved and a comprehensive peak list was drafted. Finally, batch fitting and integration was performed for all relevant files.

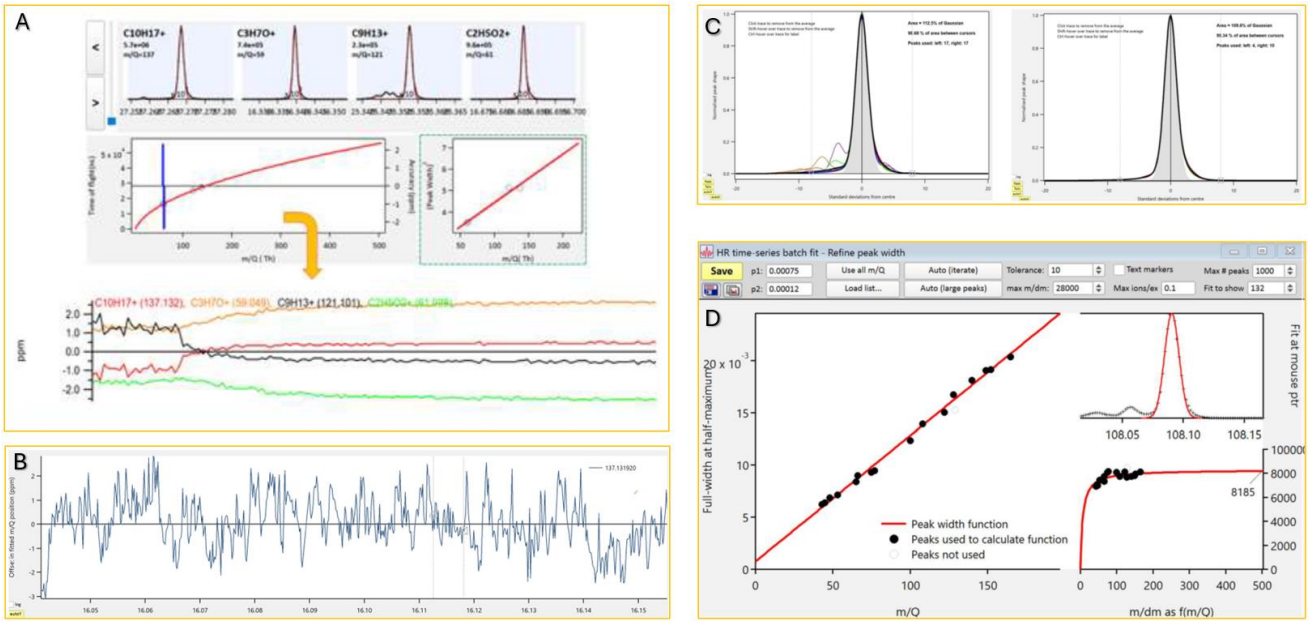

Figure 15. The work stages of raw data processing. A: Mass calibration. The accuracy of the file-specific measured time-of-flight is presented in the left-side plot and the corresponding peak-width function is shown in the right-side plot. The calibrant-specific accuracy during the entire calibrated period is presented in the timeseries below the plots. B: Selection of the reference spectrum. The y axis shows the mass accuracy of a chosen peak over measurement time (x-axis). An optimal measurement interval of low and preferably stable peak offset (i.e. highest accuracy) is chosen and averaged for a reference mass spectrum. C: Peak shape optimization. The black line is the average peak shape. The left side features the unmodified peak shape and the right the optimized peak shape. D: Peak width optimization. The left-hand plot represents the relationship of ion m/Q and its fullwidth at half-maximum. The right-hand plot illustrates the experimentally determined resolution of the instrument.

3.4.2 Further data analysis

Processed HR data was exported as csv files and imported to Matlab. As there was a 30 second lag between the recorded temperatures and the MS data, the temperature data from the VIA was converted to correspond to the timing of the recorded MS data. The MS data was then averaged to 30 second data to match the timing of the recorded temperature data. Only data for the 98 assigned peaks and the total ion concentration (TIC) was exported and analyzed further. A cursive analysis was performed for data from all VOC concentrations, after which the 90-ppb dataset was chosen as the primary focus in the combination set-up.

Thermograms were plotted for all assigned peaks and the data quality assessed first visually and then by further graphical analysis. In addition, repeatability and the effect of the concentration on the signal of the measurements were studied. Majority of the data analysis was performed on α-pinene, but a cursive analysis was also performed on the β-pinene data for sake of comparison. Results of the data analysis will be handled in the following section.

3.5 Results

3.5.1 General remarks

Mass spectra were successfully recorded in both gas phase measurements in chamber mode and particle phase measurements using the VIA. Overall, 98 ions were identified by molecular formula during the experiment. Because of the complexity of the gas phase chemistry and the lack of complementing instrumental techniques, the molecular structure of these peaks remains unknown. Of the 98 peaks, 94 ions were identified as organics, of which 18 being hydrocarbon species and 76 oxygenated species.

The quality of the plotted thermograms varied widely between different ions and measurements. Due to the uncontrolled cooling after peak temperature, mostly only data accumulated during the ramp-up period was used for plotting thermograms. Data from particle phase background measurements was considered poor and the background signal extremely high, so no conventional background subtraction was performed for the final data set. However, some useful information was observed from the behavior of the background during measurements.

Despite the fact that some MS data was successfully extracted with the VIA-Vocus set-up, the quality of the data proved to have significant room for improvement in measuring particle composition accurately. Therefore, it cannot be stressed enough, that any observations concerning particle composition in this experiment are speculative at best, and that the value of this work lies most in providing insight into the need in optimizing the VIA-Vocus set-up for future experiments.

3.6 Gas and particle comparison

The initial evaluation of the data was performed by observing signal behavior from plotted timeseries. According to expectation, VOC signals for gas phase measurements were high and stable, whereas wavelike behavior was observed during particle phase measurements. Figure 16a shows a gas phase measurement followed by a series of particle phase measurements. Next, mass spectra from both measurements were compared to ensure their fundamental difference (see Figure 16b). From observations of time series and mass spectra it became evident that while meeting our expectations to a certain extent, several discrepancies existed in the signal behaviour.

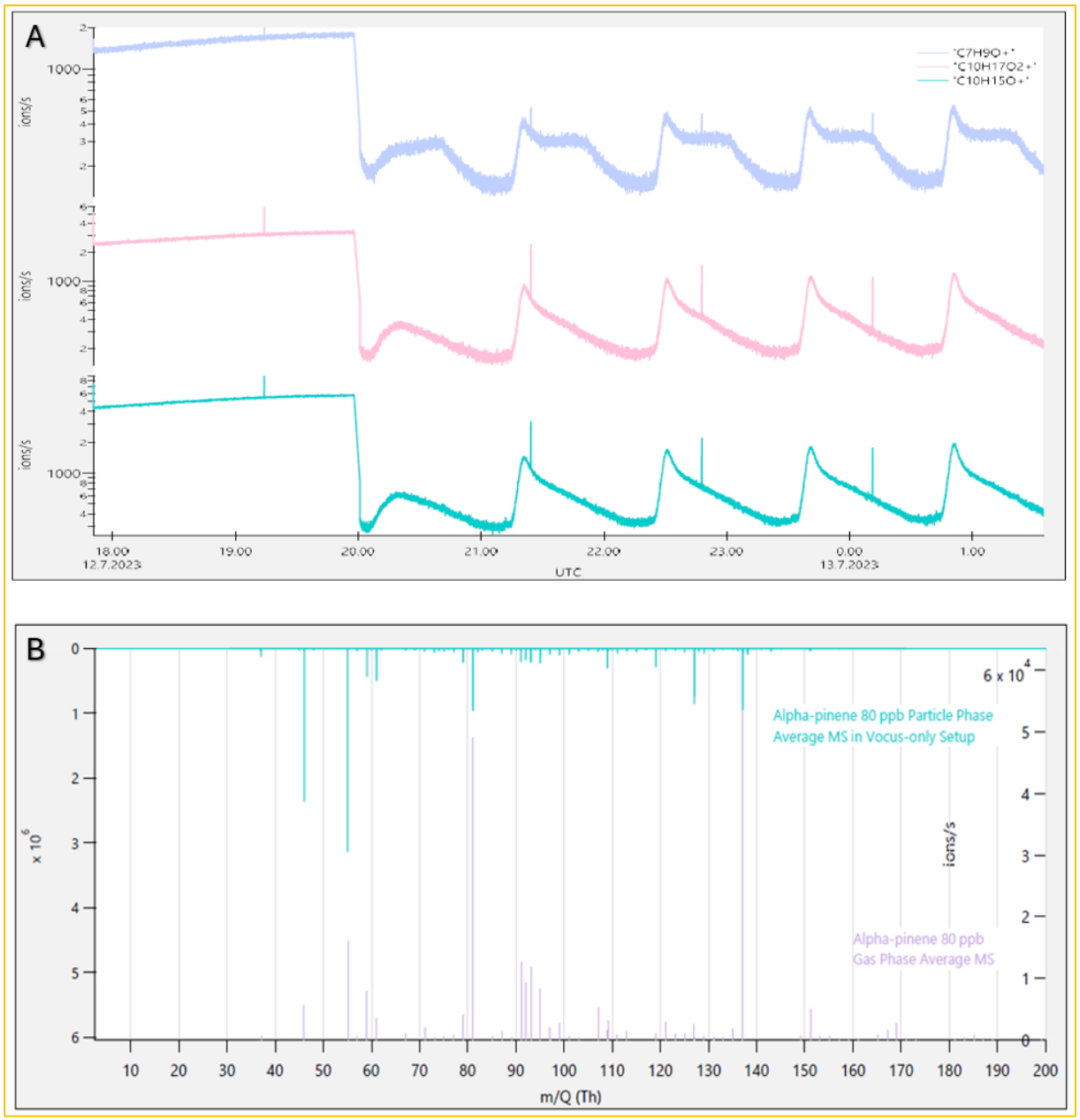

Figure 16. Measurement data for α-pinene and ozone born particles. A: Timeseries recorded for selected ions (c7h9o+, c10h17o2+ and c10h15o+) from a gas phase measurement followed by 5 consecutive particle phase measurements. Note, that the ion concentrations are presented in logarithmic scale to highlight the wavelike behavior of the signals. Periodic vertical peaks are false readings occurring during file change in data recording. B: Mass spectra measured in gas phase (lilac lines) and particle phase average (turquoise lines). Peak unit is ions/second.

Firstly, the particle phase mass spectra contained a multitude of peaks, many of which were detected throughout the temperature program. Especially questionable was the presence of hydrocarbons ranging from C_6H_x to $C_{10}H_x$, which in theory should not be detectable in particle phase studies. Alpha-pinene showed somewhat steady and high breakthrough levels throughout the particle phase measurements. This brings us to the second observed issue, namely the apparently high background signal in the particle

phase measurements. In the beginning of particle phase measurements, before heating in the VIA takes place, a zero signal should ideally be observed. A certain level of noise is indeed always expected, but as in the case of α-pinene (see Figure 17a), the background level was in the scale of 10^4 ions/s. As for ions that were considered more likely to be detectable in particle phase, it was the shape of the thermogram that raised concern. As can be observed from Figure 17b, ions were detected in relatively high concentrations in the beginning of the VIA measurements, which couldn't possibly derive from the particles. Issues with the background will be further discussed in the following sections.

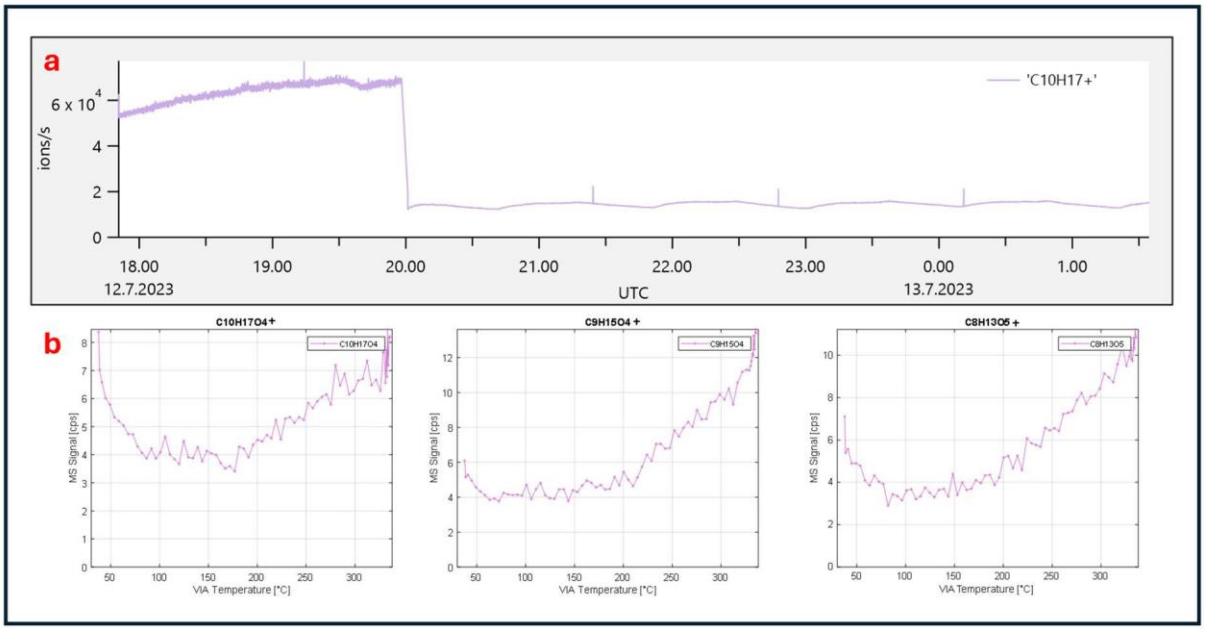

Figure 17. Background issues demonstrated by selected ion signals. The upper plot (a) shows alpha-pinene levels in chamber mode followed by consecutive VIA measurements. Thermograms in the lower half (b) present $C_{10}H_{17}O_4^+$, $C_9H_{15}O_4^+$ and $C_8H_{13}O_5^+$ concentrations from the Vocus-only measurement from left to right.

Issues with the chamber measurements were not detected, as these are performed routinely in the research group. A comparative figure of gas phase mass spectra for α-pinene and β-pinene is presented below (Figure 18) to establish that gas phase composition in the chamber varies between injected VOCs. As can be seen, the molecular composition in the chamber depends on the source VOC even in the case of structural isomers. Albeit similar, the ratio between peaks varies in these two spectra. In addition, the α-pinene MS shows the presence of oxidated species which are not present in the β-pinene spectrum despite the 10ppb difference in initial monoterpene

concentration. These peaks are circled and have been identified as $C_{10}H_{13}O_2^+$, $C_{10}H_{15}O_2^+$, $C_{10}H_{17}O_2^+$, $C_{10}H_{15}O_3^+$, and $C_{10}H_{17}O_3^+$. Minor peaks not visible in the MS below were also identified and can be read from the list of identified species in the supplements section (Attachment 1 Gas phase peak fitting data for α-pinene and β-pinene).

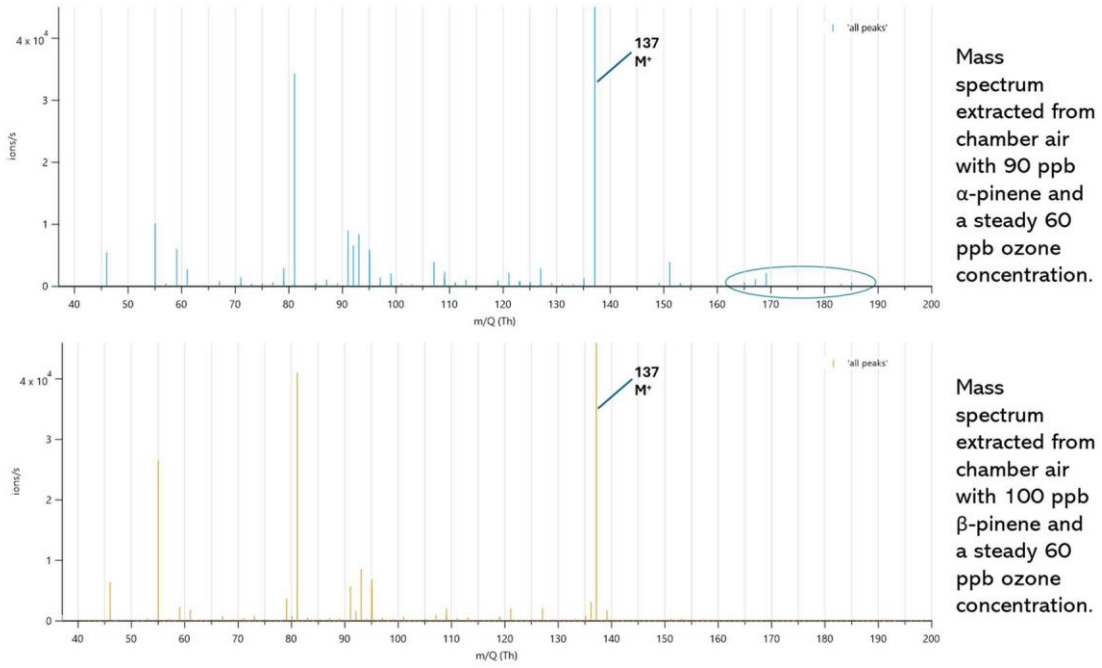

Figure 18. Comparison of mass spectra obtained from two monoterpene chamber oxidations. The circled area in the α-pinene Mass spectrum highlights the presence of peaks not present in the β-pinene mass spectrum.

Experiments in which the VIA inlet was used revealed the presence of multiple oxygenated compounds in particle phase. The length of detected carbon chains varied from $C_2H_xO_y$ to $C_{10}H_xO_y$ with the oxygen count reaching a maximum of 6. Figure 19 comprises the remaining results from the thermogram analysis, after screening out plots with unusable data.

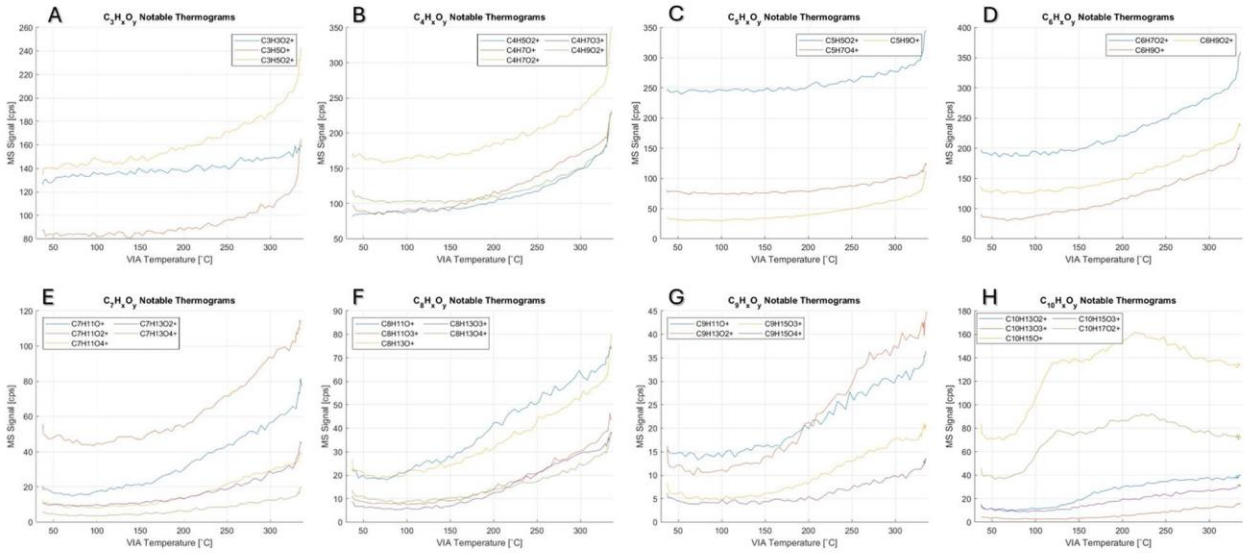

Figure 19. Plots A - H depict all notable thermograms obtained during the analysis of the Vocus-only dataset. Each graph contains thermograms with the same number of carbon atoms. Thermograms for all hydrocarbon species as well as thermograms with erratic background have been omitted here.

As can be observed from many of these plots (E - H), even here some instability in the background exists. This can be seen as a steep concentration fall in the beginning of the thermogram. In addition, attention should be drawn to the seemingly high levels of some species throughout the measurement (species with a starting level above 100 counts per second (cps) include $C_3H_5O_2^+$, $C_3H_3O_2^+$, $C_4H_7O_2^+$, $C_4H_9O_2^+$, $C_5H_5O_2^+$, $C_6H_7O_2^+$, and $C_6H_9O_2^+$). It is evident here that background levels in these cases are high and that the initial concentrations cannot be traced to particle phase. Problematic parts of the results will be discussed further in later sections.

The presence of smaller hydrocarbon species, such as the C3:s and C4:s, may be explained by a combination of breakthrough and thermal degradation. These lightweight organics should evaporate in lower temperatures, so it seems plausible that the beginning levels of the thermograms represent filter breakthrough, whereas the rising level towards the end of the thermogram would be due to thermal fragmentation of particle components. In this case wall contamination is the less likely cause, since the Vocus-only set-up was the first in the sequence of measurements. In contrast, for the bigger and more oxygenated species, the background concentration is low in the beginning and the evaporation i.e. rise in concentration occurs in the expected temperature range.

As for the C_{10} group, there exists a curious hump in two of the thermograms, analogous to the combination Vocus 90 ppb series. Observing this series further one can see that these two curves have the least amount of oxygen. Perhaps the humps are caused by oxidation reactions of breakthrough α-pinene. If this indeed is the case, any gas-phase chemistry occurring inside the VIA would complicate particle analysis even further. Unfortunately, no data of ozone concentrations passing through the VIA exists for this experiment, but the idea of O3 breaking through cannot be omitted with the existing knowledge of the compromised gas denuder performance and previous filter performance study.

3.6.1 Comparison of the instrumental set-ups

Particle phase measurements were conducted mainly in combinatory Vocus+ NO_3-CIMS set-ups. Several monoterpenes were included in a range of concentrations, but only α-pinene data will be discussed here. One short experiment was performed by Vocus-only set-up. Figure 20 shows a period of chamber phase measurement followed by VIA measurements with Vocus-only and a combination set-up. A visual comparison of a Vocus-only measurement and the new set-up shows more pronounced waves during the temperature programs and a lower background at the start of the particle phase measurement.

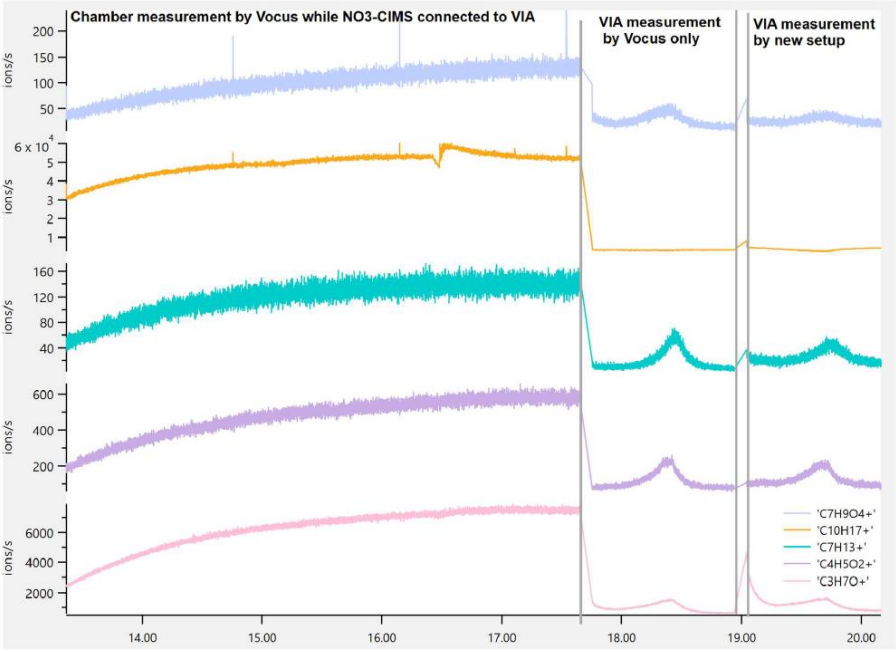

Figure 20. Selected ion signals recorded in chamber mode followed by Vocus-only particle phase measurement and finally a combination Vocus-NO3-CIMS Measurement. α-pinene was used at 80 ppb concentration in all three measurements.

Interestingly, the composition of the list of 20 most abundant ions (see Table 5) varied between the NO3-CIMS and Vocus-only set-up. Note that this list does not correlate with the thermogram findings. If anything, it highlights the fact that average MS data does not look accurate. Thermogram data of highlighted ions may be observed from attached data (Attachment 3. Highlighted species from Table 1; Vocus-only Set-up. and Attachment 4. Highlighted species from Table 1 ; combination set-up).

Table 5. Top 20 detected species based on net change in thermogram signals. cells highlighted in bluefeature ions with an increase that may be attributed to evaporation from particle phase or fragmentation of particle constituents. Species not highlighted should not be considered due to signal instability or cases of wall contamination masking potential trends.

Set-up	**Vocus-only**		**Vocus + NO3-CIMS**	
Ion Rank According to $(I_{Max} - I_{Min})$	Detected Ion	Net Change in Signal $I_{Max} - I_{Min}$ [cps]	Detected Ion	Net change in Signal $I_{Max} - I_{Min}$ [cps]
1	**C6H7O3+**	**455**	**C10H15O+**	**1921**
2	**C2H5O2+**	**346**	**C6H9+**	**1732**
3	**C6H5O2+**	**224**	**C8H11+**	**1573**
4	**C4H7O2+**	**192**	**C10H17O2+**	**1262**
5	**C6H7O2+**	**174**	**C7H7+**	**779**
6	**C4H7O+**	**147**	**C2H5O2+**	**568**
7	**C4H5O2+**	**147**	**C8H13+**	**498**
8	**C4H7O4+**	**146**	**C7H9O+**	**441**
9	**C4H5O3+**	**145**	**C7H9+**	**387**
10	**C2H7O3+**	**133**	**C6H7O+**	**382**
11	**C4H7O3+**	**129**	**C4H7O+**	**372**
12	**C6H9O+**	**128**	**C6H11O+**	**349**
13	**C6H9+**	**127**	**C6H9O+**	**338**
14	**C6H7O+**	**124**	**C4H5O2+**	**334**
15	**C6H9O2+**	**116**	**C7H11+**	**331**
16	**C5H7O2+**	**111**	**C7H8+**	**290**
17	**C3H5O2+**	**109**	**C6H7O3+**	**289**
18	**C5H5O2+**	**105**	**C2H7O3+**	**265**
19	**C10H15O+**	**92**	**C6H7O2+**	**253**
20	**C8H11+[1]**	**90**	**C5H7O2+**	**248**

[1] $C_8H_{11}^+$ as a hydrocarbon is not likely to derive from particle phase but has been highlighted as a species of interest due to its rising trend even when wall contamination is unlikely.

A significant difference between the measurements was in the shape of the thermograms. Many of the compounds detected by the Vocus+ NO3-CIMS set-up had strange bumps in their thermograms at a temperature of approximately 100 ° C (see Figure 21 A - C). In fact, the same bump was also clearly visible in the net signal consisting of hydrocarbon species (see Attachment 5. Background subtracted net signal of apparent hydrocarbon species measured with combination set-up.). These bumps were suspected to stem from possible wall condensates or fragmentation products from particles. Since the bumps were not present in thermograms plotted from the cool-down data they were considered to stem from wall contamination produced during the previous temperature program. The thermograms from the Vocus-only measurement however matched expectations more concerning thermogram shape (see Figure 21 D - F). The fact that no bumps were present in the Vocus-only measurement supports the theory that they originated from the VIA walls, since this was the first-time use of the VIA tube in this experiment.

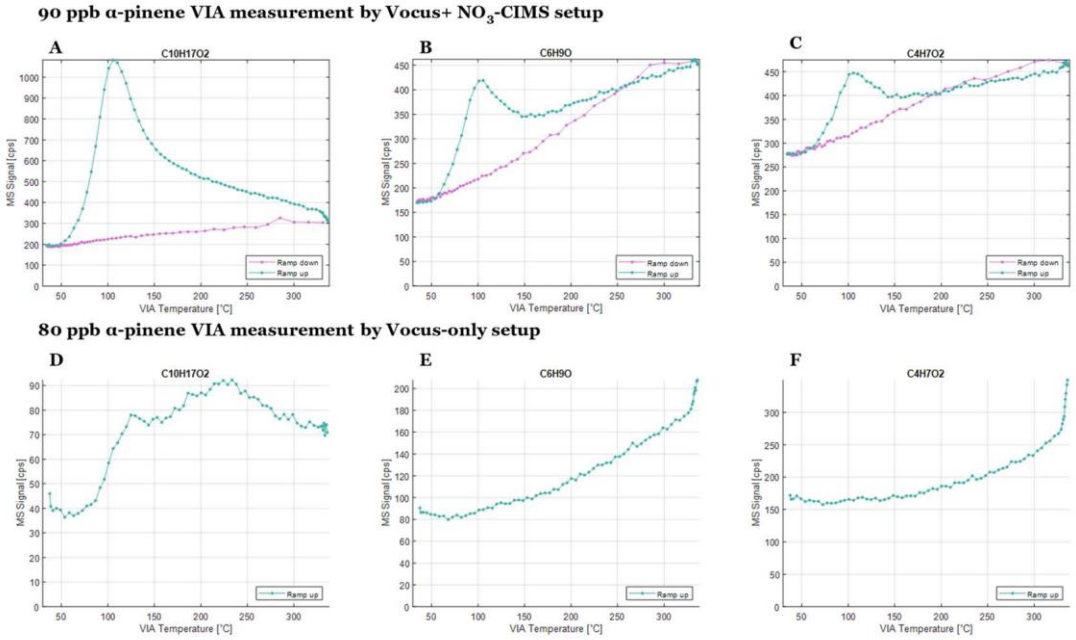

Figure 21. Selected thermograms highlighting the shape differences between set-ups. Figures A – C include thermograms from the combination set-up, the turquoise line representing the ramp-up period, and the purple line representing the cool-down period. Figures D – F include thermograms for the same species from the Vocus-only set-up. Figures A & D feature $C_{10}H_{17}O_2^+$, B & E $C_6H_9O^+$, and C & F $C_4H_7O_2^+$.

Another observation that could be made from comparing the ramp-up and ramp-down data was the converging of the plots in the minimum temperature. It would appear that

a somewhat constant level of breakthrough occurs for each detected species. Unfortunately, the behavior of the background is in some cases quite erratic, and the mentioned convergence disappears. When comparing ramp-up/ramp-down data between set-ups for $C_3H_7O^+$ and $C_3H_9O_2^+$, converging plots were observed in the combination set-up, while the Vocus-only set-up detected signals with a 100 % difference in the background between the beginning and the end of a temperature ramp (Attachment 6. Comparison of ramp-up and ramp-down data in both set-ups.).
For the most interesting species, those feasible to exist in particle phase and extremely low in signal, this meant such a high level of uncertainty in the signal-to-noise ratio that no definitive conclusions could be drawn. So, while the Vocus-only measurement may have worked better on average, neither set-up seems far form robust as is. What complicates the comparison of the two set-ups, is the lack of measurement sequences by the Vocus-only set-up. It remains unclear whether the lower background and stable signal is merely lack of contamination in the VIA walls or in fact a sign of a better instrumental set-up. Optimization of the set-up must be set as primary goal, before using the VIA-Vocus combination to study particle composition further.

3.6.2 Challenges in method development

Background behaviour Unreasonably high backgrounds were measured throughout the VIA experiment. Figure 22 illustrates the data acquisition process during a VIA experiment, but also highlights the issues observed in the particle phase data, namely the fact that too much similarity exists between these spectra. The issue with high background is not limited to the group of hydrocarbons but includes other lightweight molecules such as $C_2H_5O_2^+$ and $C_3H_7O^+$. The reason for the high background does likely not derive from just one culprit and will be further discussed in the following section on hydrocarbon presence.

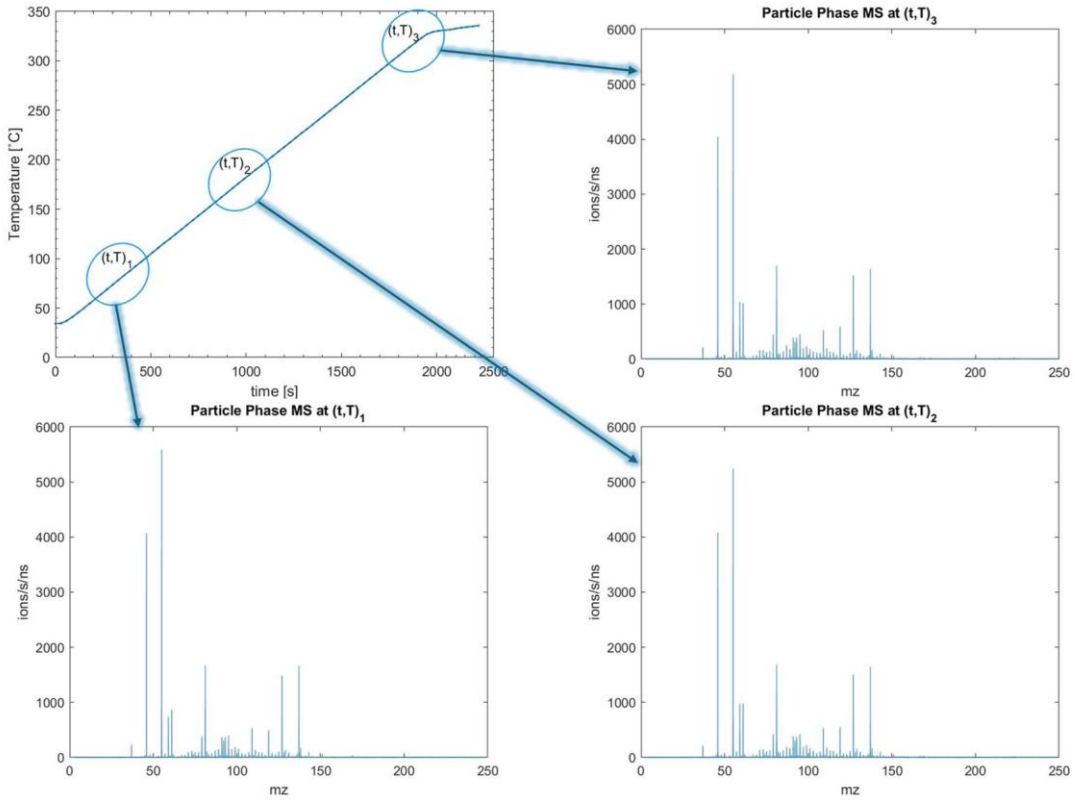

Figure 22. Mass spectra extracted from three different timepoints during the temperature program. Upper left plot shows time and temperature correlation, when ramping up the temperature.

When a series of particle phase measurements was conducted in the same set-up, repeatability plotting showed a steady increase in the background of consecutive measurements. This steady increase could possibly derive from a gradual increase in tube wall contamination and filter saturation, but it doesn't explain the high background in the beginning of the measurement. To maintain data comparability, blank measurements in-between each VIA measurement seem necessary. Filter saturation is another matter that should be considered more in future, and more frequent filter changes should be seen to.

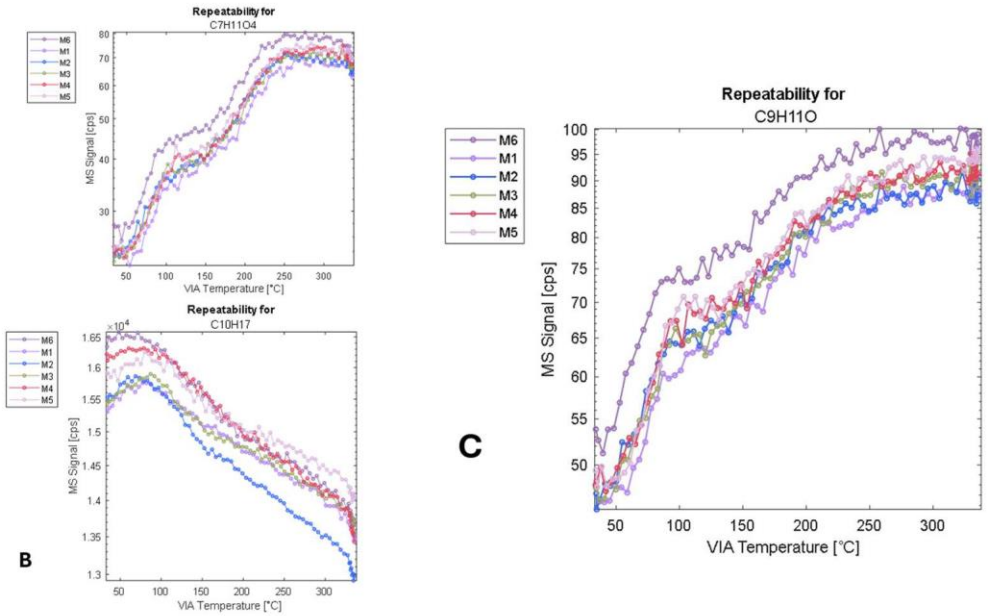

Figure 23. Repeatability plots for $C_7H_{11}O_4^+$ (A), α-pinene $C_{10}H_{17}^+$ (B) and $C_9H_{11}O$ (C). M1 through M6 represent measured data from a series of temperature ramps with no background measurements in-between, with the numbers signifying the order of measurements. Note the logarithmic scale in the y-axis.

Another interesting observation is the fall of α-pinene concentration (Figure 23B) as the tube is heated. Thermal decomposition of α-pinene has been reported to begin at 200 °C in an inert atmosphere, but in the presence of oxygen it is noted to be thermally instable.[84] The reactivity of the breakthrough α-pinene may thus contribute to the concentrations of other measured fragments. In fact, similar sharp concentration trends in the opposite direction exist for small species in the top end of the temperature range. Figure 24 outlines this sharp increase in the thermogram plots for $C_3H_5O^+$, $C_4H_9O_2^+$ and $C_7H_{13}^+$. It should be noted that the increasing trend in the thermograms may be amplified by the fact that the heating of the VIA was considerably slower when approaching maximum temperature.

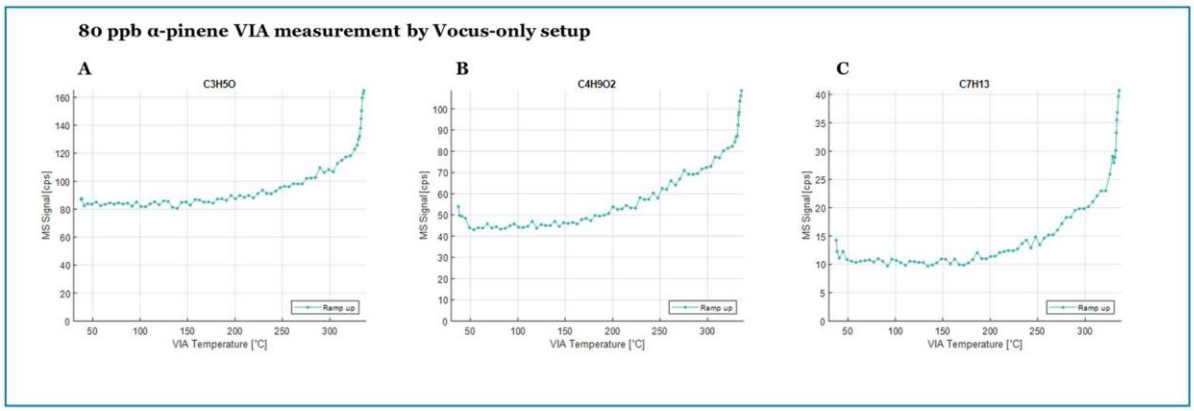

Figure 24. Selected thermograms of smaller detected particle phase species (A: $C_3H_5O^+$, B: $C_4H_9O_2^+$, and C: $C_7H_{13}^+$) by Vocus-only set-up.

Hydrocarbon presence

Hydrocarbon species were detected in all measurements including the Vocus-only set-up. Figure 26 shows a zoom-in from a Vocus-only particle phase MS, which includes a series of hydrocarbons. These are not believed to originate from particles, as only oxygenated species of organics have been shown to condense onto particle phase[80]. Performance of the gas denuders should be considered critically, since aged filters (2 years) were used in this experiment. Detection of hydrocarbons and the high backgrounds in general derive likely partly from filter breakthrough and partly from wall condensation/evaporation. Correspondingly, some thermograms depict a constant hydrocarbon presence, and others an increase with rising temperature (See Figure 25). What attracted attention, was the clear rising trend in the thermograms of some of the longer hydrocarbon species.

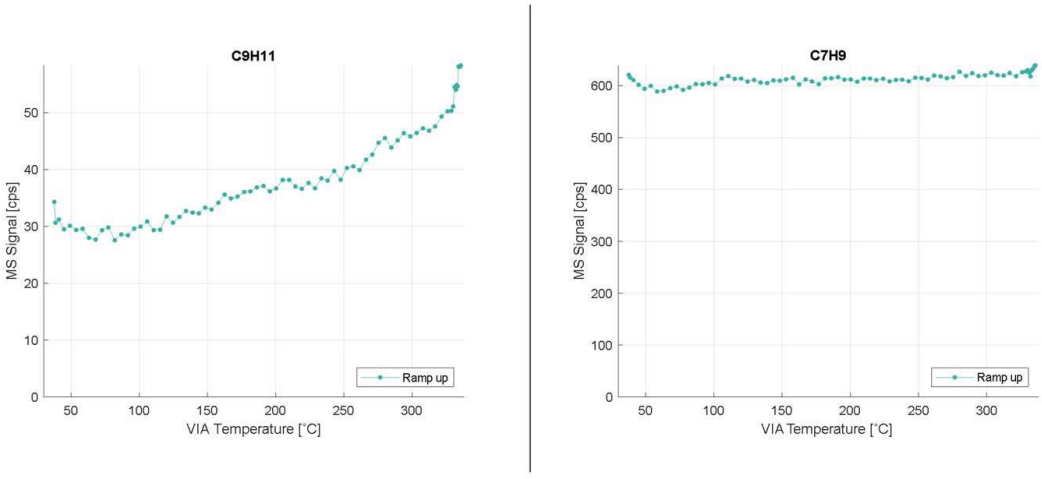

Figure 25. Thermograms for C9H11+ and C7H9+ measured with the Vocus-only set-up.

When comparing the 20 most abundant ions from the two set-ups, a considerably higher hydrocarbon presence was observed on average in the combined set-up, with 2/20 species being hydrocarbons in the Vocus-only set-up and 7/20 in the combined set-up (see Table 5).

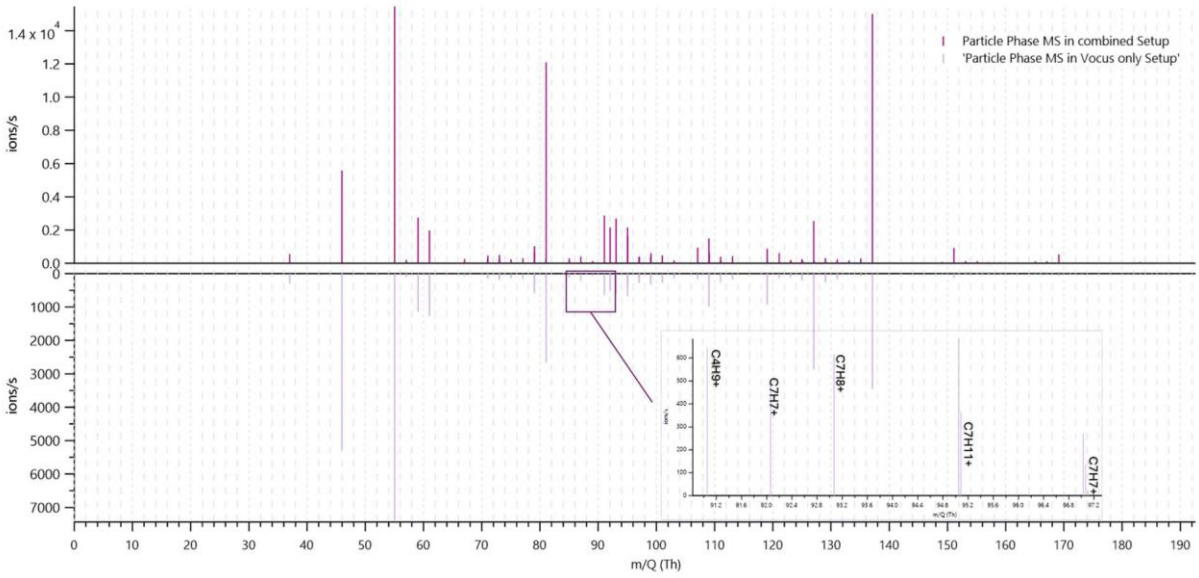

Figure 26. Particle phase mass spectral comparison between the combined Set-up (upper mass spectrum) and the Vocus-only set-up (lower mass spectrum). The relatively high peaks at low m/z for the T_{max} spectrum are not organics but a NO2+ peak at m/z 46 and a H7O3+ reagent ion peak at m/z 55. A zoom-in of the Vocus-only mass spectrum shows a strong hydrocarbon presence.

4 Concluding remarks

As demonstrated in the theoretical section of this thesis, PTR-MS possesses surprising capacity for research applications, far from limited to conventional VOC research such as source apportionment or point source analysis. From VOC emissions to aerosol precursors and oxygenated VOCs, PTR-MS can directly detect atmospheric analytes. Proceeding to indirect methods, typically comprising inlets coupled to the mass spectrometer, research on particles can be conducted. Chamber studies play a significant role in the study of various emission phenomena, usually performed by placing a solid sample into a climate-controlled chamber. The benefit of PTR-MS as a technique with the premise for on-line-measurements means that even difficult phenomena such as phase distribution can be approached via parameterization, i.e. by continuous sampling in different conditions until sufficient data is gathered.

Through its capacity for on-line trace level analysis of analyte mixtures, PTR-MS is an analytical approach most fit for use in atmospheric analysis. While the use of supporting techniques may occasionally be required, in terms of selectivity, sensitivity and time-resolution it is unrivalled. The number of publications related to PTR-MS has remained steady and the technique provides a versatile analytical detection method for VOC scientists, as well as those drawn towards creative analytical approaches.

A novel vaporization inlet for particle phase studies was tested in combination with a Vocus PTR-ToF-MS. Several set-ups and VOC concentrations were tested with varying results. The method was observed to work on a principal level, but the quality of the data was lacking. The best instrumental response was gained by a set-up in which only the Vocus was coupled with the VIA. This showed that the method has real potential when optimized to Vocus. More experimental data is however needed to confirm the role of the set-up in the success rate of the measurement, since only one particle phase measurement was performed in this way. Indeed, any future experiments designed for the optimization of a VIA-Vocus instrumental method should include numerous measurements in all set-ups to ensure data comparability.

Significant issues in the experiment were the extremely high background levels for most detected VOCs and the apparent contamination of the VIA walls. VOCs are often referred to as sticky, and this should not be underestimated in experiments involving much surface area and temperature fluctuation. It remains unclear, how much of the background was caused by filter saturation, and any future studies should address this question in context of the used VOC concentrations. In addition, background subtraction could not be performed in most cases due to an ever-fluctuating, erratic background. If reliable data is to be extracted from future measurements, a blank measurement between each use of the VIA should be performed.

Finally, the challenging nature of the topic should be stressed in light of the results. The accurate measurement of any event occurring in the study of particle composition is extremely difficult. A matter further complicating the data interpretation is the chemistry occurring within the VIA. In addition to gas phase species leaching through the gas denuder, also wall condensation and evaporation upon temperature changes must be considered, as well as thermal degradation of any thermolabile particle phase species.

For now, any results will remain speculative until eventually confirmed by experiments conducted with an optimized method. The most valuable observations were made from

thermogram data, and oxygenated organic species along with hydrocarbons were detected to the amount of 94 ions. As many as 6 oxygens were detected in some species. The concentration range of the detected organics varied widely, with the most likely particle originating species having the lowest concentrations. This highlights the importance of achieving background levels as low as possible.

With some optimizing, experiments by the VIA-Vocus set-up should provide complementing information to SOA formation gained by NO_3^--CIMS studies. This in turn may increase our comprehension of large-scale phenomena affecting our climate and well-being. The undersigned would like to encourage scientists in the field of new particle formation to tackle this challenge despite its difficulties.

References

1 A. Hansel, A. Jordan, R. Holzinger, P. Prazeller, W. Vogel and W. Lindinger, *Int. J. Mass Spectrom. Ion Process.*, 1995, **149–150**, 609–619.
2 M. Graus, M. Müller and A. Hansel, *J. Am. Soc. Mass Spectrom.*, 2010, **21**, 1037–1044.
3 T. Reinecke, M. Leiminger, A. Jordan, A. Wisthaler and M. Müller, *Anal. Chem.*, 2023, **95**, 11879–11884.
4 E. Häkkinen, J. Zhao, F. Graeffe, N. Fauré, J. E. Krechmer, D. Worsnop, H. Timonen, M. Ehn and J. Kangasluoma, *Atmospheric Meas. Tech.*, 2023, **16**, 1705–1721.
5 J. Zhao, E. Häkkinen, F. Graeffe, J. E. Krechmer, M. R. Canagaratna, D. R. Worsnop, J. Kangasluoma and M. Ehn, *Atmospheric Chem. Phys.*, 2023, **23**, 3707–3730.
6 J. H. Gross and P. Roepstorff, *Mass Spectrometry: A Textbook*, Springer, 2nd ed. 2011 edition., 2014.
7 J. Krechmer, F. Lopez-Hilfiker, A. Koss, M. Hutterli, C. Stoermer, B. Deming, J. Kimmel, C. Warneke, R. Holzinger, J. Jayne, D. Worsnop, K. Fuhrer, M. Gonin and J. de Gouw, *Anal. Chem.*, 2018, **90**, 12011–12018.
8 F. Löher, E. Borrás, A. Muñoz and A. C. Nölscher, *Atmospheric Meas. Tech.*, 2024, **17**, 4553–4579.
9 H. Li, T. G. Almeida, Y. Luo, J. Zhao, B. B. Palm, C. D. Daub, W. Huang, C. Mohr, J. E. Krechmer, T. Kurtén and M. Ehn, *Atmospheric Meas. Tech.*, 2022, **15**, 1811–1827.
10 M. M. Coggon, C. E. Stockwell, M. S. Claflin, E. Y. Pfannerstill, L. Xu, J. B. Gilman, J. Marcantonio, C. Cao, K. Bates, G. I. Gkatzelis, A. Lamplugh, E. F. Katz, C. Arata, E. C. Apel, R. S. Hornbrook, F. Piel, F. Majluf, D. R. Blake, A. Wisthaler, M. Canagaratna, B. M. Lerner, A. H. Goldstein, J. E. Mak and C. Warneke, *Atmospheric Meas. Tech.*, 2024, **17**, 801–825.
11 Y. Peng, H. Wang, Y. Gao, S. Jing, S. Zhu, D. Huang, P. Hao, S. Lou, T. Cheng, C. Huang and X. Zhang, *Atmospheric Meas. Tech.*, 2023, **16**, 15–28.
12 Y. Zhang, W. Xu, W. Zhou, Y. Li, Z. Zhang, A. Du, H. Qiao, Y. Kuang, L. Liu, Z. Zhang, X. He, X. Cheng, X. Pan, Q. Fu, Z. Wang, P. Ye, D. R. Worsnop and Y. Sun, *Sci. Total Environ.*, 2024, **919**, 170633.
13 D. Materić, A. Kasper-Giebl, D. Kau, M. Anten, M. Greilinger, E. Ludewig, E. van Sebille, T. Röckmann and R. Holzinger, *Environ. Sci. Technol.*, 2020, **54**, 2353–2359.
14 X. Zhou, Z. Li, T. Zhang, F. Wang, Y. Tao and X. Zhang, *Environ. Pollut.*, 2022, **300**, 118875.
15 K. M. Haider, F. Lafouge, Y. Carpentier, S. Houot, D. Petitprez, B. Loubet, C. Focsa and R. Ciuraru, *Sci. Total Environ.*, 2022, **838**, 155948.
16 K. M. Haider, C. Focsa, C. Decuq, B. Esnault, F. Lafouge, B. Loubet, D. Petitprez and R. Ciuraru, *J. Environ. Manage.*, 2024, **364**, 121453.
17 M. Riva, P. Rantala, J. E. Krechmer, O. Peräkylä, Y. Zhang, L. Heikkinen, O. Garmash, C. Yan, M. Kulmala, D. Worsnop and M. Ehn, *Atmospheric Meas. Tech.*, 2019, **12**, 2403–2421.
18 Q. Yuan, Z. Zhang, Y. Chen, L. Hui, M. Wang, M. Xia, Z. Zou, W. Wei, K. F. Ho, Z. Wang, S. Lai, Y. Zhang, T. Wang and S. Lee, *Sci. Total Environ.*, 2024, **908**, 168316.
19 E. C. M. Vitucci, O. Oladeji, A. A. Presto, C. L. Cannon and N. M. Johnson, *J. Expo. Sci. Environ. Epidemiol.*, 2024, 1–8.
20 D. A. Jaffe, M. Ninneman, L. Nguyen, H. Lee, L. Hu, D. Ketcherside, L. Jin, E. Cope, S. Lyman, C. Jones, T. O'Neil and M. L. Mansfield, *J. Air Waste Manag. Assoc.*, 2024, **74**, 163–180.
21 L. Hui, X. Feng, Q. Yuan, Y. Chen, Y. Xu, P. Zheng, S. Lee and Z. Wang, *Environ. Pollut.*, 2023, **335**, 122287.
22 G. Beel, B. Langford, N. Carslaw, D. Shaw and N. Cowan, *Sci. Total Environ.*, 2023, **881**, 163497.
23 D. Pan, I. B. Pollack, B. C. Sive, A. Marsavin, L. E. Naimie, K. B. Benedict, Y. Zhou, A. P. Sullivan, A. J. Prenni, E. J. Cope, J. F. Juncosa Calahorrano, E. V. Fischer, B. A. Schichtel and J. L. Collett Jr., *J. Air Waste Manag. Assoc.*, 2023, **73**, 914–929.

24 X.-B. Li, B. Yuan, S. Wang, C. Wang, J. Lan, Z. Liu, Y. Song, X. He, Y. Huangfu, C. Pei, P. Cheng, S. Yang, J. Qi, C. Wu, S. Huang, Y. You, M. Chang, H. Zheng, W. Yang, X. Wang and M. Shao, *Atmospheric Chem. Phys.*, 2022, **22**, 10567–10587.

25 H. Ø. Notø and R. Holzinger, *Int. J. Mass Spectrom.*, 2024, **504**, 117311.

26 S. Barber, R. S. Blake, I. R. White, P. S. Monks, F. Reich, S. Mullock and A. M. Ellis, *Anal. Chem.*, 2012, **84**, 5387–5391.

27 M. M. Coggon, C. E. Stockwell, L. Xu, J. Peischl, J. B. Gilman, A. Lamplugh, H. J. Bowman, K. Aikin, C. Harkins, Q. Zhu, R. H. Schwantes, J. He, M. Li, K. Seltzer, B. McDonald and C. Warneke, *Atmospheric Chem. Phys.*, 2024, **24**, 4289–4304.

28 R. Holzinger, O. Eppers, K. Adachi, H. Bozem, M. Hartmann, A. Herber, M. Koike, D. B. Millet, N. Moteki, S. Ohata, F. Stratmann and A. Yoshida, *Atmos. Environ.*, 2023, **309**, 119919.

29 M. C. Minguillón, N. Pérez, N. Marchand, A. Bertrand, B. Temime-Roussel, K. Agrios, S. Szidat, B. van Drooge, A. Sylvestre, A. Alastuey, C. Reche, A. Ripoll, E. Marco, J. O. Grimalt and X. Querol, *Faraday Discuss.*, 2016, **189**, 337–359.

30 D. Pagonis, P. Campuzano-Jost, H. Guo, D. A. Day, M. K. Schueneman, W. L. Brown, B. A. Nault, H. Stark, K. Siemens, A. Laskin, F. Piel, L. Tomsche, A. Wisthaler, M. M. Coggon, G. I. Gkatzelis, H. S. Halliday, J. E. Krechmer, R. H. Moore, D. S. Thomson, C. Warneke, E. B. Wiggins and J. L. Jimenez, *Atmospheric Meas. Tech.*, 2021, **14**, 1545–1559.

31 T. T. Hien, D. H. Huy, P. A. Dominutti, N. D. Thien Chi, J. R. Hopkins, M. Shaw, G. Forster, G. Mills, H. A. Le and D. Oram, *Atmos. Environ.*, 2022, **269**, 118872.

32 J. Jiang, X. Ding, P. Coelho, G. Wittbrod, A. J. Whelton, B. E. Boor and N. Jung, *Sci. Total Environ.*, 2024, **954**, 176056.

33 N. Brun, J. M. González-Sánchez, S. Ravier, B. Temime-Roussel, M. Brigante, G. Mailhot, J.-L. Clément and A. Monod, *Talanta*, 2024, **276**, 126176.

34 M. C. Minguillón, N. Pérez, N. Marchand, A. Bertrand, B. Temime-Roussel, K. Agrios, S. Szidat, B. Van Drooge, A. Sylvestre, A. Alastuey, C. Reche, A. Ripoll, E. Marco, J. O. Grimalt and X. Querol, *Faraday Discuss.*, 2016, **189**, 337–359.

35 O. Oladeji, M. Saitas, T. Mustapha, N. M. Johnson, W. A. Chiu, I. Rusyn, A. L. Robinson and A. A. Presto, *Environ. Sci. Technol. Lett.*, 2023, **10**, 680–685.

36 S. Shrestha, S. Yoon, M. H. Erickson, F. Guo, M. Mehra, A. A. T. Bui, B. C. Schulze, A. Kotsakis, C. Daube, S. C. Herndon, T. I. Yacovitch, S. Alvarez, J. H. Flynn, R. J. Griffin, G. P. Cobb, S. Usenko and R. J. Sheesley, *Sci. Total Environ.*, 2022, **838**, 155861.

37 Z. Zhang, H. Man, J. Zhao, Y. Jiang, M. Zeng, Z. Cai, C. Huang, W. Huang, H. Zhao, S. Jing, X. Shi, K. He and H. Liu, *J. Hazard. Mater.*, 2022, **435**, 128979.

38 Y. Wang, C. Zhao, A. Lu, D. Dong and W. Gong, *J. Hazard. Mater.*, 2024, **471**, 134294.

39 M. In 'T Veld, R. Seco, C. Reche, N. Pérez, A. Alastuey, M. Portillo-Estrada, I. A. Janssens, J. Peñuelas, M. Fernandez-Martinez, N. Marchand, B. Temime-Roussel, X. Querol and A. M. Yáñez-Serrano, *Sci. Total Environ.*, 2024, **906**, 167159.

40 M. Yang, F. Li, C. Huang, L. Tong, X. Dai and H. Xiao, *J. Environ. Sci.*, 2023, **127**, 483–494.

41 P. A. Dominutti, J. R. Hopkins, M. Shaw, G. P. Mills, H. A. Le, D. H. Huy, G. L. Forster, S. Keita, T. T. Hien and D. E. Oram, *Environ. Pollut.*, 2023, **318**, 120927.

42 W.-T. Liu, W.-C. Liao, S. M. Griffith, C.-C. Chang, Y.-C. Wu, C. H. Wang and J.-L. Wang, *Chemosphere*, 2022, **304**, 135304.

43 D. Materić, E. Ludewig, D. Brunner, T. Röckmann and R. Holzinger, *Environ. Pollut.*, 2021, **288**, 117697.

44 K. N. McPherson, L. G. Jahn, C. G. Masoud, N. Bhattacharyya, M. Modi, K. Patel, P. Abue, D. Blomdahl, P. K. Misztal and L. Hildebrandt Ruiz, *Atmos. Environ.*, 2024, **338**, 120812.

45 M. Kim, D. Kim, J.-Y. Seo and D. Park, *Toxics*, 2024, **12**, 511.

46 K. M. Haider, C. Focsa, C. Decuq, B. Esnault, F. Lafouge, B. Loubet, D. Petitprez and R. Ciuraru, *J. Environ. Manage.*, 2024, **364**, 121453.

47 R. Ciuraru, J. Kammer, C. Decuq, M. Vojkovic, K. Haider, Y. Carpentier, F. Lafouge, C. Berger, M. Bourdat-Deschamps, I. K. Ortega, F. Levavasseur, S. Houot, B. Loubet, D. Petitprez and C. Focsa, *Npj Clim. Atmospheric Sci.*, 2021, **4**, 1–10.

48 D. Kau, D. Materić, R. Holzinger, K. Baumann-Stanzer, G. Schauer and A. Kasper-Giebl, *Chemosphere*, 2024, **352**, 141410.
49 F. D. Lopez-Hilfiker, C. Mohr, M. Ehn, F. Rubach, E. Kleist, J. Wildt, T. F. Mentel, A. Lutz, M. Hallquist, D. Worsnop and J. A. Thornton, *Atmospheric Meas. Tech.*, 2014, **7**, 983–1001.
50 F. D. Lopez-Hilfiker, V. Pospisilova, W. Huang, M. Kalberer, C. Mohr, G. Stefenelli, J. A. Thornton, U. Baltensperger, A. S. H. Prevot and J. G. Slowik, *Atmospheric Meas. Tech.*, 2019, **12**, 4867–4886.
51 Y. Yang, J. Zhou, C. Xie, W. Tian, M. Xue, T. Han, K. Chen, Y. Zhang, Y. Liu, Y. Huang, H. Sun, C. Liu and S.-M. Li, *Environ. Sci. Technol.*, 2024, **58**, 12488–12497.
52 M. Farhat, C. Afif, S. Zhang, S. Dusanter, H. Delbarre, V. Riffault, S. Sauvage and A. Borbon, *Sci. Total Environ.*, 2024, **928**, 172098.
53 N. Rezaie, E. Pallozzi, P. Ciccioli, C. Calfapietra and S. Fares, *Environ. Pollut.*, 2023, **338**, 122703.
54 C.-B. Wei, G.-H. Yu, L.-M. Cao, H.-X. Han, S.-Y. Xia and X.-F. Huang, *Atmos. Environ.*, 2023, **312**, 120016.
55 K. Sekimoto, M. M. Coggon, G. I. Gkatzelis, C. E. Stockwell, J. Peischl, A. J. Soja and C. Warneke, *Environ. Sci. Technol.*, 2023, **57**, 13193–13204.
56 C. Daube, S. C. Herndon, J. E. Krechmer, D. Johnson, N. Clark, T. L. Footer and E. D. Thoma, *Atmospheric Environ. X*, 2023, **19**, 100220.
57 B. Kirchsteiger, D. Materić, F. Happenhofer, R. Holzinger and A. Kasper-Giebl, *Atmos. Environ.*, 2023, **301**, 119670.
58 Q. Wang, D. Sheng, C. Wu, D. Jing, N. Cheng, X. Cai, S. Li, J. Zhao, W. Li and J. Chen, *J. Environ. Sci.*, 2023, **130**, 114–125.
59 Q. Liu, J. Sheng, Y. Wu, Z. Ma, J. Sun, P. Tian, D. Zhao, X. Li, K. Hu, S. Li, X. Shen, Y. Zhang, H. He, M. Huang, D. Ding and D. Liu, *Sci. Total Environ.*, 2023, **860**, 160469.
60 Y. Fujitani, K. Sato, K. Tanabe, Y. Morino, K. Takahashi and J. Hoshi, *Atmospheric Environ. X*, 2023, **17**, 100197.
61 Y. Fujitani, K. Sato, K. Tanabe, K. Takahashi, J. Hoshi, X. Wang, J. C. Chow and J. G. Watson, *Environ. Sci. Technol.*, 2020, **54**, 14235–14245.
62 Y. Peng, A. P. Mouat, Y. Hu, M. Li, B. C. McDonald and J. Kaiser, *Atmos. Environ.*, 2022, **288**, 119324.
63 A. P. Mouat, C. Paton-Walsh, J. B. Simmons, J. Ramirez-Gamboa, D. W. T. Griffith and J. Kaiser, *Atmospheric Chem. Phys.*, 2022, **22**, 11033–11047.
64 D. Materić, M. Peacock, J. Dean, M. Futter, T. Maximov, F. Moldan, T. Röckmann and R. Holzinger, *Environ. Res. Lett.*, 2022, **17**, 054036.
65 A. Borbon, T. Salameh, S. Sauvage and C. Afif, *Environ. Pollut.*, 2024, **350**, 123797.
66 B. T. Jobson and J. K. McCoskey, *Atmospheric Chem. Phys.*, 2010, **10**, 1821–1835.
67 D. Materić, H. A. Kjær, P. Vallelonga, J.-L. Tison, T. Röckmann and R. Holzinger, *Environ. Res.*, 2022, **208**, 112741.
68 J. Zhao, V. Mickwitz, Y. Luo, E. Häkkinen, F. Graeffe, J. Zhang, H. Timonen, M. Canagaratna, J. E. Krechmer, Q. Zhang, M. Kulmala, J. Kangasluoma, D. Worsnop and M. Ehn, *EGUsphere*, 2023, 1–21.
69 A.-S. Lehnert, T. Behrendt, A. Ruecker, G. Pohnert and S. E. Trumbore, *Atmospheric Meas. Tech.*, 2020, **13**, 3507–3520.
70 D. Pagonis, K. Sekimoto and J. de Gouw, *J. Am. Soc. Mass Spectrom.*, 2019, **30**, 1330–1335.
71 P. Paatero and U. Tapper, *Environmetrics*, 1994, **5**, 111–126.
72 AQI Basics | AirNow.gov, https://www.airnow.gov/aqi/aqi-basics, (accessed 24 January 2025).
73 S. Keita, C. Liousse, V. Yoboué, P. Dominutti, B. Guinot, E.-M. Assamoi, A. Borbon, S. L. Haslett, L. Bouvier, A. Colomb, H. Coe, A. Akpo, J. Adon, J. Bahino, M. Doumbia, J. Djossou, C. Galy-Lacaux, E. Gardrat, S. Gnamien, J. F. Léon, M. Ossohou, E. T. N'Datchoh and L. Roblou, *Atmospheric Chem. Phys.*, 2018, **18**, 7691–7708.
74 W. P. L. Carter, *Air Waste*, 1994, **44**, 881–899.

75 M. J. Newland, G. J. Rea, L. P. Thüner, A. P. Henderson, B. T. Golding, A. R. Rickard, I. Barnes and J. Wenger, *Phys. Chem. Chem. Phys.*, 2019, **21**, 1160–1171.
76 J. Zhao, V. Mickwitz, Y. Luo, E. Häkkinen, F. Graeffe, J. Zhang, H. Timonen, M. Canagaratna, J. E. Krechmer, Q. Zhang, M. Kulmala, J. Kangasluoma, D. Worsnop and M. Ehn, *Atmospheric Meas. Tech.*, 2024, **17**, 1527–1543.
77 D. Materić, R. Holzinger and H. Niemann, *Sci. Total Environ.*, 2022, **846**, 157371.
78 A. B. Guenther, X. Jiang, C. L. Heald, T. Sakulyanontvittaya, T. Duhl, L. K. Emmons and X. Wang, *Geosci. Model Dev.*, 2012, **5**, 1471–1492.
79 F. Bianchi, T. Kurtén, M. Riva, C. Mohr, M. P. Rissanen, P. Roldin, T. Berndt, J. D. Crounse, P. O. Wennberg, T. F. Mentel, J. Wildt, H. Junninen, T. Jokinen, M. Kulmala, D. R. Worsnop, J. A. Thornton, N. Donahue, H. G. Kjaergaard and M. Ehn, *Chem. Rev.*, 2019, **119**, 3472–3509.
80 M. Ehn, J. A. Thornton, E. Kleist, M. Sipilä, H. Junninen, I. Pullinen, M. Springer, F. Rubach, R. Tillmann, B. Lee, F. Lopez-Hilfiker, S. Andres, I.-H. Acir, M. Rissanen, T. Jokinen, S. Schobesberger, J. Kangasluoma, J. Kontkanen, T. Nieminen, T. Kurtén, L. B. Nielsen, S. Jørgensen, H. G. Kjaergaard, M. Canagaratna, M. D. Maso, T. Berndt, T. Petäjä, A. Wahner, V.-M. Kerminen, M. Kulmala, D. R. Worsnop, J. Wildt and T. F. Mentel, *Nature*, 2014, **506**, 476–479.
81 E. Öström, Z. Putian, G. Schurgers, M. Mishurov, N. Kivekäs, H. Lihavainen, M. Ehn, M. P. Rissanen, T. Kurtén, M. Boy, E. Swietlicki and P. Roldin, *Atmospheric Chem. Phys.*, 2017, **17**, 8887–8901.
82 Y. Zhang, R. Liu, M. Li, Y. Guo, J. Kong and K. Hou, *J. Environ. Sci.*, 2025, **149**, 500–511.
83 J. Zhao, E. Häkkinen, F. Graeffe, J. E. Krechmer, M. R. Canagaratna, D. R. Worsnop, J. Kangasluoma and M. Ehn, *Atmospheric Chem. Phys.*, 2023, **23**, 3707–3730.
84 P. Liu, X. Liu, T. Saburi, S. Kubota, P. Huang and Y. Wada, *RSC Adv.*, 2021, **11**, 20529–20540.

Attachments

Attachment 1 Gas phase peak fitting data for α-pinene and β-pinene

alphapinene gasphase 90 ppb			betapinene gasphase 100 ppb			
Ion	m/Q	Fitted Intensity	Ion	m/Q	Fitted Intensity	
H5O2+	37.028406	557	H5O2+	37.028406	884	
NO2+	45.992355	5.59e+03	C2H2O+	42.010016	1.61	
H7O3+	55.038970	1.51e+04	C2H3O+	43.017841	44.5	
C3H5O+	57.033491	489	C3H7+	43.054227	1.2	
C4H9+	57.069877	106	C2H5O+	45.033491	76.3	
C3H7O+	59.049141	7.37e+03	NO2+	45.992355	6.46e+03	
C2H5O2+	61.028406	3.35e+03	CH3O2+	47.012756	13.3	
C5H7+	67.054227	974	C2H7O+	47.049141	1.84	
C3H3O2+	71.012756	567	H7O3+	55.038970	2.37e+04	
C4H7O+	71.049141	1.81e+03	C3H5O+	57.033491	497	
C3H5O2+	73.028406	412	C4H9+	57.069877	140	
H9O4+	73.049535	442	C3H7O+	59.049141	3.52e+03	
C4H9O+	73.064791	146	C2H4O2+	60.020581	55.8	
C3H7O2+	75.044056	512	C2H5O2+	61.028406	1.75e+03	
C3H9O2+	77.059706	745	C2H7O2+	63.044056	23.7	
C2H7O3+	79.038970	1.07e+03	C5H6+	66.046402	446	
C6H7+	79.054227	3.69e+03	C5H7+	67.054227	1.5e+03	
C5H5O+	81.033491	484	C5H9+	69.069877	398	
C6H9+	81.069877	4.44e+04	C3H3O2+	71.012756	720	
C4H5O2+	85.028406	645	C4H7O+	71.049141	405	
C5H9O+	85.064791	417	C5H11+	71.085527	65.6	
C4H7O2+	87.044056	1.32e+03	C3H5O2+	73.028406	274	
C4H9O2+	89.059706	464	H9O4+	73.049535	732	
C7H7+	91.054227	1.14e+04	C4H9O+	73.064791	83.4	
C7H8+	92.062052	8.38e+03	C3H7O2+	75.044056	384	
C7H9+	93.069877	1.06e+04	C2H5O3+	77.023320	47.1	
C7H11+	95.085527	6.75e+03	C3H9O2+	77.059706	279	
C7H13+	97.101177	141	C2H6O3+	78.031145	7.59	
C5H7O2+	99.044056	903	C6H6+	78.046402	241	
C6H11O+	99.080441	2.46e+03	C2H7O3+	79.038970	103	
C4H5O3+	101.023320	516	C6H7+	79.054227	8.39e+03	
C4H7O3+	103.038970	378	C6H8+	80.062052	1.94e+03	
C5H11O2+	103.075356	115	C6H9+	81.069877	9.35e+04	
C8H11+	107.085527	4.77e+03	C4H3O2+	83.012756	12.5	
C6H5O2+	109.028406	1.55e+03	C5H7O+	83.049141	757	
C7H9O+	109.064791	1.44e+03	C6H11+	83.085527	132	
C8H13+	109.101177	2.95e+03	C4H4O2+	84.020581	17.6	
C6H7O2+	111.044056	646	C4H5O2+	85.028406	295	

alphapinene gasphase 90 ppb			betapinene gasphase 100 ppb			
Ion	**m/Q**	**Fitted Intensity**	**Ion**	**m/Q**	**Fitted Intensity**	
C6H9O2+	113.059706	1.27e+03	C4H6O2+	86.036231	54.1	
C4H7O4+	119.033885	945	C4H7O2+	87.044056	394	
C9H11+	119.085527	516	C5H11O+	87.080441	14.4	
C9H13+	121.101177	2.64e+03	C4H9O2+	89.059706	95.2	
C3H7O5+	123.028800	188	C3H6O3+	90.031145	45.8	
C8H11O+	123.080441	989	C7H7+	91.054227	1.24e+04	
C9H15+	123.116827	931	C7H8+	92.062052	2.79e+03	
C6H5O3+	125.023320	252	C7H9+	93.069877	2e+04	
C7H9O2+	125.059706	466	C6H6O+	94.041316	173	
C8H13O+	125.096091	826	C6H7O+	95.049141	1.55e+04	
C6H7O3+	127.038970	2.67e+03	C7H11+	95.085527	1.22e+04	
C7H11O2+	127.075356	429	C5H5O2+	97.028406	407	
C6H9O3+	129.054621	549	C6H9O+	97.064791	618	
C7H13O2+	129.091006	146	C7H13+	97.101177	64.2	
C5H7O4+	131.033885	234	C5H6O2+	98.036231	65.6	
C6H11O3+	131.070271	424	C4H3O3+	99.007670	49.8	
C10H11+	131.085527	134	C5H7O2+	99.044056	434	
C7H15O2+	131.106656	31.1	C6H11O+	99.080441	145	
C10H13+	133.101177	424	C4H4O3+	100.015495	12.3	
C9H11O+	135.080441	248	C4H5O3+	101.023320	605	
C10H15+	135.116827	1.63e+03	C5H9O2+	101.059706	217	
C10H17+	137.132477	5.73e+04	C6H13O+	101.096091	2.91	
C10H13O+	149.096091	591	C4H7O3+	103.038970	160	
C10H15O+	151.111741	4.67e+03	C5H11O2+	103.075356	40.2	
C9H13O2+	153.091006	577	C3H4O4+	104.010410	3.16	
C10H17O+	153.127392	548	C3H5O4+	105.018235	120	
C7H7O4+	155.033885	35.2	C4H9O3+	105.054621	48.9	
C8H11O3+	155.070271	175	C8H9+	105.069877	633	
C9H15O2+	155.106656	490	C8H11+	107.085527	1.74e+03	
C7H9O4+	157.049535	162	C7H8O+	108.056966	36.5	
C8H13O3+	157.085921	198	C8H12+	108.093352	339	
C7H11O4+	159.065185	151	C6H5O2+	109.028406	2.01e+03	
C8H15O3+	159.101571	78.5	C7H9O+	109.064791	607	
C7H13O4+	161.080835	76.2	C8H13+	109.101177	1.1e+03	
C10H13O2+	165.091006	686	C7H10O+	110.072616	95.6	
C10H15O2+	167.106656	1.36e+03	C6H7O2+	111.044056	506	
C10H17O2+	169.122306	2.61e+03	C7H11O+	111.080441	252	
C8H11O4+	171.065185	83.9	C8H15+	111.116827	16.1	
C9H15O3+	171.101571	218	C5H5O3+	113.023320	115	
C8H13O4+	173.080835	171	C6H9O2+	113.059706	1.07e+03	
C10H13O3+	181.085921	55.3	C7H13O+	113.096091	26.6	
C10H14O3+	182.093746	28.3	C5H7O3+	115.038970	174	

alphapinene gasphase 90 ppb			betapinene gasphase 100 ppb			
Ion	**m/Q**	**Fitted Intensity**	**Ion**	**m/Q**	**Fitted Intensity**	
C9H15O4+	187.096485	204	C4H5O4+	117.018235	62.4	
C8H13O5+	189.075750	68.4	C5H9O3+	117.054621	105	
C8H15O5+	191.091400	26.8	C9H9+	117.069877	39.2	
C10H15O4+	199.096485	93.4	C6H13O2+	117.091006	55	
C10H17O4+	201.112135	112	C4H6O4+	118.026060	8.57	
C9H15O5+	203.091400	36.1	C5H10O3+	118.062446	5.44	
C8H13O6+	205.070665	11.7	C4H7O4+	119.033885	653	
C8H15O6+	207.086315	16.9	C9H11+	119.085527	223	
C10H15O5+	215.091400	32.8	C9H12+	120.093352	65.9	
C10H17O5+	217.107050	27.9	C9H13+	121.101177	3.97e+03	
C5H13O10+	233.050323	0.687	C3H7O5+	123.028800	76.6	
C10H17O6+	233.101965	5.62	C7H7O2+	123.044056	58	
			C8H11O+	123.080441	396	
			C9H15+	123.116827	213	
			C6H5O3+	125.023320	221	
			C7H9O2+	125.059706	151	
			C8H13O+	125.096091	266	
			C9H17+	125.132477	24.6	
			C6H6O3+	126.031145	21.5	
			C6H7O3+	127.038970	1.99e+03	
			C7H11O2+	127.075356	188	
			C5H5O4+	129.018235	21.1	
			C6H9O3+	129.054621	251	
			C7H13O2+	129.091006	58.9	
			C5H7O4+	131.033885	87	
			C6H11O3+	131.070271	211	
			C10H11+	131.085527	18.1	
			C7H15O2+	131.106656	4.17	
			C10H12+	132.093352	5.11	
			C5H9O4+	133.049535	73.8	
			C6H13O3+	133.085921	26.6	
			C10H13+	133.101177	139	
			C10H14+	134.109002	30.2	
			C4H7O5+	135.028800	26.1	
			C9H11O+	135.080441	92.5	
			C10H15+	135.116827	1.28e+03	
			C10H16+	136.124652	7.59e+03	
			C10H17+	137.132477	1.04e+05	
			C9H14O+	138.103916	345	
			C7H7O3+	139.038970	78.7	
			C8H11O2+	139.075356	107	
			C9H15O+	139.111741	2.96e+03	

betapinene gasphase 100 ppb			
Ion	**m/Q**	**Fitted Intensity**	
C7H9O3+	141.054621	102	
C8H13O2+	141.091006	253	
C3H10O6+	142.047189	10.7	
CH18O7+	142.104704	4.87	
C6H7O4+	143.033885	147	
C7H11O3+	143.070271	88.1	
C8H15O2+	143.106656	57.1	
C5H5O5+	145.013150	7.49	
C6H9O4+	145.049535	70	
C7H13O3+	145.085921	47.5	
C8H17O2+	145.122306	3.69	
C5H6O5+	146.020975	2.52	
C8H18O2+	146.130131	0.227	
C5H7O5+	147.028800	22.5	
C10H11O+	147.080441	45.4	
C7H16O3+	148.109396	2.59	
C10H13O+	149.096091	126	
C10H14O+	150.103916	24	
C10H15O+	151.111741	447	
C9H12O2+	152.083181	14.6	
C9H13O2+	153.091006	510	
C10H17O+	153.127392	409	
C7H7O4+	155.033885	14.6	
C8H11O3+	155.070271	67.5	
C9H15O2+	155.106656	1.42e+03	
C7H9O4+	157.049535	86.4	
C8H13O3+	157.085921	67.8	
C9H17O2+	157.122306	554	
C6H6O5+	158.020975	3.66	
C6H7O5+	159.028800	26.9	
C7H11O4+	159.065185	62.9	
C8H15O3+	159.101571	26.3	
C6H9O5+	161.044450	18.3	
C7H13O4+	161.080835	25.5	
C11H13O+	161.096091	3.37	
C8H17O3+	161.117221	1.73	
C10H11O2+	163.075356	23.8	
C7H15O4+	163.096485	2.64	
C5H8O6+	164.031539	1.33	
C6H12O5+	164.067925	3.02	
C10H12O2+	164.083181	0.0358	
C7H16O4+	164.104310	0.87	

betapinene gasphase 100 ppb			
Ion	**m/Q**	**Fitted Intensity**	
C9H10O3+	166.062446	3.44	
C9H11O3+	167.070271	16.3	
C10H15O2+	167.106656	122	
C9H12O3+	168.078096	8.93	
C9H13O3+	169.085921	129	
C10H17O2+	169.122306	174	
C8H11O4+	171.065185	44.8	
C9H15O3+	171.101571	204	
C10H19O2+	171.137956	152	
C7H9O5+	173.044450	8.02	
C8H13O4+	173.080835	100	
C9H17O3+	173.117221	24.3	
C13H17+	173.132477	4.19	
C9H2O4+	173.994760	0.49	
C6H7O6+	175.023714	3.95	
C7H11O5+	175.060100	38.4	
C8H15O4+	175.096485	8.66	
C9H20O3+	176.140696	0.251	
C7H13O5+	177.075750	17.1	
C6H10O6+	178.047189	0.787	
C7H14O5+	178.083575	0.571	
C6H11O6+	179.055014	4.46	
C7H16O5+	180.099225	5.14	
C5H9O7+	181.034279	1.58	
C9H9O4+	181.049535	1.95	
C10H13O3+	181.085921	18.5	
C10H14O3+	182.093746	5.46	
C7H18O5+	182.114875	7.21	
C9H11O4+	183.065185	5.23	
C10H15O3+	183.101571	44.5	
C4H8O8+	184.021369	0.652	
C10H17O3+	185.117221	192	
C8H11O5+	187.060100	8.95	
C9H15O4+	187.096485	71	
C7H9O6+	189.039364	1.93	
C8H13O5+	189.075750	25.2	
C13H17O+	189.127392	13.7	
C7H10O6+	190.047189	0.309	
C8H14O5+	190.083575	0.572	
C8H15O5+	191.091400	23.2	
C12H15O2+	191.106656	2.46	
C7H12O6+	192.062839	0.911	

betapinene gasphase 100 ppb			
Ion	**m/Q**	**Fitted Intensity**	
C7H13O6+	193.070665	2.67	
C8H19O5+	195.122700	6.34	
C8H20O5+	196.130525	0.178	
C10H13O4+	197.080835	3.56	
C11H17O3+	197.117221	1.79	
C10H15O4+	199.096485	16.4	
C10H16O4+	200.104310	2.08	
C9H13O5+	201.075750	4.48	
C10H17O4+	201.112135	24.7	
C9H15O5+	203.091400	17.2	
C10H19O4+	203.127785	1.9	
C16H12+	204.093352	0.473	
C8H13O6+	205.070665	5	
C8H14O6+	206.078490	0.382	
C7H11O7+	207.049929	0.63	
C8H15O6+	207.086315	4.65	
C15H12O+	208.088266	0.169	
C10H13O5+	213.075750	1.71	
C10H14O5+	214.083575	0.895	
C7H18O7+	214.104704	0.607	
C10H15O5+	215.091400	4.18	
C11H19O4+	215.127785	1.16	
C9H13O6+	217.070665	1.49	
C10H17O5+	217.107050	7.63	
C10H18O5+	218.114875	0.196	
C10H19O5+	219.122700	2.16	
C8H13O7+	221.065579	0.795	
C9H17O6+	221.101965	0.944	
C9H19O6+	223.117615	1.17	
C10H15O6+	231.086315	1.28	
C11H19O5+	231.122700	0.892	
C5H13O10+	233.050323	0.223	
C10H17O6+	233.101965	1.95	
C9H15O7+	235.081229	0.386	
C10H19O6+	235.117615	0.588	

Attachment 2 Particle phase peak fitting data for α-pinene and β-pinene

Alphapinene 90 ppb - particle phase			Alphapinene 80 ppb Vocus-only - particle phase			Betapinene 100 ppb - particle phase		
Ion	m/Q	Fitted intensity	Ion	m/Q	Fitted Intensity	Ion	m/Q	Fitted Intensity
H5O2+	37.028406	5,44E+02	H5O2+	37.028406	2,99E+02	H5O2+	37.028406	9,44E+02
NO2+	45.992355	5.64e+03	NO2+	45.992355	5.27e+03	C2H2O+	42.010016	4,42E+04
H7O3+	55.038970	1.53e+04	H7O3+	55.038970	7.44e+03	C2H3O+	43.017841	41.8
C3H5O+	57.033491	1,82E+02	C3H5O+	57.033491	1,08E+02	C3H7+	43.054227	0.939
C4H9+	57.069877	65.5	C4H9+	57.069877	4,57E+04	C2H5O+	45.033491	88.9
C3H7O+	59.049141	2.31e+03	C3H7O+	59.049141	1.14e+03	NO2+	45.992355	6.37e+03
C2H5O2+	61.028406	1.81e+03	C2H5O2+	61.028406	1.29e+03	CH3O2+	47.012756	4,58E+04
C5H7+	67.054227	2,39E+02	C5H7+	67.054227	71.9	C2H7O+	47.049141	1,14E+04
C3H3O2+	71.012756	2,31E+02	C3H3O2+	71.012756	1,44E+02	H7O3+	55.038970	2.65e+04
C4H7O+	71.049141	3,79E+02	C4H7O+	71.049141	1,44E+02	C3H5O+	57.033491	3,11E+02
C3H5O2+	73.028406	2,41E+02	C3H5O2+	73.028406	1,78E+02	C4H9+	57.069877	1,10E+02
H9O4+	73.049535	4,78E+02	H9O4+	73.049535	1,74E+02	C3H7O+	59.049141	2.39e+03
C4H9O+	73.064791	1,09E+02	C4H9O+	73.064791	74.9	C2H4O2+	60.020581	38.1
C3H7O2+	75.044056	2,20E+02	C3H7O2+	75.044056	1,44E+02	C2H5O2+	61.028406	1.82e+03
C3H9O2+	77.059706	2,56E+02	C3H9O2+	77.059706	1,60E+02	C2H7O2+	63.044056	4,58E+04
C2H7O3+	79.038970	5,65E+02	C2H7O3+	79.038970	5,85E+02	C5H6+	66.046402	2,02E+02
C6H7+	79.054227	9,74E+02	C6H7+	79.054227	2,97E+02	C5H7+	67.054227	7,29E+02
C5H5O+	81.033491	2,60E+02	C5H5O+	81.033491	1,38E+02	C5H9+	69.069877	2,36E+02
C6H9+	81.069877	1.16e+04	C6H9+	81.069877	2.67e+03	C3H3O2+	71.012756	4,18E+02
C4H5O2+	85.028406	2,42E+02	C4H5O2+	85.028406	1,34E+02	C4H7O+	71.049141	3,10E+02
C5H9O+	85.064791	1,17E+02	C5H9O+	85.064791	58.6	C5H11+	71.085527	48.8
C4H7O2+	87.044056	3,72E+02	C4H7O2+	87.044056	2,26E+02	C3H5O2+	73.028406	2,68E+02
C4H9O2+	89.059706	1,16E+02	C4H9O2+	89.059706	66.3	H9O4+	73.049535	8,50E+02
C7H7+	91.054227	2.67e+03	C7H7+	91.054227	6,46E+02	C4H9O+	73.064791	1,02E+02
C7H8+	92.062052	2.07e+03	C7H8+	92.062052	5,04E+02	C3H7O2+	75.044056	2,77E+02
C7H9+	93.069877	2.53e+03	C7H9+	93.069877	6,17E+02	C2H5O3+	77.023320	4,58E+04
C7H11+	95.085527	1.52e+03	C7H11+	95.085527	3,67E+02	C3H9O2+	77.059706	2,06E+02
C7H13+	97.101177	45.5	C7H13+	97.101177	4,59E+04	C2H6O3+	78.031145	2,24E+04
C5H7O2+	99.044056	3,88E+02	C5H7O2+	99.044056	3,25E+02	C6H6+	78.046402	1,20E+02
C6H11O+	99.080441	4,94E+02	C6H11O+	99.080441	1,22E+02	C2H7O3+	79.038970	2,66E+02
C4H5O3+	101.023320	4,75E+02	C4H5O3+	101.023320	2,77E+02	C6H7+	79.054227	3.69e+03
C4H7O3+	103.038970	1,62E+02	C4H7O3+	103.038970	1,42E+02	C6H8+	80.062052	7,36E+02
C5H11O2+	103.075356	48.9	C5H11O2+	103.075356	39.3	C6H9+	81.069877	4.08e+04
C8H11+	107.085527	7,14E+02	C8H11+	107.085527	1,61E+02	C4H3O2+	83.012756	1,30E+01
C6H5O2+	109.028406	1.53e+03	C6H5O2+	109.028406	9,86E+02	C5H7O+	83.049141	5,03E+02
C7H9O+	109.064791	2,64E+02	C7H9O+	109.064791	8,30E+01	C6H11+	83.085527	1,40E+02
C8H13+	109.101177	5,34E+02	C8H13+	109.101177	1,26E+02	C4H4O2+	84.020581	4,58E+04

Alphapinene 90 ppb - particle phase			Alphapinene 80 ppb Vocus-only - particle phase			Betapinene 100 ppb - particle phase		
Ion	m/Q	Fitted intensity	Ion	m/Q	Fitted Intensity	Ion	m/Q	Fitted Intensity
C6H7O2+	111.044056	3,63E+02	C6H7O2+	111.044056	2,55E+02	C4H5O2+	85.028406	2,58E+02
C7H11O+	111.080441	1,14E+02	C7H11O+	111.080441	43.1	C5H9O+	85.064791	1,26E+02
C6H9O2+	113.059706	3,79E+02	C6H9O2+	113.059706	1,74E+02	C4H6O2+	86.036231	4,57E+04
C4H7O4+	119.033885	8,62E+02	C4H7O4+	119.033885	9,26E+02	C4H7O2+	87.044056	4,19E+02
C9H11+	119.085527	1,37E+02	C9H11+	119.085527	41.9	C5H11O+	87.080441	4,57E+04
C9H13+	121.101177	5,71E+02	C9H13+	121.101177	1,45E+02	C4H9O2+	89.059706	79.2
C3H7O5+	123.028800	1,10E+02	C3H7O5+	123.028800	1,18E+02	C3H6O3+	90.031145	39.8
C8H11O+	123.080441	1,38E+02	C8H11O+	123.080441	47.1	C7H7+	91.054227	5.77e+03
C9H15+	123.116827	1,43E+02	C9H15+	123.116827	35.5	C7H8+	92.062052	1.58e+03
C6H5O3+	125.023320	2,42E+02	C6H5O3+	125.023320	2,05E+02	C7H9+	93.069877	8.6e+03
C7H9O2+	125.059706	1,26E+02	C7H9O2+	125.059706	74.4	C6H6O+	94.041316	1,20E+02
C8H13O+	125.096091	1,28E+02	C8H13O+	125.096091	44.5	C6H7O+	95.049141	6.85e+03
C6H7O3+	127.038970	2.59e+03	C6H7O3+	127.038970	2.86e+03	C7H11+	95.085527	5.44e+03
C7H11O2+	127.075356	1,30E+02	C7H11O2+	127.075356	73.8	C5H5O2+	97.028406	4,23E+02
C6H9O3+	129.054621	2,88E+02	C6H9O3+	129.054621	2,55E+02	C6H9O+	97.064791	3,30E+02
C7H13O2+	129.091006	43.4	C7H13O2+	129.091006	4,58E+04	C7H13+	97.101177	64.8
C5H7O4+	131.033885	1,12E+02	C5H7O4+	131.033885	9,20E+01	C5H6O2+	98.036231	60.3
C6H11O3+	131.070271	2,28E+02	C6H11O3+	131.070271	1,64E+02	C4H3O3+	99.007670	58.3
C10H11+	131.085527	4,59E+04	C10H11+	131.085527	4,22E+04	C5H7O2+	99.044056	3,65E+02
C7H15O2+	131.106656	4,37E+04	C7H15O2+	131.106656	1,95E+04	C6H11O+	99.080441	1,45E+02
C10H13+	133.101177	1,52E+02	C10H13+	133.101177	39.7	C4H4O3+	100.015495	4,57E+04
C9H11O+	135.080441	67.1	C9H11O+	135.080441	4,58E+04	C4H5O3+	101.023320	6,18E+02
C10H15+	135.116827	2,83E+02	C10H15+	135.116827	71.9	C5H9O2+	101.059706	3,73E+02
C10H17+	137.132477	1.46e+04	C10H17+	137.132477	3.44e+03	C6H13O+	101.096091	1,22E+04
C10H13O+	149.096091	64.7	C10H13O+	149.096091	4,59E+04	C4H7O3+	103.038970	1,47E+02
C10H15O+	151.111741	6,51E+02	C10H15O+	151.111741	1,32E+02	C5H11O2+	103.075356	41.7
C9H13O2+	153.091006	74.6	C9H13O2+	153.091006	4,59E+04	C3H4O4+	104.010410	4,58E+04
C10H17O+	153.127392	1,27E+02	C10H17O+	153.127392	4,59E+04	C3H5O4+	105.018235	1,09E+02
C7H7O4+	155.033885	4,58E+04	C7H7O4+	155.033885	3,17E+04	C4H9O3+	105.054621	64.4
C8H11O3+	155.070271	47.5	C8H11O3+	155.070271	4,58E+04	C8H9+	105.069877	3,82E+02
C9H15O2+	155.106656	89.4	C9H15O2+	155.106656	2,20E+01	C8H11+	107.085527	1.04e+03
C7H9O4+	157.049535	50.3	C7H9O4+	157.049535	3,40E+01	C7H8O+	108.056966	33.1
C8H13O3+	157.085921	47.9	C8H13O3+	157.085921	4,59E+04	C8H12+	108.093352	1,69E+02

Alphapinene 90 ppb - particle phase			Alphapinene 80 ppb Vocus-only - particle phase			Betapinene 100 ppb - particle phase		
Ion	m/Q	Fitted intensity	Ion	m/Q	Fitted Intensity	Ion	m/Q	Fitted Intensity
C7H11O4+	159.065185	4,30E+01	C7H11O4+	159.065185	4,57E+04	C6H5O2+	109.028406	2.07e+03
C8H15O3+	159.101571	4,57E+04	C8H15O3+	159.101571	3,42E+04	C7H9O+	109.064791	3,16E+02
C7H13O4+	161.080835	4,59E+04	C7H13O4+	161.080835	4,59E+04	C8H13+	109.101177	5,66E+02
C10H13O2+	165.091006	89.6	C10H13O2+	165.091006	4,57E+04	C7H10O+	110.072616	35.4
C10H15O2+	167.106656	96.1	C10H15O2+	167.106656	4,59E+04	C6H7O2+	111.044056	4,79E+02
C10H17O2+	169.122306	3,70E+02	C10H17O2+	169.122306	7,30E+01	C7H11O+	111.080441	1,79E+02
C8H11O4+	171.065185	4,59E+04	C8H11O4+	171.065185	1,00E+01	C8H15+	111.116827	47.6
C9H15O3+	171.101571	3,00E+01	C9H15O3+	171.101571	4,57E+04	C5H5O3+	113.023320	1,34E+02
C8H13O4+	173.080835	46.3	C8H13O4+	173.080835	2,00E+01	C6H9O2+	113.059706	5,60E+02
C10H13O3+	181.085921	1,70E+01	C10H13O3+	181.085921	1,96E+04	C7H13O+	113.096091	4,57E+04
C10H14O3+	182.093746	1,80E+04	C10H14O3+	182.093746	2,30E+04	C5H7O3+	115.038970	1,67E+02
C10H15O3+	183.101571	57.8	C10H15O3+	183.101571	4,59E+04	C9H7+	115.054227	5,40E+01
C10H17O3+	185.117221	42.9	C10H17O3+	185.117221	4,57E+04	C6H11O2+	115.075356	1,41E+02
C9H15O4+	187.096485	4,57E+04	C9H15O4+	187.096485	2,36E+04	C4H5O4+	117.018235	68.3
C8H13O5+	189.075750	1,00E+01	C8H13O5+	189.075750	2,46E+04	C5H9O3+	117.054621	1,12E+02
C8H15O5+	191.091400	7,00E+00	C8H15O5+	191.091400	1,61E+04	C9H9+	117.069877	41.1
C10H15O4+	199.096485	1,60E+01	C10H15O4+	199.096485	4,59E+04	C6H13O2+	117.091006	59.2
C10H17O4+	201.112135	4,58E+04	C10H17O4+	201.112135	2,53E+04	C4H6O4+	118.026060	1,23E+04
C9H15O5+	203.091400	5,00E+00	C9H15O5+	203.091400	4,46E+04	C5H10O3+	118.062446	4,58E+04
C8H13O6+	205.070665	4,59E+04	C8H13O6+	205.070665	3,03E+04	C4H7O4+	119.033885	6,72E+02
C8H15O6+	207.086315	2,89E+04	C8H15O6+	207.086315	2,67E+04	C9H11+	119.085527	2,71E+02
C10H15O5+	215.091400	2,42E+04	C10H15O5+	215.091400	4,57E+04	C9H12+	120.093352	4,58E+04
C10H17O5+	217.107050	3,15E+04	C10H17O5+	217.107050	2,71E+04	C9H13+	121.101177	2.14e+03
C5H13O10+	233.050323	0.239	C5H13O10+	233.050323	0.236	C3H7O5+	123.028800	66.6
C10H17O6+	233.101965	0.848	C10H17O6+	233.101965	0.781	C7H7O2+	123.044056	71.5
						C8H11O+	123.080441	1,59E+02
						C9H15+	123.116827	1,54E+02
						C6H5O3+	125.023320	2,46E+02
						C7H9O2+	125.059706	1,17E+02
						C8H13O+	125.096091	1,41E+02
						C9H17+	125.132477	4,58E+04
						C6H6O3+	126.031145	4,59E+04
						C6H7O3+	127.038970	2.05e+03

Alphapinene 90 ppb - particle phase			Alphapinene 80 ppb Vocus-only - particle phase			Betapinene 100 ppb - particle phase		
Ion	m/Q	Fitted intensity	Ion	m/Q	Fitted Intensity	Ion	m/Q	Fitted Intensity
						C7H11O2+	127.075356	1,14E+02
						C5H5O4+	129.018235	4,59E+04
						C6H9O3+	129.054621	2,36E+02
						C7H13O2+	129.091006	56.9
						C5H7O4+	131.033885	90.3
						C6H11O3+	131.070271	1,98E+02
						C10H11+	131.085527	4,59E+04
						C7H15O2+	131.106656	3,00E+04
						C10H12+	132.093352	41.3
						C5H9O4+	133.049535	70.2
						C6H13O3+	133.085921	4,58E+04
						C10H13+	133.101177	3,29E+02
						C10H14+	134.109002	65.6
						C4H7O5+	135.028800	4,58E+04
						C9H11O+	135.080441	1,00E+02
						C10H15+	135.116827	9,03E+02
						C10H16+	136.124652	3.07e+03
						C10H17+	137.132477	4.59e+04
						C9H14O+	138.103916	98.3
						C7H7O3+	139.038970	55.2
						C8H11O2+	139.075356	72.9
						C9H15O+	139.111741	1.88e+03
						C6H5O4+	141.018235	66.7
						C7H9O3+	141.054621	62.7
						C8H13O2+	141.091006	1,04E+02
						C3H10O6+	142.047189	1,37E+04
						CH18O7+	142.104704	3,25E+04
						C6H7O4+	143.033885	1,57E+02
						C7H11O3+	143.070271	45.5
						C8H15O2+	143.106656	56.3
						C5H5O5+	145.013150	1,66E+04
						C6H9O4+	145.049535	59.5
						C7H13O3+	145.085921	4,58E+04

Alphapinene 90 ppb - particle phase			Alphapinene 80 ppb Vocus-only - particle phase			Betapinene 100 ppb - particle phase		
Ion	m/Q	Fitted intensity	Ion	m/Q	Fitted Intensity	Ion	m/Q	Fitted Intensity
						C8H17O2+	145.122306	1,66E+04
						C5H6O5+	146.020975	4,68E+04
						C8H18O2+	146.130131	0.336
						C5H7O5+	147.028800	4,59E+04
						C10H11O+	147.080441	4,80E+01
						C7H16O3+	148.109396	1,76E+04
						C10H13O+	149.096091	1,12E+02
						C10H14O+	150.103916	4,58E+04
						C10H15O+	151.111741	4,06E+02
						C9H12O2+	152.083181	4,57E+04
						C9H13O2+	153.091006	2,44E+02
						C10H17O+	153.127392	3,37E+02
						C7H7O4+	155.033885	1,20E+01
						C8H11O3+	155.070271	38.5
						C9H15O2+	155.106656	2,06E+02
						C7H9O4+	157.049535	40.9
						C8H13O3+	157.085921	33.7
						C9H17O2+	157.122306	3,78E+02
						C6H6O5+	158.020975	4,58E+04
						C6H7O5+	159.028800	2,80E+01
						C7H11O4+	159.065185	38.6
						C8H15O3+	159.101571	4,57E+04
						C6H9O5+	161.044450	4,58E+04
						C7H13O4+	161.080835	4,59E+04
						C11H13O+	161.096091	3,41E+04
						C8H17O3+	161.117221	1,91E+04
						C10H11O2+	163.075356	4,59E+04
						C7H15O4+	163.096485	1,87E+04
						C5H8O6+	164.031539	4,57E+04
						C6H12O5+	164.067925	2,30E+04
						C10H12O2+	164.083181	0.87
						C7H16O4+	164.104310	4,24E+04
						C10H13O2+	165.091006	39.1

Alphapinene 90 ppb - particle phase			Alphapinene 80 ppb Vocus-only - particle phase			Betapinene 100 ppb - particle phase		
Ion	m/Q	Fitted intensity	Ion	m/Q	Fitted Intensity	Ion	m/Q	Fitted Intensity
						C9H10O3+	166.062446	3,22E+04
						C9H11O3+	167.070271	2,40E+01
						C10H15O2+	167.106656	92.7
						C9H12O3+	168.078096	2,79E+04
						C9H13O3+	169.085921	42.2
						C10H17O2+	169.122306	1,92E+02
						C8H11O4+	171.065185	4,57E+04
						C9H15O3+	171.101571	55.2
						C10H19O2+	171.137956	1,22E+02
						C7H9O5+	173.044450	2,31E+04
						C8H13O4+	173.080835	45.5
						C9H17O3+	173.117221	4,57E+04
						C13H17+	173.132477	2,96E+04
						C9H2O4+	173.994760	0.513
						C6H7O6+	175.023714	1,65E+04
						C7H11O5+	175.060100	4,57E+04
						C8H15O4+	175.096485	4,59E+04
						C9H20O3+	176.140696	4,57E+04
						C7H13O5+	177.075750	2,54E+04
						C6H10O6+	178.047189	0.912
						C7H14O5+	178.083575	0.616
						C6H11O6+	179.055014	2,67E+04
						C7H16O5+	180.099225	1,43E+04
						C5H9O7+	181.034279	2,01E+04
						C9H9O4+	181.049535	4,57E+04
						C10H13O3+	181.085921	4,59E+04
						C10H14O3+	182.093746	4,59E+04
						C7H18O5+	182.114875	4,59E+04
						C9H11O4+	183.065185	4,57E+04
						C10H15O3+	183.101571	4,57E+04
						C4H8O8+	184.021369	0.542
						C10H17O3+	185.117221	49.5
						C8H11O5+	187.060100	3,01E+04

Alphapinene 90 ppb - particle phase			Alphapinene 80 ppb Vocus-only - particle phase			Betapinene 100 ppb - particle phase		
Ion	m/Q	Fitted intensity	Ion	m/Q	Fitted Intensity	Ion	m/Q	Fitted Intensity
						C9H15O4+	187.096485	4,59E+04
						C7H9O6+	189.039364	4,60E+04
						C8H13O5+	189.075750	2,83E+04
						C13H17O+	189.127392	2,16E+04
						C7H10O6+	190.047189	0.267
						C8H14O5+	190.083575	0.274
						C8H15O5+	191.091400	3,63E+04
						C12H15O2+	191.106656	2,52E+04
						C7H12O6+	192.062839	0.47
						C15H12+	192.093352	0.175
						C7H13O6+	193.070665	1,79E+04
						C8H19O5+	195.122700	1,69E+04
						C8H20O5+	196.130525	0.265
						C10H13O4+	197.080835	4,57E+04
						C11H17O3+	197.117221	1,68E+04
						C10H15O4+	199.096485	3,01E+04
						C10H16O4+	200.104310	0.73
						C9H13O5+	201.075750	1,28E+04
						C10H17O4+	201.112135	3,53E+04
						C9H15O5+	203.091400	4,58E+04
						C10H19O4+	203.127785	2,74E+04
						C16H12+	204.093352	0.253
						C8H13O6+	205.070665	3,21E+04
						C8H14O6+	206.078490	0.167
						C7H11O7+	207.049929	0.988
						C8H15O6+	207.086315	1,28E+04
						C15H12O+	208.088266	0.152
						C10H13O5+	213.075750	4,58E+04
						C10H14O5+	214.083575	4,33E+04
						C7H18O7+	214.104704	3,22E+04
						C10H15O5+	215.091400	3,00E+04
						C11H19O4+	215.127785	0.404
						C9H13O6+	217.070665	0.926

Alphapinene 90 ppb - particle phase			Alphapinene 80 ppb Vocus-only - particle phase			Betapinene 100 ppb - particle phase		
Ion	m/Q	Fitted intensity	Ion	m/Q	Fitted Intensity	Ion	m/Q	Fitted Intensity
						C10H17O5+	217.107050	1,25E+04
						C10H18O5+	218.114875	0.15
						C10H19O5+	219.122700	0.912
						C8H13O7+	221.065579	0.464
						C9H17O6+	221.101965	0.902
						C9H19O6+	223.117615	4,25E+04
						C10H15O6+	231.086315	0.519
						C11H19O5+	231.122700	0.265
						C5H13O10+	233.050323	0.23
						C10H17O6+	233.101965	0.662
						C9H15O7+	235.081229	0.208
						C10H19O6+	235.117615	0.28

Attachment 3. Highlighted species from Table 1; Vocus-only Set-up.

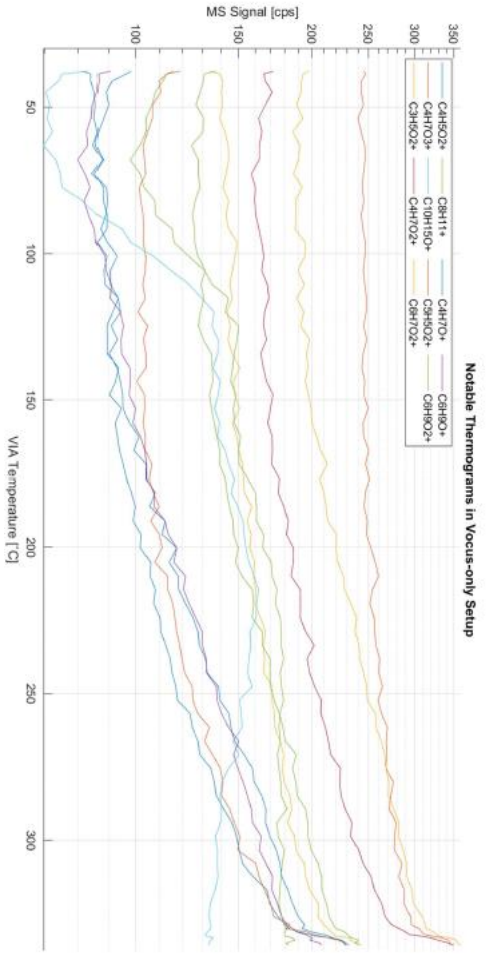

Attachment 4. Highlighted species from Table 1 ; combination set-up

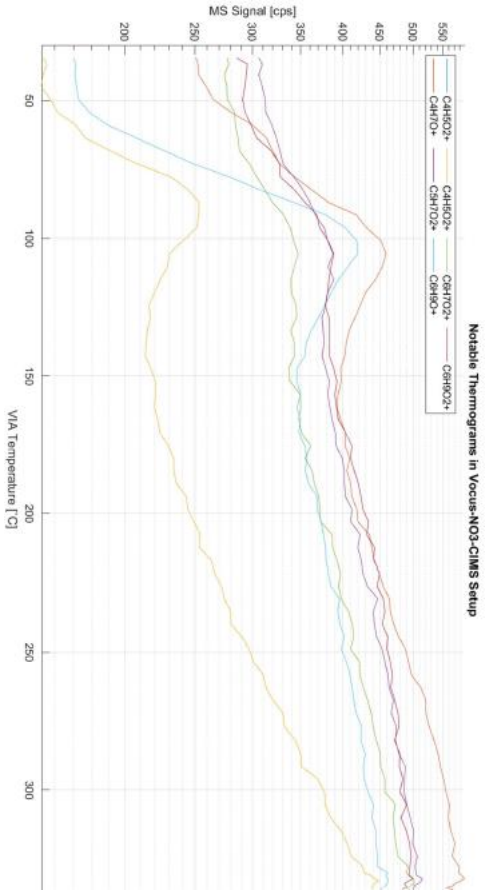

Attachment 5. Background subtracted net signal of apparent hydrocarbon species measured with combination set-up.

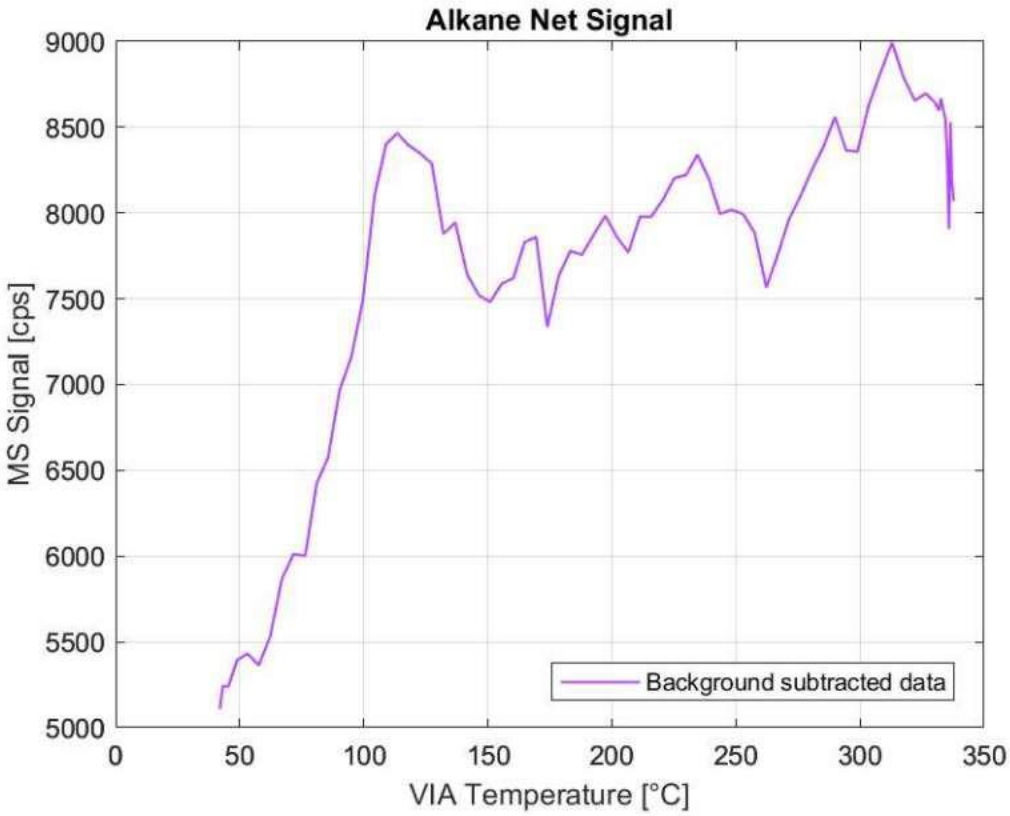

Attachment 6. Comparison of ramp-up and ramp-down data in both set-ups.

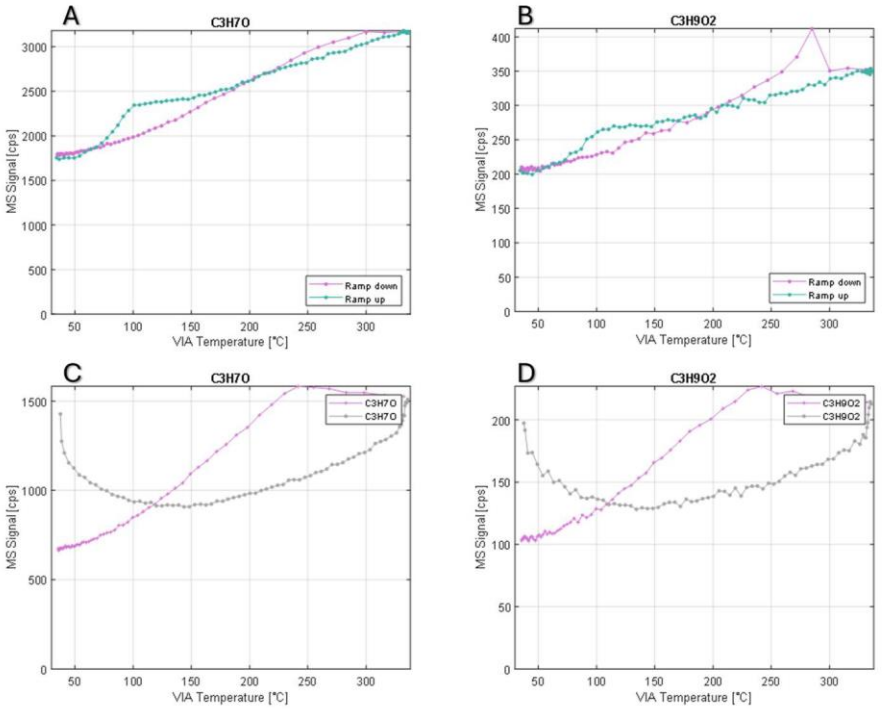

A & B:
Combination Setup with 90 ppb α-pinene concentration. The Turqoise Line Depicts Ramp-up Data and the Pink Line Respectively Ramp-down Data.

C & D:
Vocus-only Setup with 80 ppb α-pinene concentration. The Gray Line Depicts Ramp-up Data and the Pink Line Respectively Ramp-down Data.